LA-12934-MS

Earth Science Investigations for Environmental Restoration—Los Alamos National Laboratory Technical Area 21

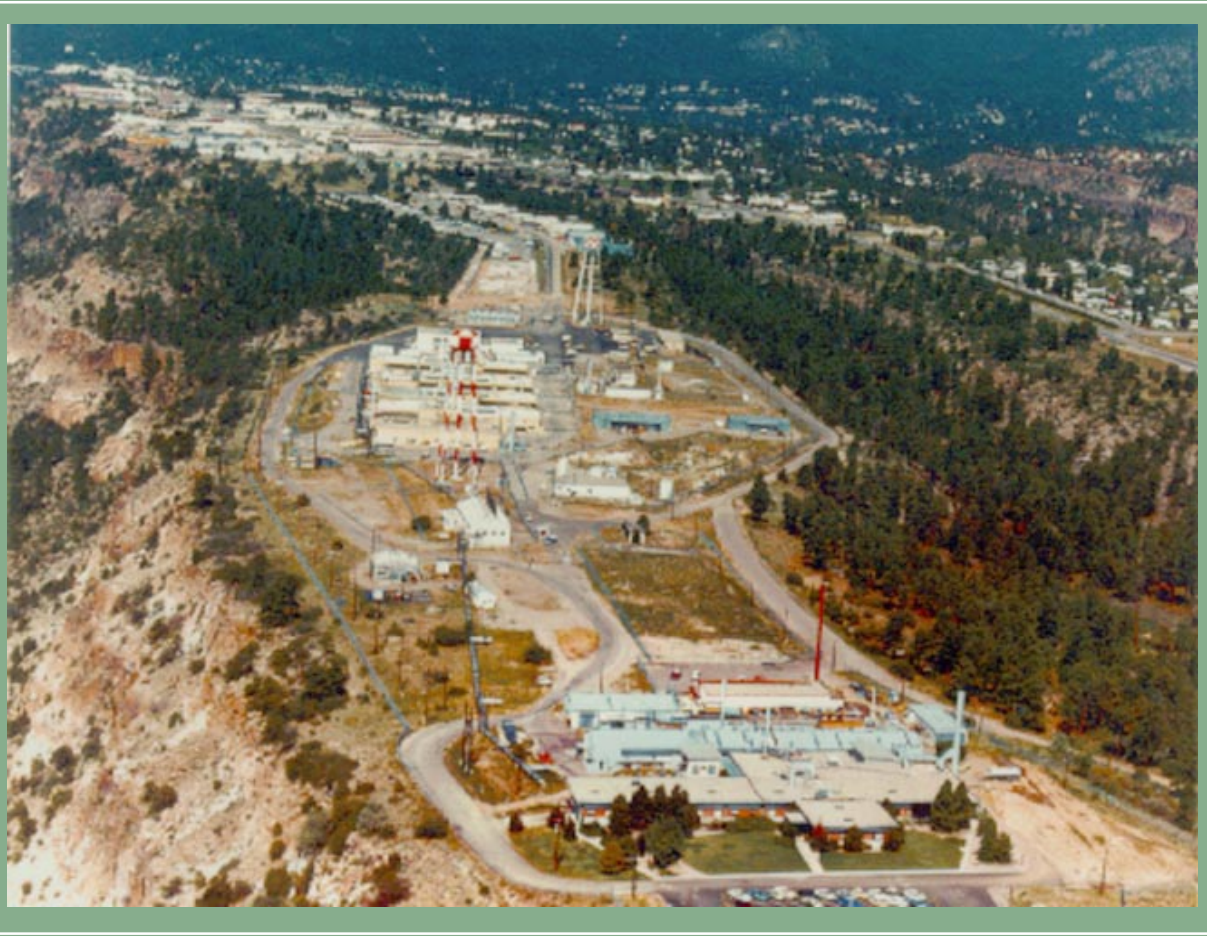

Los Alamos
NATIONAL LABORATORY

Los Alamos National Laboratory is operated by the University of California for the United States Department of Energy under contract W-7405-ENG-36.

Cover photo: Aerial view of Los Alamos Technical Area 21, looking west, with Los Alamos townsite in the background. Light-colored tuffs, which underlie TA-21, are visible on canyon walls. Variations in welding produce alternating dark-orange cliff-forming tuffs and nearly white, slope-forming tuffs. (Photograph was taken in 1982.)

LA-12934-MS

UC-903
Issued: May 1995

Earth Science Investigations for Environmental Restoration— Los Alamos National Laboratory Technical Area 21

Edited by
D.E. Broxton
P.G. Eller

Los Alamos
NATIONAL LABORATORY
Los Alamos, New Mexico 87545

ACKNOWLEDGEMENTS

This work was supported by the Environmental Restoration Program of Los Alamos National Laboratory as part of Resource Conservation and Recovery Act Facility Investigation work at TA-21. We thank Micheline Devaurs, Caroline Mason, and Garry Allen for their project support during these investigations. The Facility for Information Management and Display (FIMAD) contributed substantially to these investigations by providing spatial display of geologic information and by producing the plates in the back pocket of this report.

Contents

EARTH SCIENCE INVESTIGATIONS FOR ENVIRONMENTAL RESTORATION— LOS ALAMOS NATIONAL LABORATORY TECHNICAL AREA 21

D. E. Broxton and P. G. Eller
Editors

ABSTRACT

The investigations compiled in this report describe the geology at Los Alamos National Laboratory Technical Area-21 and form the basis for a more detailed understanding of site hydrogeological characteristics. The investigations included studies of site geology, fractures, stratigraphy, petrography, mineralogy, and geomorphology. These studies were conducted in support of the Resource Conservation and Recovery Act Facility Investigation for Los Alamos National Laboratory. Although these investigations specifically address geologic conditions at TA-21, they have substantial relevance to other Laboratory operable units.

INTRODUCTION

This report describes geologic field investigations conducted in 1992 and 1993 in support of the Resource Conservation and Recovery Act Facility Investigation (RFI) at Technical Area (TA)-21; Operable Unit (OU) 1106 at Los Alamos National Laboratory. The investigations included studies of the site geology, fractures, stratigraphy, petrography, mineralogy, and geomorphology. Some of these investigations were reported to Region VI of the US Environmental Protection Agency (EPA) as part of an earlier phase report (LANL, 1993). However, this report includes some additional data and minor revisions not encompassed by the earlier phase report. This report also provides new information about drilling activities in the autumn of 1993 (Fig. 1) and about a fluorescein tracer experiment in DP Canyon.

Photo of Technical Area-21, Los Alamos National Laboratory, Los Alamos, New Mexico (1975 photo).

specifically address TA-21, they have substantial relevance to other Laboratory Environmental Restoration (ER) Investigations. The work forms the basis for more detailed understanding of site hydrogeological characteristics to be developed in greater detail during subsequent RFI investigations. This work was supported by the TA-21 RFI and the Earth Sciences Technical Team of the ER Program.

SITE DESCRIPTION

TA-21 is located on the northern edge of the Laboratory, at an elevation of 7140 ft. It is centrally located on the Pajarito Plateau, roughly midway between the steep flanks of the Jemez Mountains on the west and the White Rock Canyon of the Rio Grande to the east. TA-21 centers on DP Mesa, immediately east-southeast of the Los Alamos townsite. The operable unit extends from the mesa top to the stream channels in the adjacent canyons, DP Canyon to the north, and Los Alamos Canyon to the south. Additional information relevant to general site conditions of TA-21 and vicinity is presented in the TA-21 RFI work plan (LANL, 1991) and the Installation Work Plan (IWP) (LANL, 1992).

SITE HISTORY

TA-21 was used primarily for plutonium research and metal production from 1945 to 1978. Subsequent offices and small-scale research activities have used the facilities up until the present time. Because the major industrial activity was related to plutonium recovery, the major waste disposal activities were plutonium related as well. Hazardous constituents are likely to be present in most waste streams as a result of the process chemistry. The 112 solid waste management units (SWMUs) fall into four conceptual categories:

- deep liquid releases, such as seepage pits and absorption beds, into which plutonium-bearing liquids were discharged;
- near-surface liquid releases, such as surface discharges from septic systems, that may have contained industrial liquid wastes;
- subsurface solid-waste disposal areas, such as Material Disposal Areas (MDAs), where contaminated equipment, industrial materials, stabilized process residues, and radioactive or hazardous wastes were buried in shallow trenches or isolated shafts; and
- surface contamination areas, where limited quantities of contaminants were released at the surface, such as stack-release fallout and surface spills.

Detailed historical data for TA-21 are presented in Chapter 3, TA-21 Operable Unit Background Information, of the RFI work plan (LANL, 1991). The state of knowledge of the environmental setting, geology, and surface and groundwater hydrology for the Pajarito Plateau in general and of TA-21 in particular, was summarized in RFI work plan Chapter 4, Environmental Setting. Additional relevant information is contained in the IWP (LANL, 1992). The grouping of SWMUs into conceptual categories, as well as a discussion of the potential migration pathways of importance for each type of SWMU is presented in RFI work plan Chapter 5, Potential Contaminant Migration Pathways.

INVESTIGATIONS REPORTED

Investigations described in this report are the TA-21-specific geologic and geomorphic studies that were outlined in RFI work plan Section 12.3, Geomorphologic Sampling Plan (LANL 1991). The studies include the sections described as follows:

Geologic mapping. Goff presents a geologic map and cross sections that were prepared to identify geologic units outcropping at TA-21 and those that can be expected in the subsurface below the mesa.

Faults and fractures. Wohletz mapped and characterized fractures on the face of Los Alamos Canyon below TA-21. His investigation assesses fracture abundance, size, and orientation as indications of faulting, as well as relevance of fractures to potential contaminant migration into the subsurface.

TA-21 is located on top of DP Mesa, which is underlain by a thick sequence of ashflow tuffs.

Stratigraphy, petrography, and mineralogy. Broxton, Heiken, Chipera, and Byers discuss the stratigraphy, petrography, and mineralogy of rock units underlying DP Mesa, using three stratigraphic sections on the cliff faces of Los Alamos Canyon. Their investigation examines vertical and lateral variability of stratigraphic, lithologic, and mineralogic properties and provides a preliminary subdivision of five hydrogeological units at the site.

Tuff color and erosion characteristics reflect differences in welding and secondary alteration.

The north wall of Los Alamos Canyon below TA-21 was mapped for fractures.

Geomorphology. Reneau investigated and mapped the geomorphic features of DP Mesa, DP Canyon, and Los Alamos Canyon. This work involved a general assessment of the rate and mechanisms of cliff retreat in addition to descriptions of erosional and depositional areas in drainages leading from DP Mesa.

Cliff retreat is noted along the margins of DP Mesa.

Preliminary Drilling Results. Broxton, Eller, and Flores summarize the preliminary geologic and hydrologic results from boreholes LADP-3 (in Los Alamos Canyon) and LADP-4 (in DP Canyon). A shallow alluvial aquifer and an intermediate-depth (325-ft) perched zone were encountered in LADP-3. The intermediate-depth perched water zone contains small amounts of tritium. Borehole LADP-4 was drilled to 800 ft but did not encounter perched water zones. Elevated tritium was found associated with high-moisture contents at the "vapor-phase notch" in the upper Bandelier Tuff in this borehole.

Preliminary results were obtained from the drillholes LADP-3 and LADP-4.

Fluorescein Dye Experiment. Adams, DeMuth, Counce, and Goff show that elevated tritium conncentrations at DP Spring are not caused by tritiated effluent from the sewage treatment plant at TA-21. Fluorescein dye and water chemistry were used to show that DP Spring is fed by a source that is not connected to the sewage treatment plant.

The biodegradable fluorescein dye used to trace tritiated effluent shows vivid green in this photo.

REGULATORY RELEVANCE

These investigations were conducted as a requirement of the HSWA Module VIII of the Laboratory's Resource Conservation and Recovery Act (RCRA) Part B operating permit (EPA, #1990). Section P, Task Ill, Facility Investigation, Subtask A.l of the Hazardous Solid Waste Act (HSWA) module, requires a program to evaluate site hydrogeologic conditions. The permit requires the aquisition and assessment of the the types of information listed in Table I.

In addition, Module VIII of the Laboratory's RCRA Part B permit requires a soils program to characterize soil and rock units above the water table in the vicinity of contaminant release(s). Section P, Task 111, A.2 specifies that this characterization program will include, but is not limited to, the information listed in Table II.

In summary, Module VIII requires comprehensive hydrogeologic and soils characterization of the vadose zone to the watertable. Specifically, Section P, Task 111, A.l.d states, "...a representative and accurate classification and description of the hydrogeologic units which may be part of the migration pathways at the facility [is required]...."
Aspects of the above requirements that are not included in this report will be addressed in other investigations described in the work plan in Chapter 12, Mesa Top Sampling Plan (LANL, 1991).

SUMMARY

The investigations compiled in this report describe the geology at TA-21 and form the basis for a more detailed understanding of site hydrogeological characteristics. These studies were conducted in support of the RFI for Los Alamos National Laboratory. The investigations specifically address geologic conditions at TA-21 but have substantial relevance to other Laboratory operable units.

TABLE I
SITE HYDROLOGIC STUDIES REQUIRED BY HSWA MODULE VIII, LOS ALAMOS NATIONAL LABORATORY'S RCRA PART B PERMIT

Description of regional- and facility-specific geologic and hydrogeologic characteristics affecting groundwater flow beneath the facility

Analysis of topographic features that might influence the groundwater flow system

Analysis of fractures within the tuff; tectonic trend fractures *vs* cooling fractures

Representative and accurate classification and description of hydrogeologic units that may be part of the migration pathways at the facility; based on field data, tests, and cores.

Structural geology and hydrogeologic cross sections showing the extent of hydrogeologic units that may be part of the migration pathways; based on field studies and cores:

- Unconsolidated sand and gravel deposits
- Zones of fracturing or channeling in consolidated or unconsolidated deposits
- Zones of high or low permeability that might direct and restrict the flow of contaminants

Representative description of water level of fluid pressure monitoring; based on data obtained from groundwater monitoring wells and piezometers installed upgradient and downgradient of the potential contaminant source

TABLE II
SITE CHARACTERIZATION OF SOILS REQUIRED BY HSWA MODULE VIII, LOS ALAMOS NATIONAL LABORATORY'S RCRA PART B PERMIT

Soils

Surface soil distribution
Soil profile, including classification of soil
Transects of soil stratigraphy
Soil pH
Particle size distribution
Residual concentration of contaminants in soil

Hydrology

Effect of stratification on unsaturated flow
Infiltration
Evapotranspiration
Water balance scenarios
Moisture content

Mineralogy/Chemistry

Mineral and metal content
Cation exchange capacity
Trace element geochemistry as a means of differentiating units within the tuff

REFERENCES

EPA, 1990, US Environmental Protection Agency. RCRA Permit No. NMO890010515, EPA Region VI, issued to Los Alamos National Laboratory, Los Alamos, NM 87545, effective May 23, 1990.

LANL, 1991, TA-21 Operable Unit RFI Work Plan for Environmental Restoration, Los Alamos National Laboratory document LAUR-91-962, Los Alamos National Laboratory, Los Alamos, NM 87545.

LANL, 1992, Installation Work Plan for Environmental Restoration. Los Alamos National Laboratory document LAUR-92-3795, Los Alamos National Laboratory, Los Alamos, NM 87545.

LANL, 1993, Phase Report 1A, TA-21 Operable Unit RCRA Facility Investigation, June 14, 1993.

GEOLOGIC MAP OF TECHNICAL AREA 21

by

F. Goff

A geologic map of TA-21 was prepared by using color photographs of canyon walls as well as conventional field mapping (scale of 1:4200, or 1 in. = 350 ft), and the general bedrock relations were studied. Exposed bedrock geology consists of three stratigraphic units (bottom to top): (1) the Otowi Member, Bandelier Tuff (consisting primarily of nonwelded, lithic-rich, rhyolitic ignimbrite), (2) the Cerro Toledo interval (interbedded rhyolitic pyroclastic falls and epiclastic gravels of dominately dacitic composition), and (3) the Tshirege Member, Bandelier Tuff (nonwelded to welded rhyolitic ignimbrite). The Bandelier Tuff and fall deposits in the Cerro Toledo interval were derived primarily from explosive volcanic eruptions in the Valles caldera west of TA-21. In addition, the Tshirege Member is subdivided into five units because of the distinct boundaries caused by deposition of flow units, variations in welding, and variations in alteration. Bedrock units are partially covered by alluvium, terrace gravels, talus/colluvium, mesa top soils, and disturbed alluvium. Contacts between the three bedrock units are generally undulatory as a result of the periods of erosion between emplacement. However, thicknesses of most units, except for the bedded Cerro Toledo interval, are relatively constant. No faults were found in the map area in exposed bedrock units. One cold spring (DP Spring) was found in eastern DP canyon issuing from a contact between colluvial and valley fill deposits and Tshirege unit 1g. This spring discharges from the north cliff face about 20 ft above the canyon bottom.

INTRODUCTION AND PREVIOUS MAPPING OF TA-21 AND THE SURROUNDING AREA

This study presents a geologic map and cross sections of units at TA-21. The map supports RFI studies at TA-21 by showing the distribution and thickness of units. These data provide both a geologic framework for evaluating potential contaminant transport pathways and background information for evaluating various remediation alternatives.

TA-21 (also known as DP site) lies on the Pajarito Plateau, which is located on the east flank of the Jemez Mountains and the west margin of the Española Basin. The Pajarito Plateau is composed primarily of the slightly eroded Tshirege Member of the Bandelier Tuff, a large-volume, rhyolitic ash-flow tuff (ignimbrite) erupted from the Valles caldera

of the Jemez volcanic field (Smith and Bailey, 1966). All designated waste sites at TA-21 are built in the upper zones of this ignimbrite sheet or in overlying deposits. Discussions of the geology of the upper portions of DP Mesa and the history of disposal facilities can be found in several reports (Rogers, 1977; Nyhan *et al.*, 1984; Gerety *et al.*, 1989; Merrill, 1990; LANL, 1991).

Regional geologic maps that cover all or part of the Pajarito Plateau include those of Griggs (1964) for geohydrologic investigations centered around Los Alamos, Smith *et al.* (1970) for volcanologic investigations of the Jemez Mountains, and Kelley (1978) for tectonic investigations associated with the Rio Grande rift. Geologic maps of nearby areas that have bearing on the stratigraphic and tectonic context of the Pajarito Plateau in the greater regional picture have been published by Weir and Purtymun (1963), Baltz *et al.*, (1963), Galusha and Blick (1971), Aubele (1978), Dethier and Manley (1985), Goff *et al.* (1990), and Dethier (in press). Detailed geologic mapping and fracture measurements were completed for an area around TA-55 (Vaniman and Wohletz, 1990). Unpublished mapping was completed for large areas of US Department of Energy land on the plateau by M.A. Rogers. The most recent syntheses of geologic and tectonic studies on the Pajarito Plateau have been published by Dransfield and Gardner (1985) and Gardner and House (1987) as part of the Los Alamos investigation of the seismic hazard of faults within the region. The latter report includes recent detailed mapping along strands of the Pajarito fault zone.

GEOLOGY OF BEDROCK UNITS

Stratigraphic units described within the Tshirege Member of the Bandelier Tuff follow the usage of Vaniman and Wohletz (1990). Estimates of the degree of welding in the Bandelier ignimbrites are based on hand-sample evaluations of pumice compaction. Detailed descriptions of lithologic and mineralogical variations are found in Broxton *et al.* (Sec. IV, this report). No mappable faults or folds cross the TA-21 site, although zones of intense fracturing correspond to the southern projections of mapped faults (Wohletz, Sec. III, this report). Descriptions of post-Bandelier alluvium, colluvium, landslides, terrace gravels, soils, and disturbed fill are given in Reneau (Sec. V, this report).

Because the cliffs along most of the south side of the TA-21 area (north wall, Los Alamos Canyon) are extremely steep, bedrock geology of this zone was mapped on a set of color photographs that will be available through the Environmental Restoration records processing facility. The geologic map (Plate 1 of this report) and cross-sections (Fig. 1) show the distribution of rock units at the site. The geologic map is a compilation of bedrock geology (this report) and post-Bandelier sedimentary deposits (Reneau, Sec. V, this report). The cross-sections use thicknesses obtained from the geologic map and from projected thicknesses from three nearby deep wells (Fig. 2). Representative photographs of rock units are displayed in Figs. 3 through 5.

Otowi Member, Bandelier Tuff

The upper part of the Otowi Member of the Bandelier Tuff (1.50 Ma, Spell *et al.*, 1990; 1.61 Ma, Izett and Obradovich, 1994) is very poorly exposed in Los Alamos Canyon because of extensive cover by talus and colluvium (Plate 1). Better exposures occur in the mouth of DP Canyon. The base of the Otowi is not exposed but is described from cuttings taken in well Otowi-4 at the mouth of DP Canyon (Stoker *et al.*, 1992), in unpublished lithologic descriptions for EGH-LA-1 at Sigma Mesa, and from core recovered at hole SHB-1 at TA-55 (Gardner *et al.*, 1993).

Where exposed, the Otowi Member consists of white, massive, nonwelded, rhyolitic ignimbrite containing about 5% pumice clasts >2 cm in diameter and about 5% clasts of pre-Bandelier lithologies of sand to cobble size

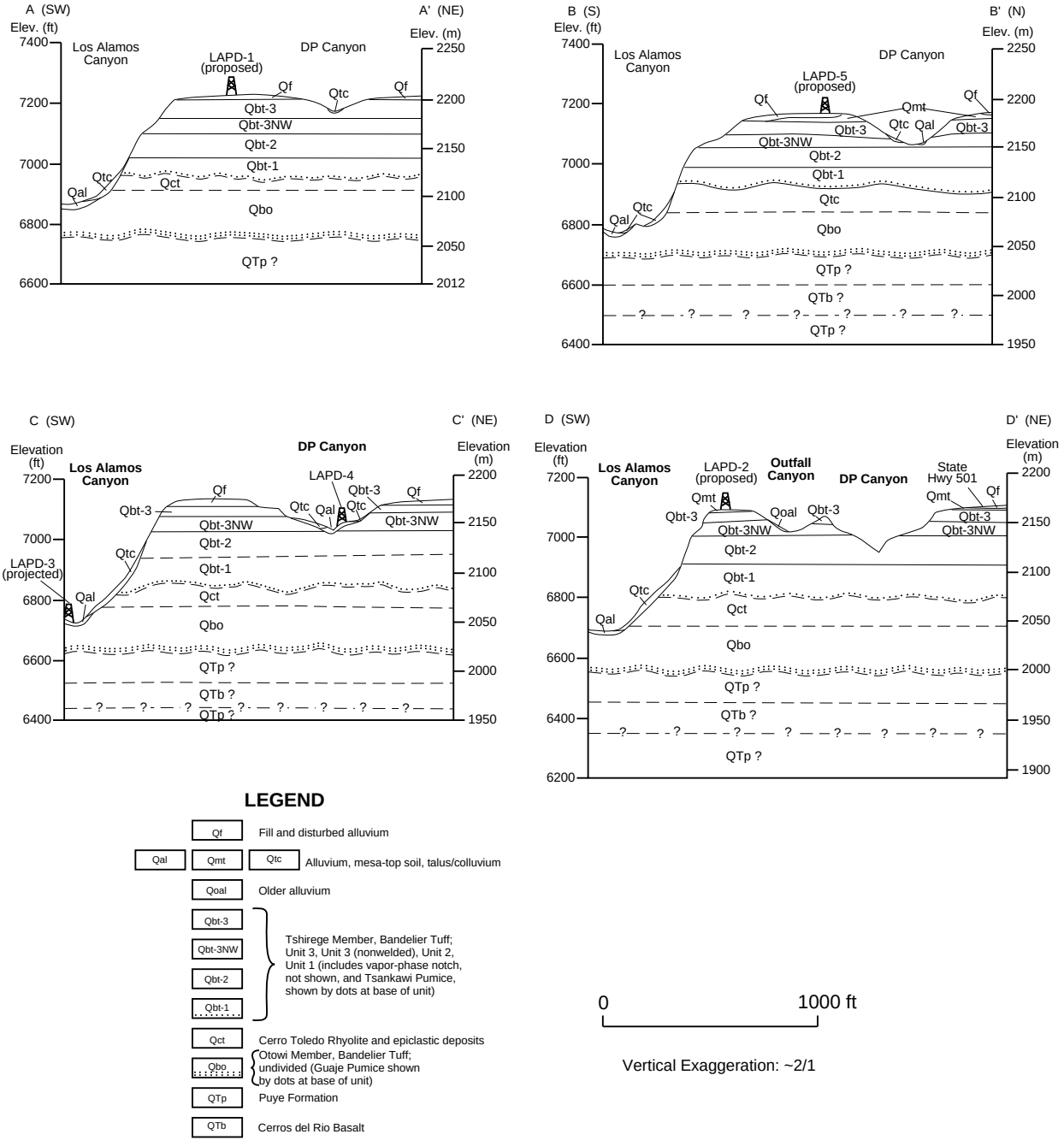

Fig. 1. Cross sections for geologic map of TA-21. Line of cross sections shown on geologic map (Plate 1, pocket inside back cover of this report). These cross sections are vertically exaggerated and reduced. Units Qtp and Qtb are not exposed at the surface in the map area; thus, their depth and thickness are approximate.

(mostly intermediate-composition volcanics). The ignimbrite matrix consists of poorly sorted ash, pumice, crystal, and lithic fragments. Phenocrysts in pumice clasts consist of quartz (~20%) and sanidine (~80%). Tiny black phenocrysts of clinopyroxene are rare and difficult to see in hand specimens. No flow-unit boundaries are observable in the few outcrops of Otowi found within the map area.

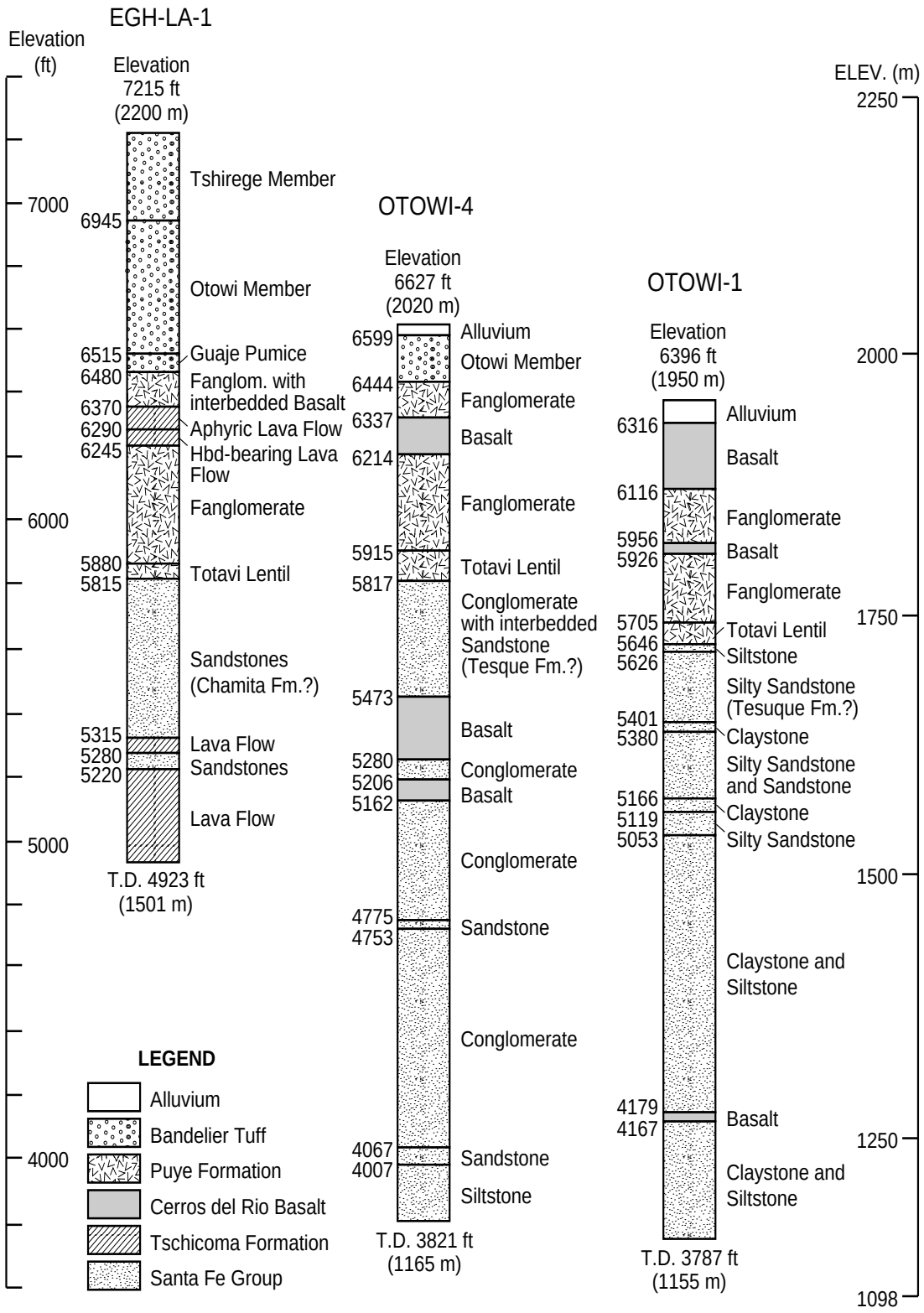

Fig. 2. Lithologic logs of well EGH-LA-1 (Sigma Mesa) and wells Otowi-1 and Otowi-4 (Pajarito and Los Alamos Canyons); lithology from C. Potzick (unpublished data), Stoker* et al. *(1992), and Purtymun* et al. *(1993). Elevations at left of columns are in feet.

The Otowi Member is relatively soft and easily eroded. An exposure in the bottom of Los Alamos Canyon along the dirt road (site C-1, Plate 1) reveals several feet of massive Otowi ignimbrite overlain by a small remnant of older alluvium (Qoal) composed primarily of dacitic rocks from sources upstream. The older alluvium is ≤3 ft thick (too small to show on the map) and is overlain by colluvium of mostly Tshirege Member, Bandelier Tuff.

Near the mouth of DP Canyon (sites C-2 and C-4, Plate 1), the top of the Otowi Member consists of an irregular erosional surface overlain by either bedded tuffs and epiclastic sedimentary rocks of the Cerro Toledo interval or by older alluvium (Qoal, too small to show on map) and recent talus and colluvium (Qtc).

The base of the Otowi Member contains a pyroclastic fall unit named the Guaje Pumice Bed (Griggs, 1964; Bailey *et al.*, 1969), which is not exposed in the map area but is found in nearby wells. It is shown diagramatically on the cross sections of Fig. 1.

Cerro Toledo Interval

Many discontinuous exposures of the Cerro Toledo interval can be observed in the lower slopes and cliffs of Los Alamos Canyon and near the mouth of DP Canyon. Complete sections occur only in DP Canyon (Plate 1). The Cerro Toledo interval in the map area consists of at least five pyroclastic eruption sequences of the Cerro Toledo Rhyolite interbedded with epiclastic deposits of mostly fluvial origin (Fig. 3). Cross-cutting relations, pinch-outs of beds, and the channeling of fluvial and sheet-wash deposits into underlying pyroclastic beds are commonly observed characteristics. Locally, old soils are preserved within the unit. Tuffaceous deposits associated with the Cerro Toledo Rhyolite are described by Griggs (1964), Bailey *et al.* (1969), Heiken *et al.* (1986), Gardner *et al.* (1986), and Stix *et al.* (1988). Heiken *et al.* (1986) and Gardner *et al.* (1993) also describe epiclastic sediments associated with the Cerro Toledo interval.

Pyroclastic sequences consist of 1.7- to 5.0-ft-thick beds of white fine ash, pumice, and pumice lapilli and contain up to 5% lithic clasts of pre-Bandelier volcanic units (Heiken *et al.*, 1986; Stix *et al.*, 1988). Most pyroclastic beds are normally graded. Phenocrysts are rare in pumice clasts of the Cerro Toledo Rhyolite (usually <2%). Most phenocrysts consist of quartz and sanidine but may include trace amounts of pyroxene, biotite, hornblende, and opaque oxides; thus, Cerro Toledo Rhyolite

Fig. 3. Photo of the Cerro Toledo interval, eastern DP Canyon in the general area of site C-4 (Plate 1). The Cerro Toledo interval consists of several layers of pyroclastic falls interbedded with layers and lenses of fluvial sands and gravels. The Cerro Toledo interval overlies the massive ignimbrite of Otowi Member, Bandelier Tuff, and underlies Tsankawi Pumice Bed and unit 1g ignimbrite of Tshirege Member, Bandelier Tuff.

pumice is usually distinct from Bandelier Tuff pumice because the latter has abundant quartz and sanidine and sparse mafic phenocrysts.

Epiclastic deposits display tremendous variations in thickness, cobble size, and sorting. An outcrop in Los Alamos Canyon (site C-8, Plate 1) exposes the upper part of a poorly sorted bed of boulders (diameters ≤ 3 ft) overlain by a series of pyroclastic deposits. In lower DP Canyon, several poorly sorted epiclastic deposits (≤ 10 ft thick) show channeling into relatively soft pyroclastic layers (Fig. 1). Cobble sizes are mostly <1.7 ft in diameter but can be as large as 3 ft in diameter. Epiclastic clasts are dominantly composed of dacitic-to-andesitic rocks from sources to the west, but the finer grained matrix between fragments contains some rhyolitic ash and pumice. These epiclastic beds resemble many of the deposits of the older Puye Formation because the sources of materials (dacitic rocks to the west) and mechanisms of deposition are similar.

The thickness of the Cerro Toledo interval is variable. Although Gardner *et al.* (1993) report about 140 ft at TA-55, the maximum thickness in DP Canyon is about 66 ft, but the thickness decreases to the east to as little as 13 ft. Exposed thickness on the west side of the map area (site C-12, Plate 1) near Omega East is about 50 ft. Some top and bottom contacts of the Cerro Toledo interval are irregular, although most contacts appear planar. The Cerro Toledo interval is overlain by the Tsankawi Pumice Bed of the Tshirege Member. In lower DP Canyon near site C-4 (Plate 1), the Cerro Toledo interval is overlain by ≤3 ft of older alluvium (too small to show on the map) that post-dates the Tshirege Member.

Tshirege Member, Bandelier Tuff

The Tshirege Member of the Bandelier Tuff (1.13 Ma, Spell *et al.*, 1990; 1.22 Ma, Izett and Obradovich, 1994) is well exposed in the map area and forms most of the spectacular cliffs throughout the Pajarito Plateau. Thick sections are observable at several locations along Los Alamos Canyon and near the mouth of DP Canyon. Because of variations in both welding and devitrification textures and in distribution of flow units and cooling units, other workers (Baltz *et al.*, 1963; Weir and Purtymun, 1963; Crowe *et al.*, 1978; Vaniman and Wohletz, 1990, 1991) have subdivided the Tshirege member into mappable units whose continuity across the Pajarito Plateau is not yet demonstrated. The basic unit subdivisions of Vaniman and Wohletz are used for this report and map (Plate 1) because their recent map overlaps with the TA-21 map area and because their subunits are based on the physical property of erodability—a property easy to recognize in the field.

According to Vaniman and Wohletz (1990; 1991), the Tshirege Member on the Pajarito Plateau consists of five units of ignimbrite and a basal pyroclastic fall unit named the Tsankawi Pumice Bed (Bailey *et al.*, 1969). For the purposes of this report, the Tsankawi pumice is described separately but, because it is ≤3 ft thick, the Tsankawi is included at the bottom of the lowermost ignimbrite unit in the map and cross-sections.

Tsankawi Pumice Bed

The Tsankawi Pumice Bed is roughly 1.7 to 3 ft thick in the map area (Fig. 4) and consists of a distinct package of ashfalls composed of bedded ash, crystal-rich ash, pumice and <5% lithic fragments (Bailey *et al.*, 1969). Tsankawi pumice contains "sparse phenocrysts of quartz and sanidine and rare black specks of oxides and ferromagnesian minerals" (Bailey *et al.*, 1969). The Tsankawi Pumice Bed also contains rare (0 to 10%) hornblende dacite pumice that is quite distinctive because of its contrasting grey color and phenocryst assemblage (Bailey *et al.*, 1969). In addition, the Tsankawi Pumice Bed commonly rests on a poorly developed soil in the uppermost pyroclastic fall of the Cerro Toledo interval. This

Fig. 4. Photograph of 3-ft-thick Tsankawi Pumice Bed on nose of DP Mesa (site C-6, Plate 1) . The Tsankawi Pumice Bed overlies soil at top of the Cerro Toledo interval (next to lower half of hammer handle) and underlies unit 1g massive ignimbrite, Tshirege Member, Bandelier Tuff.

soil horizon is often damp or erodes differentially. In spite of these features, there is some argument about assignment of individual beds to the Tsankawi Pumice Bed or the Cerro Toledo Rhyolite based on chemical and petrographic criteria (Self *et al.*, 1986; Heiken *et al.*, 1986; Stix *et al.*, 1988). For the purposes of the maps and cross sections, in this report, the original definition of Bailey *et al.* (1969, p.14) is used.

Tshirege Unit 1 Ignimbrite

Unit 1 Ignimbrite is divided into units 1g (glassy) and 1v (vapor phase) in Fig. 5 and by Vaniman and Wohletz (1990 and 1991), but it is shown only as unit 1 on the geologic map (Plate 1). Units 1g and 1v are separated from each other by a persistent and mappable pink-colored, erosional notch, in which the pumices are extremely "soft" (Vaniman and Wohletz, 1990). Pumice clasts at this horizon fall apart with the touch of a finger, and they have a distinctive greyish-purple color. This notch, also described by Crowe *et al.* (1978), is referred to as the vapor-phase notch (Fig. 5). Vaniman and Wohletz (1991) and Broxton *et al.* (Sec. IV, this report) include the vapor-phase notch as the lowermost part of unit 1v.

Unit 1g rests on the Tsankawi Pumice Bed (Fig. 4) and underlies the vapor-phase notch. It consists of ≤83 ft of white-to-gray nonwelded tuff that weathers to pale orange. Although the ignimbrite is soft, unit 1g generally forms cliffs where it is not covered by talus and colluvium. Unit 1g commonly contains abundant holes ≤ 5 ft in diameter arranged in vertical tiers that give a "swiss-cheese" appearance to the unit (Fig. 5). These holes are caused by preferential erosion of pumice clasts in the ignimbrite.

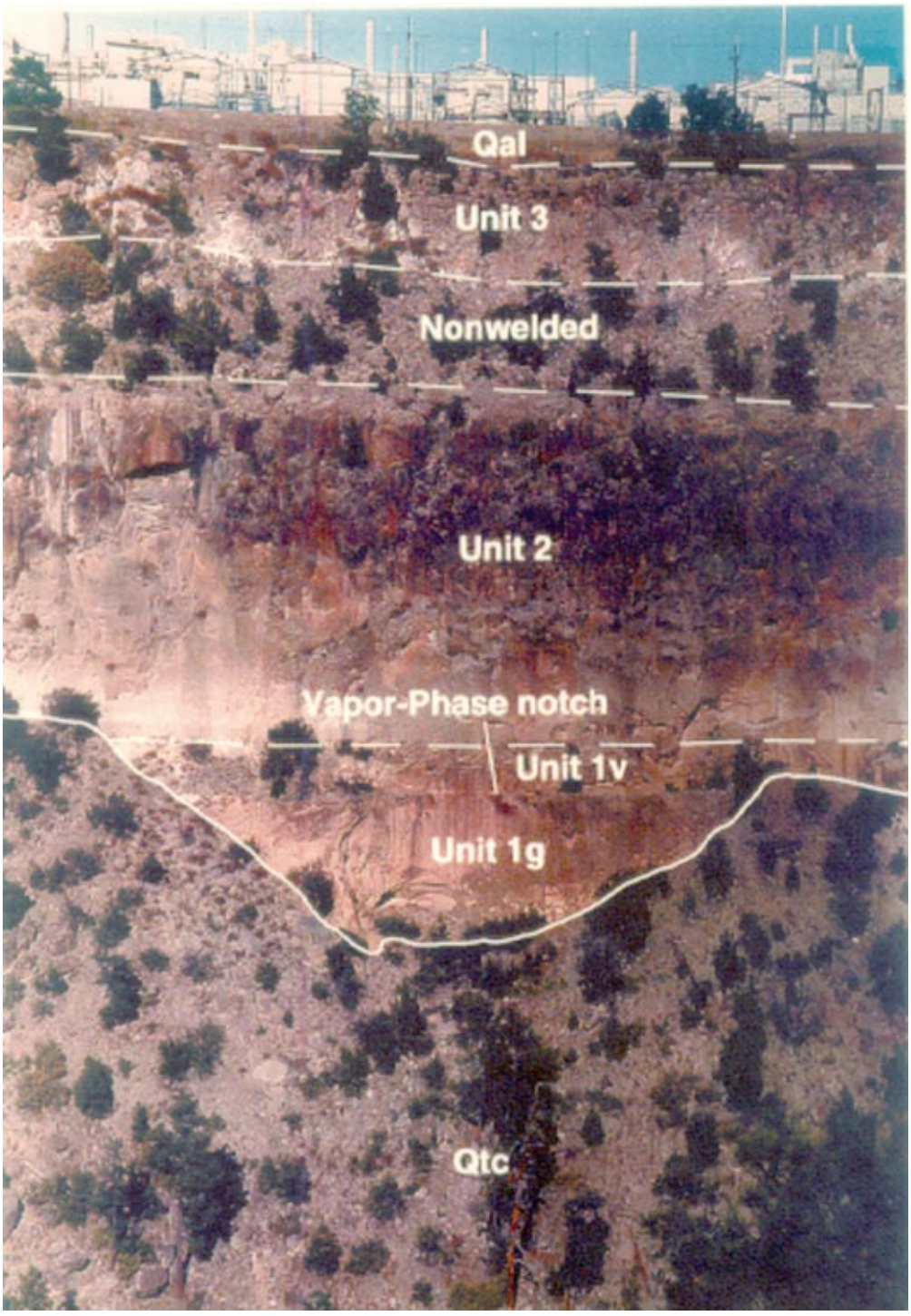

Fig. 5. Representative photograph of the south wall of DP Mesa (north wall of Los Alamos Canyon); locations of photographs are shown on geologic map (Photo 2/5, Plate 1). Symbols: Unit 1g, Unit 1v, Unit 2, Unit 3-Nonwelded, and Unit 3 are various subdivisions of the Tshirege Member, Bandelier Tuff; vpn = vapor-phase notch; Qtc = post-Bandelier talus and colluvium; Qal on photos refers to post-Banderlier mesa top soils, alluvium, and disturbed fill shown as Qmt and Qf on geologic map and cross sections. Buildings of TA-21 are visible at the top of the mesa.

Unit 1v overlies unit 1g. Within the map area, unit 1v is consistently ≤40 ft in thickness. It consists of white-to-pink nonwelded to slightly welded tuff that weathers to pale orange. Vapor-phase alteration of individual pumice fragments is pervasive and distinctive because of the color and textural changes described above. Although the ignimbrite is soft, unit 1v also forms cliffs. The top of unit 1v is often defined by a thin bench, but the actual contact between units 1v and 2 is not sharp. More often than not, the contact is defined by a change in color (orange to white ascending) and erodability.

Tshirege Unit 2 Ignimbrite

Unit 2 ignimbrite, further subdivided into welded and nonwelded units by Vaniman and Wohletz (1991), is described as one unit and shown as one unit on the geologic map in this report. The contact between welded and nonwelded units is gradational in the map area. Unit 2 ignimbrite consists of ≤100 ft of white-to-orange-to-brown nonwelded (bottom) to moderately welded (top) tuff. Both pumice and groundmass of moderately welded tuff are dense and hard. The nonwelded base weathers white-to-pale-pink and generally forms a steep slope, whereas the moderately welded top weathers dark-brown-to-orange and forms broadly jointed cliffs. The bottom contact of unit 2 ignimbrite often forms a thin erosional bench with unit 1v. The top of unit 2 forms a wide bench below the mesa top, extending along the entire length of the north wall of Los Alamos Canyon within the map area (Fig. 5).

Tshirege Unit 3 Ignimbrite

Unit 3 ignimbrite is divided into welded and nonwelded units by Vaniman and Wohletz (1991). These units are shown separately on the west and central parts of the geologic map (Plate 1) but are undivided on the eastern part of the map because the units thin and become indistinguishable eastward.

The nonwelded unit is ≤50 ft thick where subdivided on the map and consists of white-to-gray pumice-rich ignimbrite that weathers to pale pink. The nonwelded unit forms broad slopes that are generally covered with talus, brush, and scattered trees.

Unit 3 ignimbrite is nonwelded to partially welded tuff that is ~50 ft thick on the east side of the map area but as thin as 26 ft in the central map area. Differences in relative thickness were noted in north-south directions, as shown in the cross sections. Where partially welded, the ignimbrite consists of gray tuff that weathers to a pale orange and forms broadly jointed, low cliffs that can be climbed at numerous locations. The upper surface of unit 3 ignimbrite is covered with mesa top soil and alluvium or with disturbed alluvium from construction of roads and buildings (Reneau, Sec. V, this report).

CONCLUSIONS

Bedrock geology of TA-21 consists primarily of Otowi and Tshirege Members of the Bandelier Tuff. The thickness of the Tshirege Member is rather constant over the map area, but thickness of the Otowi Member is only known approximately. In contrast, the Cerro Toledo interval, which lies between the two members of the Bandelier Tuff, varies from 13 to 66 ft in thickness. The Cerro Toledo interval deposits display large-scale variations in lithologic properties both vertically and laterally. No obvious surface expression of faults was found in the map area. One cold spring (DP Spring), found in eastern DP Canyon, issues from a contact between colluvial and valley-fill deposits and Tshirege unit 1g.

The geologic map presented in this report and the detailed stratigraphic and lithologic descriptions (Broxton *et al.*, Sec. IV, this report) complete the geologic characterization of bedrock geologic units in the upper vadose zone for the TA-21 RFI work plan. Additional work is under way to characterize the fracture mineralogy of these bedrock units; results of

these studies will be reported at a later date. The data in this report provide a geologic framework for evaluating potential subsurface transport pathways and will be particularly useful for understanding the distribution of contaminants when characterization boreholes for the MDAs are completed. The map accompanying this report shows the thickness and distribution of geologic units in the upper part of the vadose zone and will support the interpretation of subsurface geologic units penetrated by planned boreholes at TA-21.

ACKNOWLEDGEMENTS

J. Gardner, D. Broxton, G. Eller, L. Maassen, J. Nyhan, and S. Reneau provided critical reviews of this paper.

REFERENCES

Aubele, J.C., 1978, Geology of the Cerros del Rio volcanic field, New Mexico, M.S. Thesis, University of New Mexico, Albuquerque, 136 pp. (with geologic map, 1:24,000 scale).

Bailey, R.A., Smith, R.L., and Ross, C.S., 1969, Stratigraphic nomenclature of volcanic rocks in the Jemez Mountains, New Mexico, US Geological Survey Bulletin 1274-P, 19 pp.

Baltz, E.H., Abrahams, J.H., Jr., and Purtymun, W.D., 1963, Preliminary report on the geology and hydrology of Mortandad Canyon near Los Alamos, with reference to disposal of liquid, low-level radioactive waste, US Geological Survey Open-File Report 63-6, 105 pp.

Broxton, D.E., Heiken, G., Chipera, S.J., and Byers, F.M., 1995, Stratigraphy, petrography, and mineralogy of Bandelier Tuff and Cerro Toledo deposits, Los Alamos National Laboratory, New Mexico, this report.

Crowe, B.M., Linn, G.W., Heiken, G., and Bevier, M.L., 1978, Stratigraphy of the Bandelier Tuff in the Pajarito Plateau, Los Alamos National Laboratory report LA-7225-MS, 57 pp.

Dethier, D.P. and Manley, K., 1985, Geologic map of the Chili Quadrangle, Rio Arriba County, New Mexico, US Geological Survey Miscellaneous Field Studies Map MF-1814 (1 sheet, 1:24,000 scale).

Dethier, D.P., in press, Geology of the White Rock Quadrangle, Santa Fe and Los Alamos Counties, New Mexico Counties, New Mexico, New Mexico Bureau of Mines and Mineral Resources Map (1 sheet, color, 1:24,000 scale).

Dransfield, B.J. and Gardner, J.N., 1985, Subsurface geology of the Pajarito Plateau, Española Basin, New Mexico, Los Alamos National Laboratory report LA-10455-MS, 15 pp. (with maps, 1:62500 scale).

Galusha, T. and Blick, J.C., 1971, Stratigraphy of the Santa Fe Group, New Mexico, American Museum of Natural History Bulletin 144, 127 pp. (with geologic map, 1:100,000 scale).

Gardner, J.N. and House, L., 1987, Seismic hazards investigations at Los Alamos National Laboratory, 1984-1985, Los Alamos National Laboratory report LA-11072-MS, 76 pp. (with maps).

Gardner, J.N., Goff, F., Garcia, S., and Hagan, R.C., 1986, Stratigraphic relations and lithologic variations in the Jemez volcanic field, New Mexico, *J. Geophys. Res. 91*, 1763-1778.

Gardner, J.N., Kolbe, T., and Chang, S., 1993, Geology, drilling, and some hydrologic aspects of seismic hazards program core holes, Los Alamos National Laboratory, New Mexico, Los Alamos National Laboratory report LA-12460-MS, 19 pp.

Gerety, M., Nyhan, J., and Oliver, R., 1989, History and geophysical description of hazardous waste disposal area A, Technical Area 21, Los Alamos National Laboratory report LA-11591-MS, 90 pp.

Goff, F., Gardner, J.N., and Valentine, G., 1990, Geologic map of the St. Peter's Dome area, Jemez Mountains, New Mexico, New Mexico Bureau of Mines and Mineral Resources Map 69 (2 sheets, color, 1:24,000 scale).

Griggs, R.L., 1964, Geology and groundwater resources of the Los Alamos area, New Mexico, US Geological Survey Water Supply Paper 1753, 107 pp. (with map, color, 1:62,500 scale).

Heiken, G., Goff, F., Stix, J., Tamanyu, S., Shafiqullah, M., Garcia, S., and Hagan, R., 1986, Intracaldera volcanic activity, Toledo caldera and embayment, Jemez Mountains, New Mexico, *J. Geophys. Res. 91*, 1799-1815.

Izett, G.A. and Obradovich, J.D., 1994, $^{39}Ar/^{40}Ar$ age constraints for the Jaramillo Normal Subchron and the Matuyama-Brunhes geomagnetic boundary, *J. Geophys. Res. 99*, 2925-2934.

Kelley, V.C., 1978, Geology of the Española Basin, New Mexico, New Mexico Bureau of Mines and Mineral Resources Map 48 (1 sheet, color, 1:125,000 scale).

LANL, 1991. TA-21 Operable Unit RFI Work Plan for Environmental Restoration, Los Alamos National Laboratory document LAUR-91-962, Los Alamos, New Mexico 87545.

Merrill, E.S., 1990, A history of waste disposal at Technical Area 21, 1943-1978, unpublished report from Earth and Environmental Science Group 15, Los Alamos National Laboratory report, 19 pp.

Nyhan, J.W., Drennon, B.J., Abeele, W.V., Trujillo, G., Herrera, W.J., Wheeler, M.L., Booth, J.W., and Purtymun, W.D., 1984, Distribution of radionuclides and water in Bandelier Tuff beneath a former Los Alamos liquid waste disposal site after 33 years, Los Alamos National Laboratory report LA-10159-LLWM, 51 pp.

Purtymun, W.D., McLin, S.G., Stoker, A.K., Maes, M.N., and Hammock, B.G., 1993, Water supply at Los Alamos during 1990, Los Alamos National Laboratory report LA-12471-PR, 50 pp.

Reneau, S., 1995, Geomorphic studies at DP Mesa and vicinity, Los Alamos National Laboratory, New Mexico, this report.

Rogers, M.A., 1977, History and environmental setting of LASL near-surface land disposal facilities for radioactive wastes (Areas A, B, C, D, E, F, G, and T), Los Alamos Scientific Laboratory report LA-6848-MS, Vol.1, 55 pp.

Self, S., Goff, F., Gardner, J.N., Wright, J.V., and Kite, W.M., 1986, Explosive rhyolitic volcanism in the Jemez Mountains, vent locations, caldera development, and relation to regional structure, *J. Geophys. Res. 91*, 1779-1798.

Smith, R.L. and Bailey, R.A., 1966, The Bandelier Tuff, A study of ash-flow eruption cycles from zoned magma chambers, *Bull. Volcanol. 29*, 83-104.

Smith, R.L.,Bailey, R.A., and Ross, C.S., 1970, Geologic map of the Jemez Mountains, New Mexico, US Geological Survey Miscellaneous Geological Investigations Map I-571 (1 sheet, color, 1:125,000 scale).

Spell, T., Harrison, M.T., and Wolff, J.A., 1990, $^{40}Ar/^{39}$ Ar dating of the Bandelier Tuff and San Diego Canyon ignimbrites, Jemez Mountains, New Mexico: Temporal constraints on magmatic evolution, *J. Volcanol. Geotherm. Res., 43*, 175-193.

Stix, J., Goff, F., Gorton, M.P., Heiken, G., and Garcia, S., 1988, Restoration of compositional zonation in the Bandelier silicic magma chamber between two caldera-forming eruptions, geochemistry and origin of the Cerro Toledo Rhyolite, Jemez Mountains, New Mexico, *J. Geophys. Res. 93*, 6129-6147.

Stoker, A.K., McLin, S.G., Purtymun, W.D., Maes, M.N., and Hammock, B.G., 1992, Water Supply at Los Alamos during 1989, Los Alamos National Laboratory report LA-12276-PR, 51 pp.

Vaniman, D. and Wohletz, K., 1990, Results of geological mapping/fracture studies, TA-55 area, Los Alamos National Laboratory Seismic Hazards Memo EES1-SH90-17, 25 pp. (with map, color, 1:7800 scale).

Vaniman, D. and Wohletz, K., 1991, Revisions to report EES1-SH90-17, Los Alamos National Laboratory Seismic Hazards Memo EES1-SH91-12, 2 pp.

Weir, J.E. and Purtymun, W.D., 1963, Geology and hydrology of Technical Area 49, Frijoles Mesa, Los Alamos County, New Mexico, US Geological Survey (Albuquerque, New Mexico) Administrative Release Report, 225 pp.

Wohletz, K., 1995, Measurement and analysis of rock fractures in the Tshirege Member of the Bandelier Tuff along Los Alamos Canyon adjacent to TA-21, Los Alamos National Labor-atory, this report.

MEASUREMENT AND ANALYSIS OF ROCK FRACTURES IN THE TSHIREGE MEMBER OF THE BANDELIER TUFF ALONG LOS ALAMOS CANYON ADJACENT TO TECHNICAL AREA-21

by

K. H. Wohletz

A total of 1662 fractures was measured in unit 2 of the Tshirege Member of the Bandelier Tuff along a section of Los Alamos Canyon adjacent to TA-21. Beginning 1200 ft east of Omega Site (TA-2), the section extends eastward 7312 ft to near the end of DP mesa. Photomosaic maps were constructed to document each fracture, and measurements were entered into an RS/1 database for analysis. Background linear fracture density averages around 20 fractures/ 100-ft interval with a notable increase to about 70 fractures/100 ft over a zone that extends ~1500 ft east-west and is centered directly south of MDA V. Within this same zone, mean fracture apertures increase from background values of ~0.8 to ~1.25 cm. Fractures make up a conjugate set of NW and NE strikes. Overall, the average strike is about N12E, but the 988 NE-trending fractures show a mean strike of N43E, and the 674 NW-trending fractures have a mean strike of N33W. Fracture dips are generally steep, averaging between 73°N and 70°S. Both fracture mean strikes and dips show rotations of several degrees in the most highly fractured zone.

INTRODUCTION

Abundant rock fractures extend throughout the Tshirege Member of the Bandelier Tuff underlying DP Mesa (Fig. 1) at TA-21. These fractures are important geological features because they constitute potential pathways for contaminant infiltration from MDAs on the mesa; they also affect slope stability along the canyon margins. This report documents an extensive field survey of exposed fractures carried out at TA-21 in 1992. It builds upon previous fracture studies conducted by Vaniman and Wohletz (1990) and employs the detailed procedure developed in that study.

The origin of the fractures in the Bandelier Tuff has never been described fully. Work by Vaniman and Wohletz (1990) suggests, by analogy to numerous other studies of welded tuffs and by consideration of tectonics of the Pajarito Plateau (Gardner and House, 1987), that most of the fractures can be explained by brittle failure of the tuff during cooling contraction. Tectonic movement over the last million years along the Pajarito fault system caused subsequent fracture extension and development in the tuff. Because the exact origin of the fractures is still in question, this study does not attempt to classify fractures according to their geological origins.

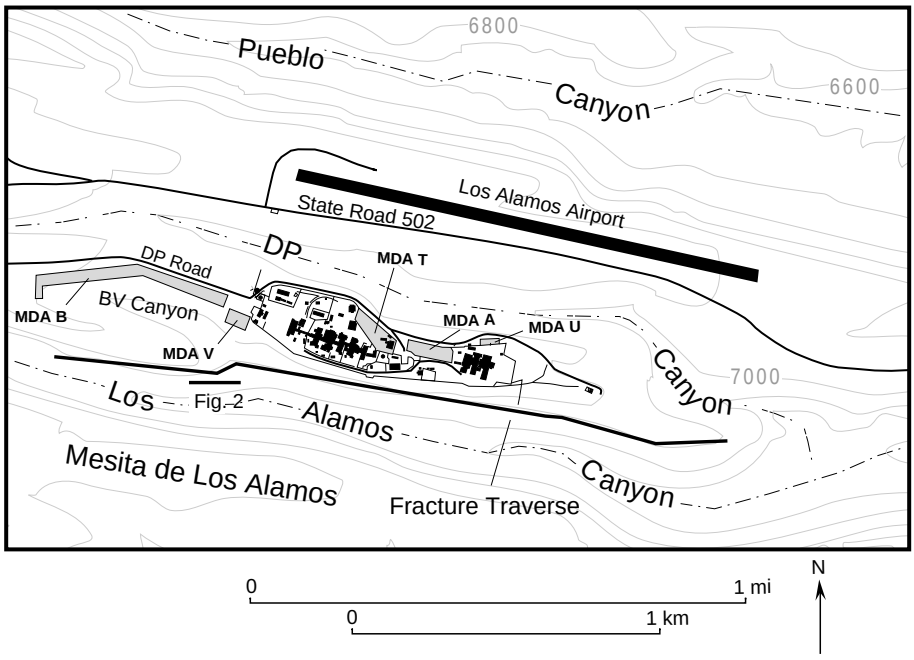

Fig. 1. Topographic map of TA-21. The fracture traverse extends along the north wall of Los Alamos Canyon from 1200 ft east of Omega Site (not shown) to 8512 ft east of Omega Site. Fourteen photomosaic fracture maps cover this traverse. Figure 2 shows an example of the photomosaic maps for the area adjacent to MDA V.

METHODS

The methodology consists of three phases, as outlined by the *SOP for Fracture Characterization* (LANL-ER-SOP-03.06): (1) photographic documentation of area or traverse along which fractures will be characterized and construction of a photomosaic map base, (2) measurement and plotting of fracture dimensions on the photomosaic map, and (3) statistical analysis of fracture data by the procedures described below.

The south-facing cliff exposures along Los Alamos Canyon were chosen for this study because they provide the only continuous vertical exposure of the Tshirege Member of the Bandelier Tuff beneath TA-21 (Fig. 2). Unit 2 of Vaniman and Wohletz (1990) is partly welded along this traverse and shows the best exposure of fracture surfaces; consequently, the results of this study are from unit 2. The documented section begins 1200 ft east of the Omega Site (TA-2) access gate to the canyon and continues 7312 ft to the east.

Photo Documentation

When unit 2 of the Tshirege Member was photographed, successive stations at the base of the unit (where slopes are accessible) were set up so that focal distances of 40 to 60 ft were maintained and photographs had ~ 20% overlap. Because of the curvature of the cliff face and its irregular vertical extent, each photograph covered between 30 to 50 ft of lateral exposure; scales added to the photomosaics reflect this variable lateral scale. After construction of the photomosaic, tracing paper was overlaid to make a map of outcrop features, including key topographic points such as cliff tops and bottoms, prominent fractures, and geographic objects such as buildings, trees, and large signposts. This map was attached to the base of the photomosaic so that there is a 1:1 correspondence between mapped and photographed features. The 7312-ft traverse required 14 individual photomosaic maps, each covering ~500 ft of lateral exposure.

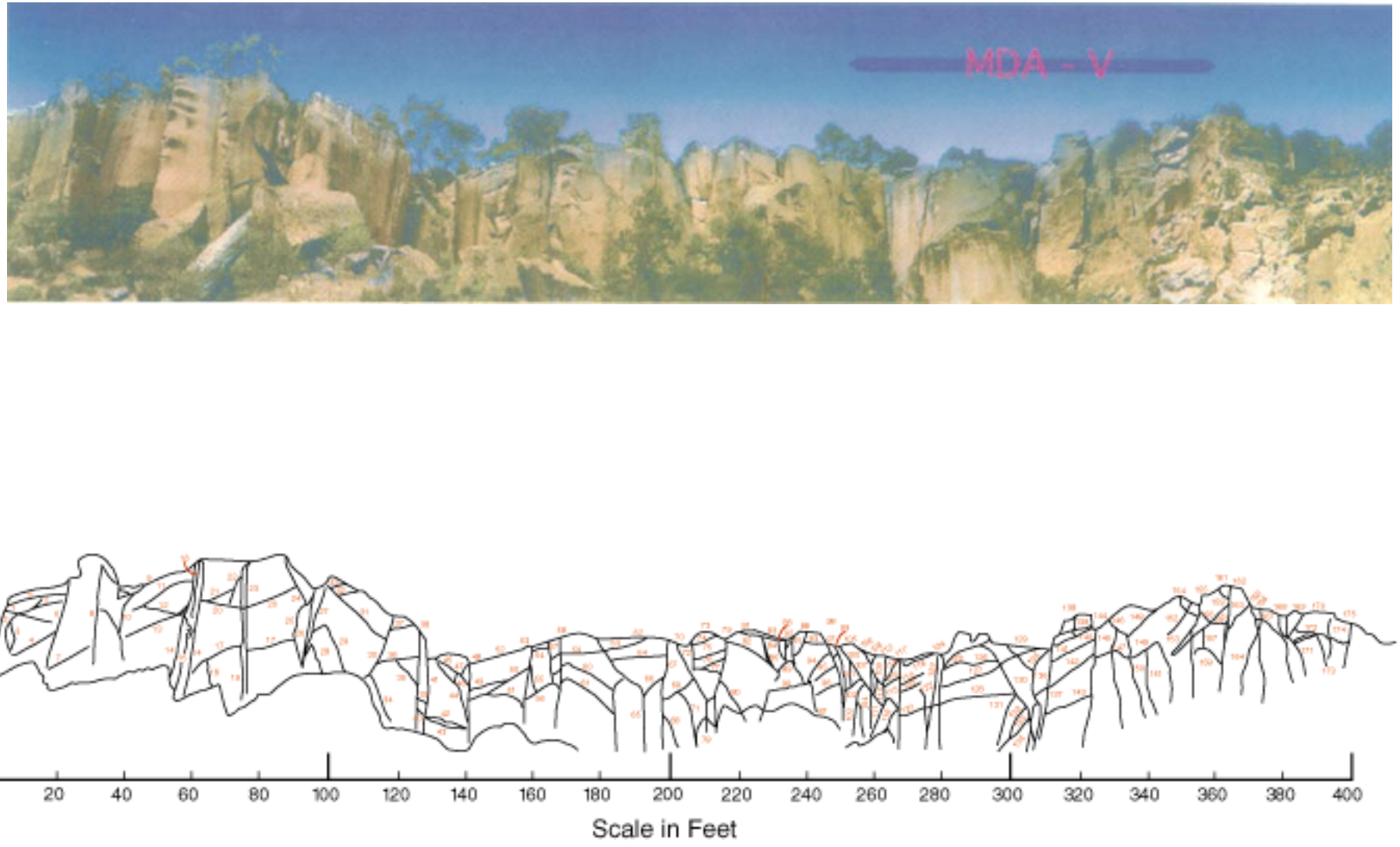

Fig. 2. Photomosaic and fracture map of the north wall of Los Alamos Canyon in the vicinity of MDA V. (See Fig. 1 for location of photograph.)

Fracture Measurement

The horizontal scale for the fracture maps was determined by measuring distance on the topographic map between topographic points identified on the photomosaics. This scale was then placed on each map to show the distance between mapped features. Because of the exposure irregularities in cliff face described above, this scale will have an error of ±10% of each map's total width.

Starting from one end of the fracture traverse, each fracture was sketched on the map and designated by a number. These numbers increase from west to east and are pertinent only to the photomosaic map on which they are shown (for example, fracture numbers 1 though 80 of photomosaic map 1, fracture numbers 1 through 66 of photomosaic map 2, etc.). The location of each fracture is its average point of intersection on the map. All observed fractures have been recorded with some parallel sets too closely spaced to be given individual numbers on the map, but nonetheless they are recorded in the database. Fracture strike and dip were measured to an accuracy of ±2° with the Brunton compass, and fracture opening width was measured perpendicular to fracture surfaces. In cases where fractures could not be safely accessed, standard application of Brunton compass techniques were applied; these require measurements using the compass alignment sights with cautious observation of the relationship between true and apparent orientations.

Fracture Data Base and Analysis

The fracture data recorded in the field notebook were entered into a database, which allowed application of several statistical procedures. The database consists of a table with a column for each fracture, listing the fracture's number designation, horizontal location on the fracture map, dip and strike, and aperture. From these data, several other columns are statistically calculated: (1) a linear fracture density calculated as a moving average by counting the number of fractures contained in a given distance interval (10 and 100 ft) that is centered on each fracture, (2) a cumulative fracture width over a specified interval (10 and 100 ft) that is centered on each fracture, and (3) the relative dip of fracture from vertical, (negative values indicate southerly inclinations). Because fractures in the Bandelier Tuff show apparent NW- and NE-strike groupings and cross-cutting relationships suggest that these two groups are coeval, I have considered fractures to represent a conjugate set. Accordingly, additional columns for the table are separately calculated for each of the three above columns for each conjugate set. This conjugate relationship is an hypothesis I attempt to support in later data analysis. Numerical procedures for the above include: (1) calculation of linear fracture densities for several different distance intervals, taking into account section end effects by extrapolating the gradient of density with distance, (2) transformation of dip measurements to degrees from vertical, and (3) computation of cumulative fracture widths for 10- and 100-ft distance intervals. Although more sophisticated statistical analyses can be applied to these data, those used are sufficient to characterize the fractures.

Fracture data were then displayed on several different plots:

(1) fracture density (10- and 100-ft intervals) *vs* horizontal distance along the traverse;
(2) histograms of fracture strike;
(3) fracture strike *vs* horizontal distance, where positive strikes represent strike in degrees east of north and negative strikes are west of north (these data are smoothed using the RS/1 data-smoothing option to show the trend of northeast and northwest fracture sets as well as the overall trend of all fracture strikes);

(4) fracture dips *vs* horizontal distance, where vertical plots at zero, dips toward the northeast or northwest are positive inflections from vertical, and southerly dips are negative inflections from vertical (again, smoothing of data shows average trends for fracture sets);
(5) fracture widths *vs* horizontal distance with smoothed trends for fracture sets;
(6) cumulative fracture widths (per 10-ft intervals *vs* horizontal distance with smoothed trends for fracture sets; and
(7) fracture widths >10 cm *vs* horizontal distance.

RESULTS AND ANALYSIS

A total of 1662 fractures was documented and measured along the 7312-ft section located along Los Alamos Canyon, as is shown in Fig. 1. An example photomosaic and fracture map documenting part of this section is shown in Fig. 2. The measurements for each of the numbered fractures on this map are archived in a computer database, as described above. The tabulated data for fracture strike, dip, and aperture are shown statistically in Tables 1, 2, and 3.

Fracture Density

In general, the background spacing of fractures is ~5 ft, which is similar to a value found for nearby areas in the Bandelier Tuff, by Vaniman and Wohletz (1990). However, over the zone from 2500 to 4000 ft east of Omega Site, the fracture spacing is much closer (1 to 2 ft). Figure 3 is a plot of linear fracture density for 10- and 100-ft intervals centered around each fracture. Note that very little lateral variation in fracture density is immediately apparent for the data plotted for 10-ft intervals; this represents the density generally apparent to an individual viewing the section while in the field. The 100-ft interval is arbitrarily chosen

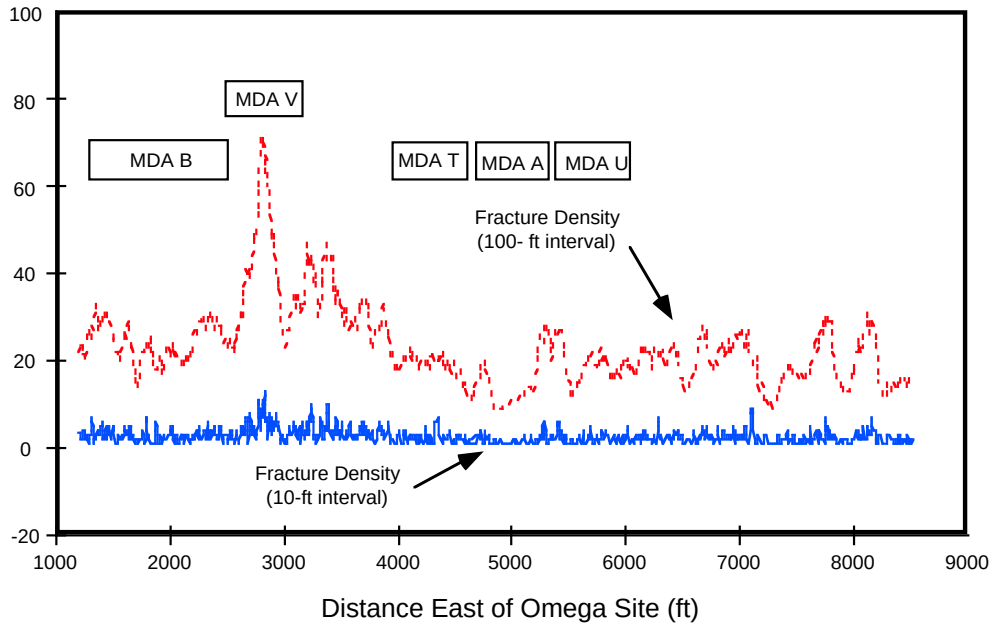

Fig. 3. Plot of linear fracture density vs distance east of Omega Site. The curves show fracture density over 100- and 10-ft intervals.

to represent the width of potential tectonic features. Data plotted for 100-ft intervals shows a background density of ~20 fractures per 100 ft; a notable increase at horizontal locations between 2500 and 4000 ft that reaches a high of about 75 fractures/100-ft interval.

The notable rise in fracture density occurs abruptly 2500 ft east of Omega site and then falls off more gradually to the east, reaching background values at ~4000 ft. This zone corresponds to a fracture zone running N-S that Vaniman and Wohletz (1990) mapped but did not document by fracture studies. It likely represents a fabric of the Pajarito fault system. The zone's northerly projection runs directly through MDA V at TA-21. In all, 554 fractures were documented in this 1500-ft-wide fracture zone, whereas 310 fractures were found over a distance of 1300 ft to the west, and 828 fractures were found over a distance of 4512 ft east of the zone.

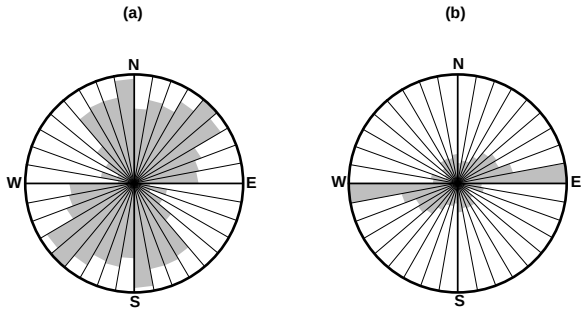

Fig. 4. Rose diagrams of fracture strikes measured in Los Alamos Canyon plotted in 10° classes. (a) Observed distribution of the 1662 fractures measured for which maximum petal magnitude is 140 occurrences. (b) Calculated distribution corrected for angle between fracture strike and the E-W line of Los Alamos Canyon exposures (maximum petal magnitude is 495 occurrences). Here, an additional 1109 fractures were inferred by the relationship of n = n/sin α, where n is the number observed for each class and α is the angle between each class's strike and E-W.

Fracture Strikes

Because observed fractures are likely to have been formed during the cooling contraction of the Bandelier Tuff, a conjugate system with 60° fracture intersections should be expected. This simple hypothesis is complicated by the fact that the tuff compacted over a preexisting topography with a strong E-W fabric, which would cause a dominant N-S strain component to be accommodated by the fractures. Figure 4a is a rose diagram of fracture strike frequency measured along the approximately E-W trend of Los Alamos Canyon. Because of its orientation, this canyon exposes fractures as a sine function of the angle between the fracture strike and the canyon wall; hence, the abundance of E-W trending fractures is greatly reduced. This figure portrays a weak bimodality of fracture strikes with modes in the NW and NE quadrants. The distribution of strikes is generally symmetric around the N-S axis and, because of their mutually cross-cutting relationships, these two modes define a conjugate fracture set. By applying a trigonometric correction for the exposure bias, Fig. 4b shows that there is likely a dominant E-W trend in fracture strikes and that the NW and NE modes are subordinate. If one assumes the dominant E-W fractures shown in Fig. 4b are real, then dominant fracture intersections reproduce 60° angles (~N30W, ~N30E, ~E-W), as expected for a cooling contraction origin.

Because the E-W component is inferred, fracture data are further represented with respect to only the NW and NE strike modes. Table 1 lists fracture strike data for the section, showing that of the 1662 fractures measured, 988 trend NE and 674 trend NW. In Table 1, fractures are differentiated into three zones: those occurring west of 2500 ft (western background), those between 2500 and 4000 ft (fracture zone), and those east of 4000 ft (eastern background). Whereas the NW set shows a mean strike of N33W, the NW set shows a mean of N43E—indicating an average intersection angle with the NE set ~15° greater than the expected angle of 60°. This result is likely a reflection of the dominating influence of E-W

TABLE 1.
FRACTURE STRIKE DATA FOR TA-21[a]

Fracture Set	Number	Mean Strike	Standard Deviation
All Fractures			
NE	988	42.7	±24.5
NW	674	-32.8	±23.1
Background (West)			
NE	182	44.3	±26.8
NW	128	-33.8	±22.0
Fracture Zone			
NE	312	45.0	±24.5
NW	212	-40.6	±25.5
Background (East)			
NE	494	40.7	±23.5
NW	334	-27.4	±20.3

[a] Strikes shown in degrees from due north, NW strikes designated by negative values. Fracture zone corresponds to horizontal distances from 2500 to 4000 ft east of Omega Site.

fractures in calculation of the NE set mean strike. Note the slight rotation of mean strikes west to east over the fracture zone from N44E and N34W to N41E and N27W, respectively. This rotation may represent the influence of tectonic movement on fracture orientations in the fracture zone.

Fig. 5 shows a plot of fracture strikes as a function of horizontal location. In this plot, smoothed curves for the data show average orientations of all fractures, only NE-trending fractures, and only NW-trending fractures. Note in Fig. 5 that azimuths west of due north plot as negative values in degrees. A composite average of all fractures varies between due north and N20E, with the NE set averaging around N40E and the NW set averaging around N30W. There is notable fluctuation of these curves over a zone extending from 2500 to 4000 ft west of Omega Site, which corresponds to the fracture zone with increased fracture density. Over the fracture zone, strikes are divergent (spreading apart), but to the east of this zone, the angle between them stays fairly constant (sympathetic).

Fracture Dips

Fracture dips range from nearly horizontal to vertical; northerly dipping fractures show a mean dip from horizontal of about 74 ± 22° and southerly dipping ones have a mean at about 68 ± 20°. Table 2 lists results of fracture dip data, showing statistics for all fractures both those in the fracture zone (2500 to 4000 ft) and those on either side of the fracture zone (considered background values). Note that dips are shown in degrees from vertical (Table 2, Figs. 6 and 7) so that northerly dips could be averaged with southerly dips (noted as negative values). As with strikes, a NE- and a NW-trending set are designated. Where northerly and southerly dips are not discriminated in Table 2, the greater abundance of northerly dipping fractures gives mean values of 8.5° (N) for both the NE and NW sets. In Fig. 6, fracture dips are plotted against horizontal location. Curves for all fractures, the NE set alone, and the NW set alone are shown with dips indicated as degrees from vertical such that southerly dips plot below 0° (vertical). For most of the section, the NE and NW sets show sympathetic

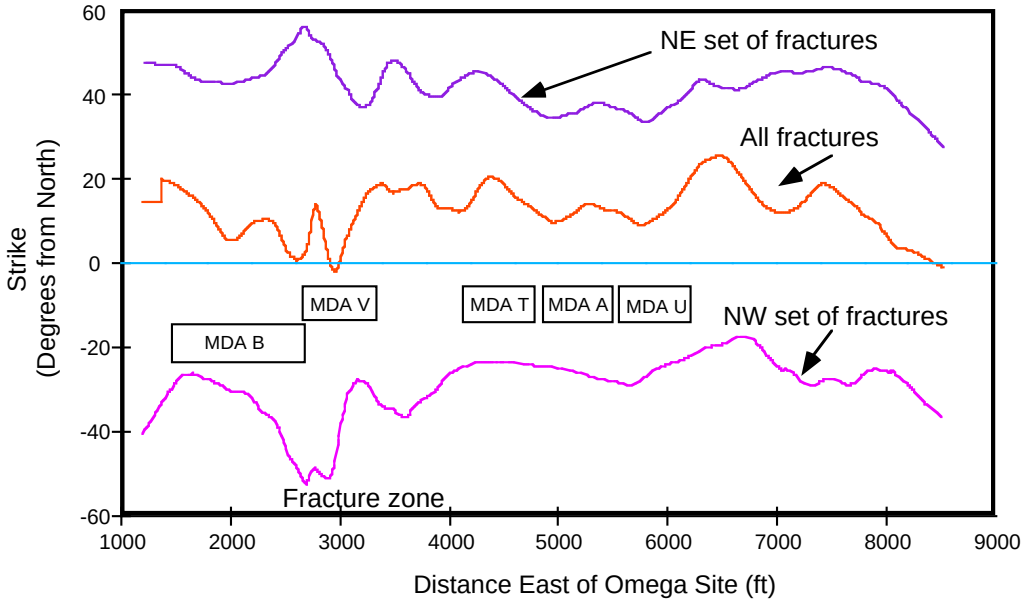

Fig. 5. Plot of linear fracture strikes vs distance east of Omega Site. Curves show smoothed running averages (0.1 smoothed = 162 fractures averaged about each fracture) for all fractures, for those of the NE set alone, and for those of the NW set alone.

TABLE 2.
FRACTURE DIP DATA FOR TA-21 [a]

Fracture Set	*Number*	*Mean Dip from Vertical (°)*	*Standard Deviation*
All Fractures			
NE	988	9	±27
N	768	17	±24
S	220	-20	±19
NW	674	9	±26
N	559	16	±21
S	115	-25	±21
Background (West)			
NE	182	4	±25
NW	128	6	±21
Fracture Zone			
NE	312	10	±31
NW	212	11	±33
Background			
NE	494	9	±25
NW	334	8	±23

[a] Dips shown in degrees from vertical, southerly dips designated by negative values. Fracture zone corresponds to horizontal distances from 2500 to 4000 ft east of Omega Site.

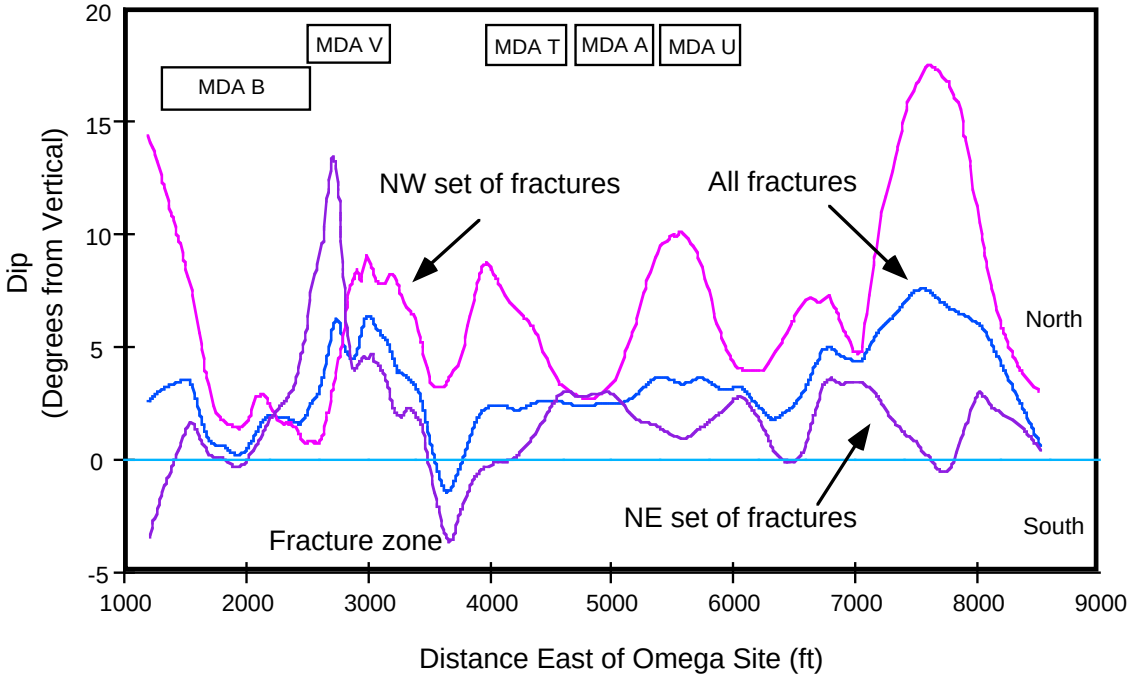

Fig. 6. Plot of fracture dips (relative to vertical at 0°) vs distance east of Omega Site, comparing all fractures to those NW and NE ones. As in Fig. 5, 0.1 smoothed data curves are shown for all fractures, for those of the NE set, and for those of the NW set.

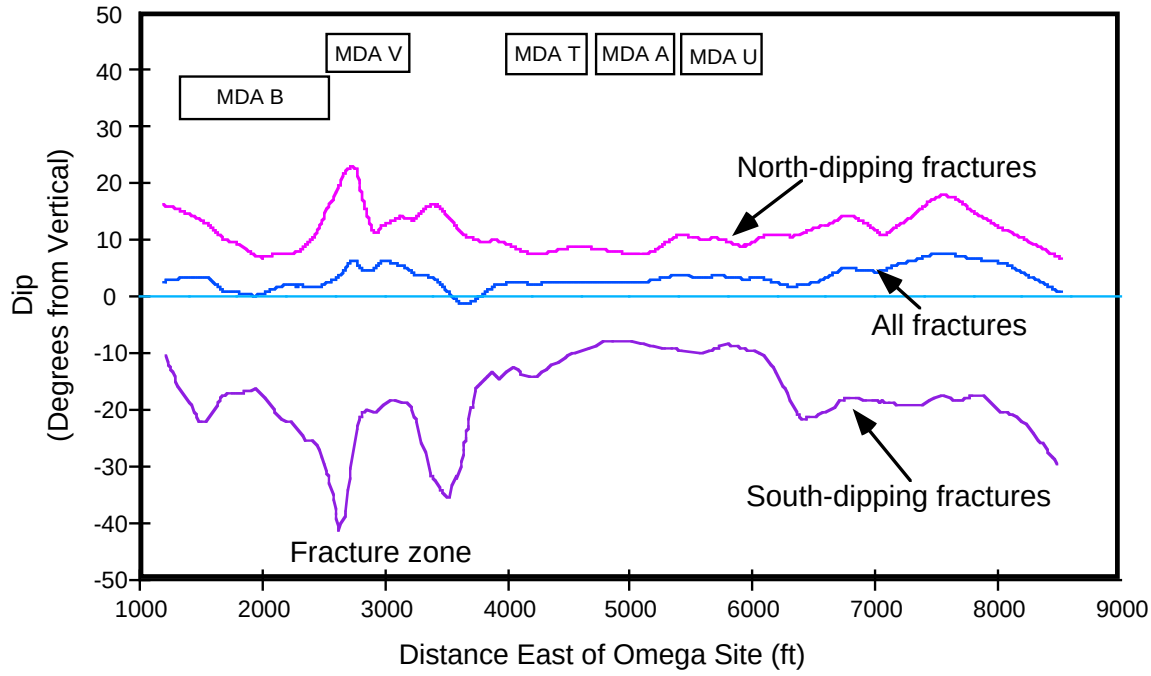

Fig. 7. Plot of fracture dips (relative to vertical at 0°) vs distance east of Omega Site, comparing all fractures to those north- and south-dipping fractures. As in Fig. 5, the 0.1 smoothed data curves are shown for all fractures, for the north-dipping set alone, and for the south-dipping set alone.

dips going east into the fracture zone; east of the fracture zone, they become antithetical and show opposite trends. Figure 7 shows a plot of dips for all fractures, northerly dipping fractures only, and southerly dipping fractures only as a function of horizontal location. For most of the section, as northerly dips become less vertical with distance, so do southerly ones. An increased fluctuation in dip is noted over the fracture zone—again, a possible effect of tectonic movement.

Fracture Apertures

Fracture apertures ranged from 0 cm (closed) to 15 cm (open). Aperture statistics (Table 3) show mean openings of 0.82 and 0.93 cm for the NE and NW sets, respectively; however, the standard deviations of between ±1.08 and ±1.33 cm indicate that most apertures vary between 0 and about 2 cm. Table 3 shows that mean apertures increase from ~0.84 cm west of the fracture zone, to 1.11 cm for the NE set, to slightly more (1.52 cm) for the NW set within the fracture zone. East of the fracture zone, apertures again fall off to mean values around 0.61 cm and standard deviations are about one-half as much as those found to the west of the most highly fractured zone. It is not known to what degree (if any) fracture apertures have been modified by their proximity to the canyon walls. No visible erosive widening was observed; the fractures show more or less pristine, case-hardened surfaces. However, apertures were observed to decrease above and below unit 2. Fracture-filling materials are sparse to absent in unit 2, but they become prominent in unit 3.

Figure 8 is a plot of fracture widths *vs* horizontal location. The data have been smoothed and compared to the linear fracture density curve of Fig. 3. Note the strong correspondence of fracture widths with linear fracture density. From background values of ~ 0.85 cm, fracture widths rise to values >3 cm over the fracture zone. In Fig. 9, cumulative fracture widths for 100-ft intervals centered on each fracture are plotted against horizontal location and compared to the linear fracture density

TABLE 3.
FRACTURE APERTURE DATA [a]

Fracture Set	*Number*	*Mean Aperture (cm)*	*Standard Deviation*
All Fractures			
NE	988	0.8	±1.1
NW	674	0.9	±1.3
Background (West)			
NE	182	0.9	±1.2
NW	128	0.8	±1.1
Fracture Zone			
NE	312	1.1	±1.5
NW	212	1.5	±2.0
Background (East)			
NE	494	0.6	±0.6
NW	334	0.6	±0.6

[a] Fracture zone corresponds to horizontal distances from 2500 to 4000 ft east of Omega Site.

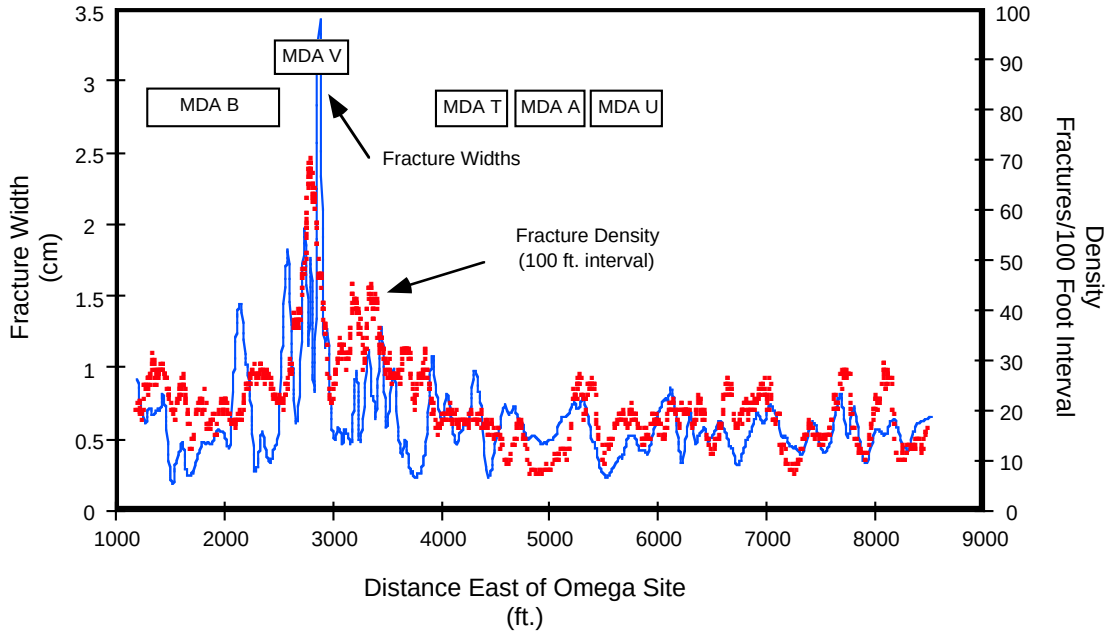

Fig. 8. Plot of fracture widths (apertures) vs distance east of Omega Site compared to linear fracture density from Fig. 3. The fracture data are represented by a 0.2 smoothed curve (81-point moving average).

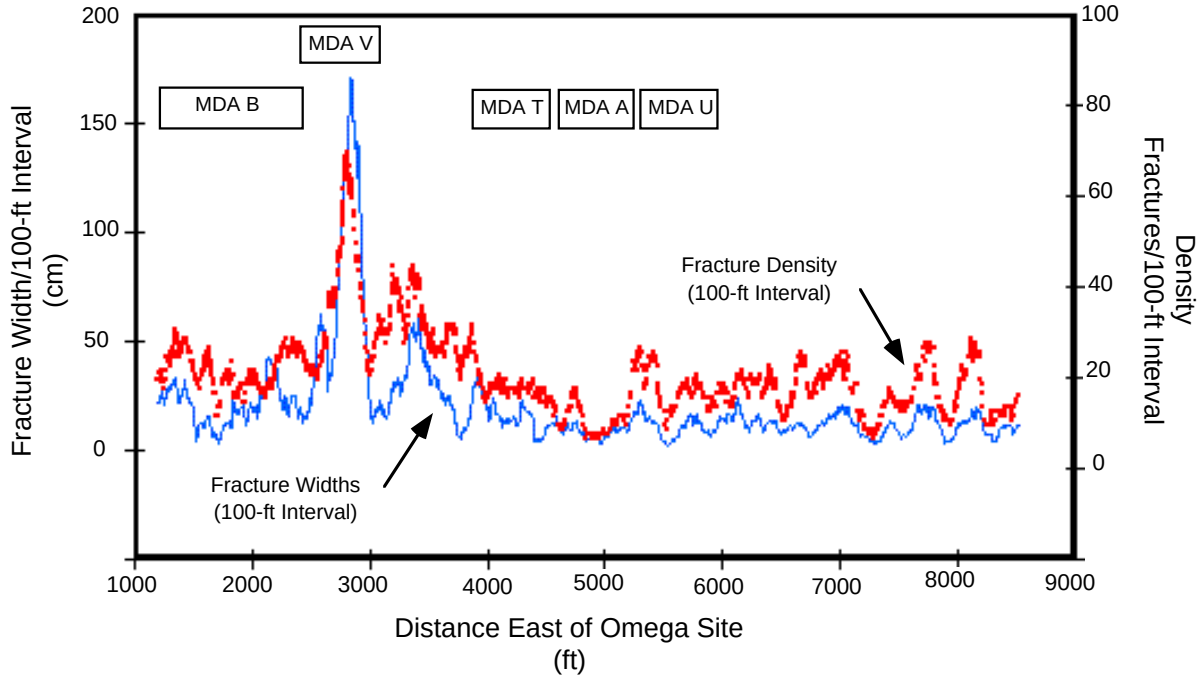

Fig. 9. Cumulative fracture widths over 100-ft interval centered on each fracture plotted against horizontal location.

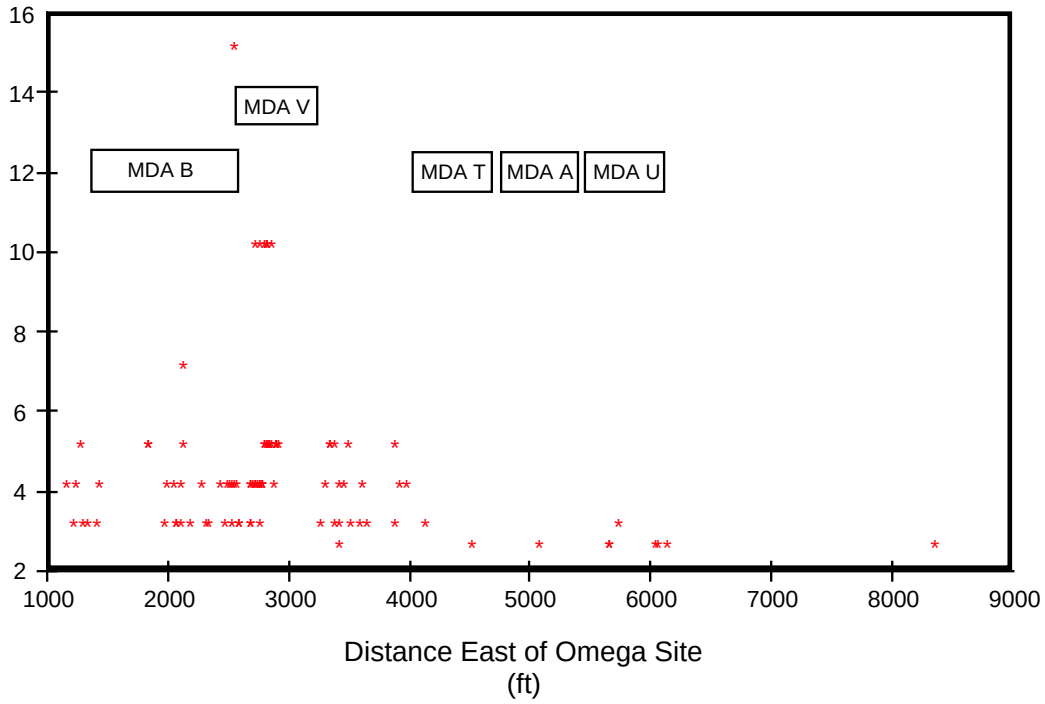

Fig. 10. Fractures with widths >2 cm plotted against horizontal location.

data. From a background of ~0.5 m of fracture opening over 100-ft intervals, the cumulative fracture opening rises to about 1.4 m/100-ft interval over the fracture zone. The importance of the fracture zone with respect to fracture apertures is further emphasized in Fig. 10, where only fractures with openings >2 cm are plotted with location.

CONCLUSIONS

The fracture characteristics described above apply to unit 2 of the Tshirege member, but their similarity to those described by Vaniman and Wohletz (1990) for unit 3 of the Tshirege Member suggests that these results for unit 2 can be extrapolated to the rocks directly underlying TA-21. The results of this present study also support the conclusion that a fracture zone probably related to the Pajarito Fault system runs on a northerly course through MDA-V of TA-21. The fracture zone appears as an area of increased fracture density from 2500 to 4000 ft east of Omega Site. Over this 1500 ft of increased fracture density, there is a cumulative fracture aperture of nearly 6.7 m. It is not known whether tectonic movement produced the increased number of fractures by creating new ones or by opening rock discontinuities originally formed by cooling contraction.

Study of the potential for contaminant migration will be pursued by coring below MDAs. Trigonometric analysis of these fracture data will provide optimum slant-drilling orientations for intersecting the greatest number of fractures in a given length of drill core. From the data in Tables 1 through 3, it is apparent that NE-striking fractures are ~30% more abundant than NW-striking ones. Furthermore, the NE-striking fractures (those that dip north into the NW quadrant) are over three times more abundant than south-dipping ones. Hence, as a first approximation, slant drilling in the direction S48E should

optimize fracture intersections. However, if calculated E-W fractures (Fig. 4b) are realistic, then N-S slant drilling should also be pursued.

This report concludes the field characterization of fracture orientations and apertures for the upper vadose zone at TA-21. The data presented in this report will be used to design drilling programs for characterization of the MDAs. These data will also be used to evaluate the role of fractures in contaminant migration at TA-21. Additional fracture characterization is planned for deep boreholes when the drilling is completed. In addition, there is an ongoing mineralogical study of fracture-lining and fracture-filling minerals at TA-21. The results of the fracture mineralogy studies will be reported separately.

AKNOWLEDGEMENTS

J. Gardner, K. Carter, D. Broxton, and G. Eller provided critical reviews of this paper.

REFERENCES

Gardner, J.N., and House, L., 1987, Seismic hazards investigations at Los Alamos National Laboratory, 1984-1985, Los Alamos National Laboratory report LA-11072-MS, 76 pp. (7 maps, 1:62500 scale).

Vaniman, D., and Wohletz, K., 1990, Results of geological mapping/fracture studies: TA-55 area, Los Alamos National Laboratory Seismic Hazards Memo EES1-SH90-17, 25 pp. (3 plates, map, 1:7800 scale).

STRATIGRAPHY, PETROGRAPHY, AND MINERALOGY OF BANDELIER TUFF AND CERRO TOLEDO DEPOSITS

by

D. E. Broxton, G.H. Heiken, S. J. Chipera, and F. M. Byers, Jr.

A total of 86 samples was collected in three measured sections on the north wall of Los Alamos Canyon to determine the lithology, petrography, and mineralogy of tuffs at TA 21. Methods of investigation included field observations, modal point counts, petrographic descriptions, x-ray diffraction, and image analysis. These data were collected to develop conceptual models for the hydrogeology of the site, evaluate potential transport pathways and processes, and provide bounds on parameters used in models for evaluating the migration of water and contaminants.

Bedrock stratigraphic units in Los Alamos Canyon consists of (in ascending order) the Otowi Member of the Bandelier Tuff, epiclastic deposits of the Cerro Toledo interval, and the Tshirege Member (including the Tsankawi Pumice Bed) of the Bandelier Tuff. The exposed upper 18 to 21 m of the Otowi Member is a simple cooling unit made up of massive, nonwelded, vitric ignimbrite. The Otowi Member is easily eroded and crops out as gentle slopes near the bottom of Los Alamos Canyon. The Cerro Toledo interval is an informal name given to a complex sequence of epiclastic sediments and tephras of mixed provenance. This unit contains deposits normally assigned to the Cerro Toledo Rhyolite, including well-stratified tuffaceous sandstones and siltstones as well as primary ash-fall and pumice-fall deposits. The Cerro Toledo interval also contains intercalated deposits not normally assigned to the Cerro Toledo Rhyolite; these include sand, gravel, cobble, and boulder deposits derived from the Tschicoma Formation. The thickness of the Cerro Toledo interval ranges from 3 to 9 m. The Tsankawi Pumice Bed is a 0.7- to 0.9-m-thick rhyolitic pumice-fall deposit that consists of two normally graded pumice falls separated by a thin ash bed. The Tshirege Member is a multiple-flow rhyolitic ignimbrite that forms a series of step-like vertical cliffs and sloping ledges in Los Alamos Canyon. It is a compound cooling unit whose physical properties vary both vertically and laterally; the thickness of this unit ranges from 89 to 98 m.

The bulk-rock mineralogy of tuffs at TA-21 consists primarily of alkali feldspar + quartz ± cristobalite ± tridymite ± glass. Minor constituents include smectite, hornblende, mica, hematite, calcite, and kaolinite. Volcanic glass is the dominant constituent in the Otowi Member, tuffs of the Cerro Toledo interval, and the lower part of the Tshirege Member. The upper two-thirds of the Tshirege Member have undergone extensive devitrification and vapor-phase alteration; the mineral assemblage in these tuffs consists of alkali feldspar + quartz ± cristobalite ± tridymite. Smectite and hematite occur in small (<2%) amounts throughout the stratigraphic sequence. These two trace minerals are important because they are highly sorptive of certain radionuclides and could provide important natural barriers to their migration. Although these minerals occur in small quantities, they are disseminated throughout all stratigraphic units, and their aggregate abundance and surface area are large when integrated over long groundwater flow paths through the tuffs.

The exposed tuffaceous rocks at TA-21 are provisionally subdivided into eight hydrogeological units based upon their lithological and mineralogical properties. Complete delineation of all hydrogeological units at TA-21 must await characterization of subsurface units and systematic measurements of hydrological properties from all rock units.

INTRODUCTION

This study is conducted as part of on-going ER Program RFI work for OU 1106 located at TA-21 (Fig. 1). This report supports the RFI studies by providing geological data for developing and testing hydrogeological conceptual models for the site, evaluating potential transport pathways and processes, and collecting data for parameters used in models for evaluating the migration of water and contaminants. The data also provide a geological framework for evaluating various types of remediation that could be applied at the site. This study supports these goals by delineating important hydrogeological units whose physical and chemical properties control the movement of moisture and contaminants.

The general stratigraphy of tuffaceous rocks of the Pajarito Plateau is described by Bailey *et al.* (1969), Baltz *et al.* (1963), Weir and Purtymun (1962), Griggs (1964), Smith *et al.* (1970), Crowe *et al.* (1978), Heiken *et al.* (1986), Vaniman and Wohletz (1990 and 1991), and Gardner *et al.* (1993). This report builds on the earlier studies and provides geological information specific to TA-21. It includes information about vertical and lateral changes in lithology, petrography, and mineralogy within the tuffs that underlie the SWMUs at TA-21. Together, the geologic map (Goff, Sec. II, this report) and this paper provide a stratigraphic framework for future studies.

Reneau (Sec. V, this report) describes geomorphic characteristics of TA-21, as well as post-Bandelier deposits not discussed here. This paper documents some observations about fracture characteristics at TA-21, but the data presented may have only local significance and should be used as supplemental information to the more systematic study of fractures by Wohletz (Sec. III, this report). An ongoing study of fracture mineralogy by D. Vaniman, LANL, is evaluating the potential for contaminant transport within fractures

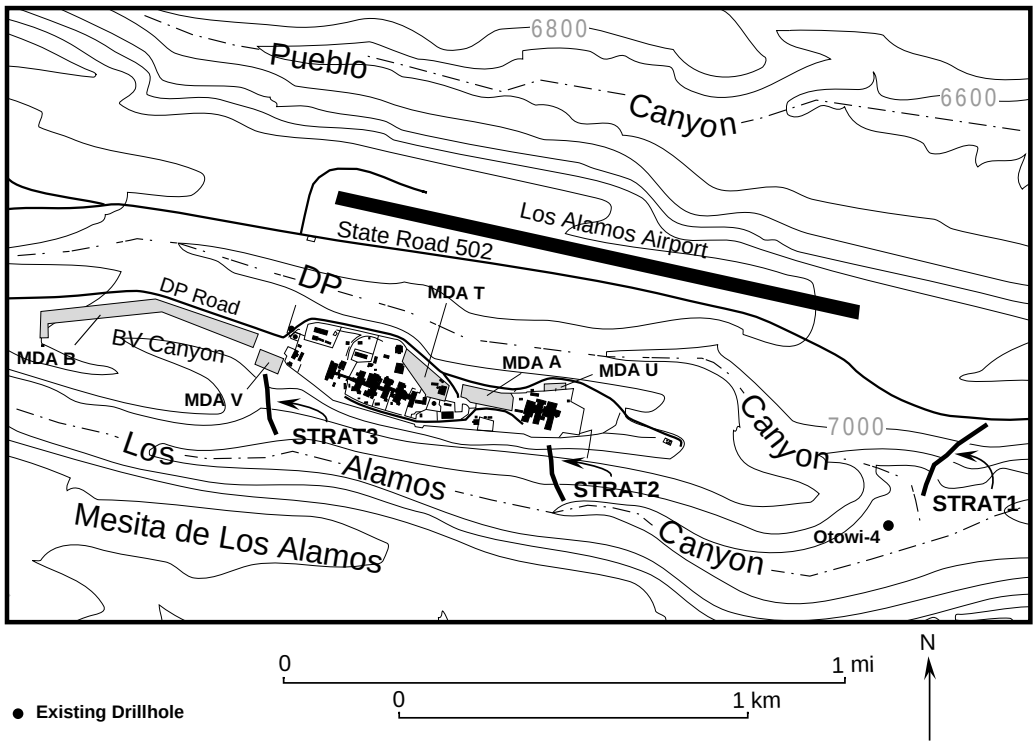

Fig. 1. Map showing the locations of the three stratigraphic sections (for example, STRAT-1) measured on the north wall of Los Alamos Canyon at TA-21.

by examining these structures for evidence of past groundwater transport. Vaniman's study also is identifying mineral assemblages that may retard contaminant transport in fractures.

METHODS

For this study, 86 bulk-rock samples were collected from outcrops of bedrock units exposed on the north wall of Los Alamos Canyon. Three stratigraphic sections were measured and sampled (Fig. 1). Section OU-1106-STRAT-1 (34 samples), near the confluence of DP Canyon and Los Alamos Canyon, is the easternmost of the three sections. Section OU-1106-STRAT-2 (25 samples) is south of MDA U in the eastern part of the TA-21 complex. Section OU-1106-STRAT-3 (27 samples), south of MDA V, is the westernmost section. Samples were collected at a nominal vertical spacing of 5 m or at major changes in lithology. Metal tags mark sample sites in the field. Initially, vertical control was maintained by Jacob staff and Abney level. Later, Merrick & Company surveyed locations and elevations of all sample sites (Table I).

Field work was performed under procedures described in LANL-ER-SOP-03.07 (*Characterization of Lithologic Variations within the Rock Outcrops of a Volcanic Field*). Observations at each sample site generally include descriptions of rock type, type and degree of alteration, welding and compaction, phenocryst assemblage and abundance, color on fresh and weathered surfaces, pumice size and abundance, and weathering characteristics. Bedding characteristics, fractures and their filling materials, and lithic assemblage, size, and abundance were also noted.

TABLE I

LOCATION OF SAMPLES COLLECTED IN STRATIGRAPHIC SECTIONS AT TA-21

Sample Number	Stratigraphic Unit [a]	Location Identification	Bar Code Number	Coordinates North (ft) [b]	Coordinates East (ft) [b]	Latitude [c]	Longitude [c]	Elevation (ft)
Stratigraphic Section #1 (Easternmost Section)								
OU-1106-STRAT1-1	Qbo	21-1485	AAA2549	1637657	1773468	35 52 28.16223	106 15 23.98251	6662.9
OU-1106-STRAT1-2	Qbo	21-1486	AAA2550	1637736	1773513	35 52 28.24855	106 15 22.88122	6683.4
OU-1106-STRAT1-3	Qbo	21-1487	AAA2551	1637730	1773554	35 52 28.65329	106 15 22.74758	6692.7
OU-1106-STRAT1-4	Qbo	21-1488	AAA2552	1637793	1773558	35 52 28.42660	106 15 22.02381	6715.8
OU-1106-STRAT1-5	Qbo	21-1489	AAA2553	1637767	1773585	35 52 28.77987	106 15 22.17646	6726.1
OU-1106-STRAT1-6	Qct	21-1490	AAA2554	1637802	1773582	35 52 28.61254	106 15 21.81482	6722.0
OU-1106-STRAT1-7	Qct	21-1491	AAA2555	1637801	1773582	35 52 28.61228	106 15 21.82369	6722.3
OU-1106-STRAT1-8	Qct	21-1492	AAA2556	1637803	1773582	35 52 28.61088	106 15 21.79562	6723.7
OU-1106-STRAT1-9	Qct	21-1493	AAA2557	1637803	1773582	35 52 28.60573	106 15 21.79343	6726.4
OU-1106-STRAT1-10	Qct	21-1494	AAA2558	1637805	1773583	35 52 28.60683	106 15 21.76694	6727.5
OU-1106-STRAT1-11	Qbt-1g	21-1495	AAA2559	1637831	1773577	35 52 28.44729	106 15 21.51588	6727.3
OU-1106-STRAT1-12	Qbt-1g	21-1496	AAA2560	1637833	1773577	35 52 28.44223	106 15 21.49522	6729.2
OU-1106-STRAT1-13	Qbt-1g	21-1497	AAA2561	1637833	1773577	35 52 28.44209	106 15 21.49060	6729.5
OU-1106-STRAT1-14	Qbt-1g	21-1498	AAA2562	1637826	1773577	35 52 28.46674	106 15 21.56521	6731.3
OU-1106-STRAT1-15	Qbt-1g	21-1499	AAA2563	1637828	1773577	35 52 28.46022	106 15 21.54553	6732.3
OU-1106-STRAT1-16	Qbt-1g	21-1500	AAA2564	1637855	1773583	35 52 28.41357	106 15 21.21451	6747.4
OU-1106-STRAT1-17	Qbt-1g	21-1501	AAA2565	1637878	1773578	35 52 28.27199	106 15 20.98241	6763.2
OU-1106-STRAT1-18	Qbt-1g	21-1502	AAA2566	1637907	1773582	35 52 28.19501	106 15 20.64471	6779.2
OU-1106-STRAT1-19	Qbt-1g	21-1503	AAA2567	1637936	1773577	35 52 28.03657	106 15 20.35014	6794.9
OU-1106-STRAT1-20	Qbt-1g	21-1504	AAA2568	1637932	1773595	35 52 28.21381	106 15 20.29730	6810.4
OU-1106-STRAT1-21	Qbt-1v	21-1505	AAA2569	1637972	1773613	35 52 28.22467	106 15 19.77126	6827.1
OU-1106-STRAT1-22	Qbt-1v	21-1506	AAA2570	1638063	1773630	35 52 28.01135	106 15 18.67055	6843.3
OU-1106-STRAT1-23	Qbt-1v	21-1507	AAA2571	1638099	1773640	35 52 27.89166	106 15 18.23308	6858.8
OU-1106-STRAT1-24	Qbt-1v	21-1508	AAA2572	1638133	1773653	35 52 27.88309	106 15 17.79429	6875.5
OU-1106-STRAT1-25	Qbt-1v	21-1509	AAA2573	1638164	1773668	35 52 27.94535	106 15 17.36887	6891.5
OU-1106-STRAT1-26	Qbt-1v	21-1510	AAA2574	1638201	1773682	35 52 27.92736	106 15 16.88596	6908.5
OU-1106-STRAT1-27	Qbt-2	21-1511	AAA2575	1638221	1773703	35 52 28.03250	106 15 16.55617	6924.1
OU-1106-STRAT1-28	Qbt-2	21-1512	AAA2576	1638255	1773722	35 52 28.07319	106 15 16.08919	6941.3
OU-1106-STRAT1-29	Qbt-2	21-1513	AAA2577	1638287	1773743	35 52 28.13243	106 15 15.63606	6957.5
OU-1106-STRAT1-30	Qbt-nw	21-1514	AAA2578	1638313	1773764	35 52 28.40968	106 15 15.16071	6974.2
OU-1106-STRAT1-31	Qbt-3	21-1515	AAA2579	1638340	1773790	35 52 28.34285	106 15 14.80976	6990.1
OU-1106-STRAT1-32	Qbt-3	21-1516	AAA2580	1638367	1773812	35 52 28.44040	106 15 14.40026	7006.4
OU-1106-STRAT1-33	Qbt-3	21-1517	AAA2581	1638394	1773833	35 52 28.52247	106 15 13.99805	7023.4
OU-1106-STRAT1-34	Qbt-3	21-1518	AAA2582	1638414	1773850	35 52 28.59649	106 15 13.68466	7036.2
Stratigraphic Section #2 (Central DP Mesa)								
OU-1106-STRAT2-1	Qbo	21-1519	AAA2583	1634069	1773288	35 52 25.19541	106 16 15.04309	6746.4
OU-1106-STRAT2-2	Qbo	21-1520	AAA2584	1634060	1773315	35 52 25.45641	106 16 15.14924	6761.3
OU-1106-STRAT2-3	Qct	21-1521	AAA2585	1634061	1773331	35 52 25.61154	106 16 15.13543	6769.7
OU-1106-STRAT2-4	Qct	21-1522	AAA2586	1634062	1773332	35 52 25.62654	106 16 15.12766	6771.2
OU-1106-STRAT2-5	Qbt-1g	21-1523	AAA2587	1634046	1773357	35 52 25.87707	106 16 15.31583	6788.0
OU-1106-STRAT2-6	Qbt-1g	21-1524	AAA2588	1634037	1773377	35 52 26.06879	106 16 15.42439	6800.9
OU-1106-STRAT2-7	Qbt-1g	21-1525	AAA2589	1634032	1773401	35 52 26.30941	106 16 15.48825	6816.6
OU-1106-STRAT2-8	Qbt-1g	21-1526	AAA2590	1634019	1773424	35 52 26.54083	106 16 15.65041	6831.8
OU-1106-STRAT2-9	Qbt-1g	21-1527	AAA2591	1634004	1773449	35 52 26.78304	106 16 15.82704	6847.4
OU-1106-STRAT2-10	Qbt-1g	21-1528	AAA2592	1633991	1773462	35 52 26.91627	106 16 15.99124	6858.1
OU-1106-STRAT2-11	Qbt-1g	21-1529	AAA2593	1633961	1773470	35 52 26.99011	106 16 16.35070	6873.5
OU-1106-STRAT2-12	Qbt-1g	21-1530	AAA2594	1633961	1773479	35 52 27.08237	106 16 16.35146	6886.5
OU-1106-STRAT2-13	Qbt-1g	21-1531	AAA2595	1633970	1773486	35 52 27.14748	106 16 16.24466	6889.0
OU-1106-STRAT2-14	Qbt-1v	21-1532	AAA2596	1633973	1773548	35 52 27.76515	106 16 16.20145	6906.6
OU-1106-STRAT2-15	Qbt-1v	21-1533	AAA2597	1633970	1773574	35 52 28.02387	106 16 16.24818	6923.7
OU-1106-STRAT2-16	Qbt-1v	21-1534	AAA2598	1633976	1773579	35 52 28.06672	106 16 16.16677	6941.2
OU-1106-STRAT2-17	Qbt-2	21-1535	AAA2599	1633998	1773593	35 52 28.20469	106 16 15.90616	6958.2
OU-1106-STRAT2-18	Qbt-2	21-1536	AAA2600	1634053	1773609	35 52 28.37063	106 16 15.23458	6977.1
OU-1106-STRAT2-19	Qbt-2	21-1537	AAA2601	1634031	1773618	35 52 28.45657	106 16 15.50194	6998.0
OU-1106-STRAT2-20	Qbt-2	21-1538	AAA2602	1634023	1773635	35 52 28.62002	106 16 15.59348	7015.8
OU-1106-STRAT2-21	Qbt-nw	21-1539	AAA2603	1634028	1773669	35 52 28.96302	106 16 15.53294	7025.9
OU-1106-STRAT2-22	Qbt-3	21-1540	AAA2604	1634054	1773699	35 52 29.25793	106 16 15.22048	7053.8
OU-1106-STRAT2-23	Qbt-3	21-1541	AAA2605	1634054	1773711	35 52 29.37201	106 16 15.22184	7069.3
OU-1106-STRAT2-24	Qbt-3	21-1542	AAA2606	1634060	1773745	35 52 29.71054	106 16 15.14659	7086.7
OU-1106-STRAT2-25	Qbt-3	21-1570	AAA5678	1634076	1773738	35 52 29.63926	106 16 14.95713	7103.0

[a] *Stratigraphic Unit - Nomenclature of Vaniman and Wohletz (1990, 1991); Qbo = Otowi Member of the Bandelier Tuff; Qct = Cerro Toledo interval; Qbt-1g = Tshirege unit 1g; Qbt-1v = Tshirege unit 1v; Qbt-2 = Tshirege unit 2; Qbt-nw = nonwelded tuff; Qbt-3 = Tshirege unit 3.*

[b] *State plane coordinate system NAD 83.*

[c] *Degrees, minutes, and seconds.*

TABLE I (cont)

LOCATION OF SAMPLES COLLECTED IN STRATIGRAPHIC SECTIONS AT TA-21

Sample Number	Stratigraphic Unit[a]	Location Identification	Bar Code Number	Coordinates North (ft)[b]	Coordinates East (ft)[b]	Latitude[c]	Longitude[c]	Elevation (ft)
Stratigraphic Section #3 (Westernmost Section)								
OU-1106-STRAT3-1	Qbo	21-1543	AAA2607	1631540	1773813	35 52 30.37632	106 16 45.77789	6779.1
OU-1106-STRAT3-2	Qct	21-1544	AAA2608	1631480	1774005	35 52 32.27278	106 16 46.50356	6831.9
OU-1106-STRAT3-3	Qct	21-1545	AAA2609	1631475	1774032	35 52 32.54528	106 16 46.55871	6849.5
OU-1106-STRAT3-4	Qct	21-1546	AAA2610	1631475	1774032	35 52 32.54385	106 16 46.56527	6850.7
OU-1106-STRAT3-5	Qct	21-1547	AAA2611	1631464	1774034	35 52 32.53960	106 16 46.69725	6857.3
OU-1106-STRAT3-6	Qct	21-1548	AAA2612	1631457	1774037	35 52 32.59736	106 16 46.78694	6861.4
OU-1106-STRAT3-7	Qbt-1g	21-1549	AAA2613	1631445	1774036	35 52 32.58614	106 16 46.92924	6864.2
OU-1106-STRAT3-8	Qbt-1g	21-1550	AAA2614	1631442	1774043	35 52 32.64717	106 16 46.96656	6867.7
OU-1106-STRAT3-9	Qbt-1g	21-1551	AAA2615	1631419	1774061	35 52 32.83190	106 16 47.23737	6885.0
OU-1106-STRAT3-10	Qbt-1g	21-1552	AAA2616	1631409	1774077	35 52 32.98752	106 16 47.36636	6901.5
OU-1106-STRAT3-11	Qbt-1g	21-1553	AAA2617	1631401	1774101	35 52 33.22538	106 16 47.46172	6917.5
OU-1106-STRAT3-12	Qbt-1g	21-1554	AAA2618	1631392	1774118	35 52 33.39489	106 16 47.57456	6931.1
OU-1106-STRAT3-13	Qbt-1g	21-1555	AAA2619	1631392	1774121	35 52 33.42131	106 16 47.56606	6933.2
OU-1106-STRAT3-14	Qbt-1v	21-1556	AAA2620	1631395	1774119	35 52 33.40229	106 16 47.53020	6934.3
OU-1106-STRAT3-15	Qbt-1v	21-1557	AAA2621	1631393	1774121	35 52 33.42113	106 16 47.56266	6937.9
OU-1106-STRAT3-16	Qbt-1v	21-1558	AAA2622	1631373	1774139	35 52 33.60113	106 16 47.79883	6954.3
OU-1106-STRAT3-17	Qbt-1v	21-1559	AAA2623	1631363	1774158	35 52 33.78689	106 16 47.92711	6968.8
OU-1106-STRAT3-18	Qbt-1v	21-1560	AAA2624	1631373	1774175	35 52 33.95934	106 16 47.80735	6985.8
OU-1106-STRAT3-19	Qbt-2	21-1561	AAA2625	1631300	1774213	35 52 34.33600	106 16 48.68449	6999.0
OU-1106-STRAT3-20	Qbt-2	21-1562	AAA2626	1631292	1774220	35 52 34.39941	106 16 48.78404	7014.6
OU-1106-STRAT3-21	Qbt-2	21-1563	AAA2627	1631168	1774217	35 52 34.37489	106 16 50.29901	7048.2
OU-1106-STRAT3-22	Qbt-nw	21-1564	AAA2628	1631199	1774288	35 52 35.07360	106 16 49.91321	7063.7
OU-1106-STRAT3-23	Qbt-nw	21-1565	AAA2629	1631271	1774351	35 52 35.69898	106 16 49.03948	7084.5
OU-1106-STRAT3-24	Qbt-3	21-1566	AAA2630	1631301	1774372	35 52 35.90971	106 16 48.68351	7100.8
OU-1106-STRAT3-25	Qbt-3	21-1567	AAA2631	1631306	1774395	35 52 36.13487	106 16 48.61992	7117.7
OU-1106-STRAT3-26	Qbt-3	21-1568	AAA2632	1631319	1774416	35 52 36.33778	106 16 48.46275	7133.9
OU-1106-STRAT3-27	Qbt-3	21-1569	AAA2633	1631316	1774473	35 52 36.90362	106 16 48.49517	7150.8

The mineralogy of all 86 bulk-rock samples was characterized by x-ray diffraction analyses (XRD). Samples were first powdered in a tungsten-carbide shatter box and then mixed with an internal standard of 1-μm metallurgical-grade Al_2O_3 (corundum) powder in a ratio of 80% sample to 20% internal standard by weight. The samples were then ground under acetone in an automatic Brinkmann-Retsch mill fitted with an agate mortar and pestle to produce an average particle size of <5 μm. This fine size is necessary to ensure adequate particle statistics and to minimize primary extinction (Klug and Alexander 1974, pp. 365-367). Particle-size distributions have been verified using a Horiba CAPA-500 centrifugal particle-size distribution analyzer calibrated with Duke Scientific glass microsphere standards.

The XRD data were collected on a Siemens D-500 theta-theta diffractometer using copper-Kα radiation, incident- and diffracted-beam Soller slits, and a Kevex solid-state (SiLi) detector. Data were typically collected from 2.0 to 50.0° 2θ using a 0.02° step size and at least 2 s per step. Quantitative analyses employed the internal standard or "matrix-flushing" method of Chung (1974a,b), which requires adding an internal standard to each sample. Details for analysis can be found in Bish and Chipera (1988; 1989). In addition, the following YMP procedures were used for sample preparation and analysis of XRD samples: LANL-EES-DP-130 (*Geologic Sample Preparation*), LANL-EES-DP-56 (*Brinkmann Automated Grinder Procedure*), LANL-EES-DP-16 (*Siemens X-Ray Diffraction Procedure*), and LANL-EES-DP-116

(*Quantitative X-Ray Diffraction Data Reduction Procedure*). The YMP quality assurance requirements are comparable in rigor to those used by the Los Alamos ER Program.

Thin-section modal point counts were made on 23 of the 25 bulk rock samples and on one pumice lump from section OU-1106-STRAT2 (bulk rock sample #8 was not prepared in time for analysis). Between 2374 and 6057 gridded points were counted for each thin section. The point counts tallied percentages of phenocrysts, lithic fragments, pumice, shards, perlite chips (solid glass or altered glass fragments), and voids, following the draft procedure LANL-ER-SOP-03.05 (*Determination of Volume Constituents in Thin Sections of Rock*). Thin sections were prepared according to YMP procedure LANL-EES-DP-130 (*Geologic Sample Preparation*). Opaque oxide minerals were qualitatively identified using criteria outlined in YMP procedure TWS-ESS-DP-128 (*Procedure for Counting Opaque Minerals in Polished Thin Sections*). Image analysis with a microscope (200x, reflected light) attached to a minicomputer was used to determine magnetite abundances as well as statistics for grain areas, grain dimensions, and grain perimeters for two samples (OU-1106-STRAT2-16 and OU-1106-STRAT3-10). Additional petrographic observations of textures, alteration features, and accessory minerals were collected using procedure LANL-ER-SOP-03.04 (*Petrography*).

RESULTS AND DISCUSSION

Plate 1 in the pocket of this volume is the geologic map of TA-21 by Goff (Sec. II, this report) and Reneau (Sec. V, this report). Plate 2 contains detailed lithologic logs for the three stratigraphic sections measured in this study. Table I correlates sample field numbers with site identifiers and lists the surveyed coordinates of samples. Table II and Fig. 2 present modal petrographic data for stratigraphic section OU-1106-STRAT2; Fig. 3 correlates stratigraphic nomenclature used in this report (that of Vaniman and Wohletz (1990, 1991) with the nomenclature used by earlier workers. Table III and Fig. 4 summarize the field data for the vapor-phase notch, an important stratigraphic marker horizon in the Tshirege Member of the Bandelier Tuff. Table IV and Fig. 5 summarize mineralogical data for all three stratigraphic sections.

Lithologic Characteristics of Tuffs in Los Alamos Canyon

The stratigraphic sequence is similar in each of the three measured sections and consists of (in ascending order) the Otowi Member of the Bandelier Tuff (1.613 ± 0.011 Ma; Izett and Obradovich, 1994), epiclastic sediments and tephras of the Cerro Toledo interval, and the Tshirege Member of the Bandelier Tuff (1.223 ± 0.018 Ma; Izett and Obradovich, 1994). Within the Tshirege Member, mappable subunits are described separately because of their distinct physical properties. Reneau (Sec. V, this report) describes younger soils and alluvial deposits for TA-21.

In this report, we use the term *ignimbrite* to describe all deposits formed by the emplacement of pyroclastic flows. The term *surge beds* is used to describe laminated ash deposits with sandwaves and to refer to pyroclastic surge deposits of any type, including ground-surge, ash-cloud, and base-surge deposits (Fisher and Schmincke, 1984). A *simple cooling unit* is made up of a single pyroclastic flow or successive pyroclastic flows that were emplaced at essentially uniform temperature and cooled as a unit without a break in time or cooling properties (Smith, 1960a,b). A *compound cooling unit* is made up of successive pyroclastic flows emplaced at radically different temperatures and/or emplaced over a sufficiently long period of time that abrupt changes in the temperature gradient caused welding and crystallization patterns to deviate from those found in a simple cooling unit (Smith, 1960a,b).

The *degree of welding* in tuffs described in this report is based on flattening of pumices in hand specimens and flattening of pumice and shards in thin section. These criteria describe the degree to which pyroclasts have undergone plastic deformation during compaction of the tuff. Strickly speaking, *welding* refers to the fusing together of adjacent pyroclasts in a cooling ash-flow sheet (Smith, 1960b). Nevertheless, as used in this report *welding* is a common and useful field term that differentiates between tuffs that are uncompacted and porous and tuffs that are compacted and less porous. [This terminology was adopted and slightly modified from that of Peterson (1979).] Ignimbrites in which pumice lapilli show no flattening are called *nonwelded*. Ignimbrites with aspect ratios of 1.5:1 to 2:1 are termed *partly* or *partially welded*; those with aspect ratios of 2:1 to 6:1 are *moderately welded;* and those with aspect ratios >6:1 are *densely welded*.

Otowi Member

The exposed portion of the Otowi Member of the Bandelier Tuff in Los Alamos Canyon is a simple cooling unit made up of nonwelded, vitric ignimbrite. This poorly indurated tuff crops out in shallow drainages that incise gentle colluvial-covered slopes on the canyon floor. Bedding or parting features are absent in the exposed portions of the Otowi Member, suggesting that the upper part of this ash-flow sheet is a single, thick, ash-flow deposit. The exposed portion of the Otowi Member is 18 to 21 m thick above the canyon floor, and an additional 47 m (including the Guaje Pumice Bed) was penetrated at water-supply well Otowi 4 (Stoker *et al.*, 1992). Therefore, the total thickness of this unit is ~67 m in the vicinity of borehole Otowi-4 (Fig. 1). Borehole LADP-4 in DP Canyon penetrated 85 m of Otowi Member, including 8.5 m of the basal Guaje Pumice Bed.

The Otowi Member consists of light-gray to pinkish-orange pumice lapilli supported by a white-to-tan, ashy matrix. The matrix is made up of glass shards, broken pumice fragments, phenocrysts, and fragments of nonvesiculated perlite. Glass shards are glassy and clear, showing no evidence for either post-emplacement high-temperature devitrification or subsequent low-temperature diagenetic alteration. Pumice lapilli typically make up 10 to 30% of the tuff, are equant to subequant (aspect ratios = 1:1 to 2:1), and range from 0.5 to 6 cm in diameter. Pumices are larger (up to 20 cm) and more abundant (~40% of the rock) at the top of the Otowi Member. These pumices have a vitreous luster on fresh surfaces, and the excellent preservation of delicate tubular vesicles imparts a fibrous appearance. Pumice and matrix materials acquire a pinkish-orange coloration near the top of the unit. This coloration may be the result of either the oxidation of iron by escaping vapors as the ash-flow sheet cooled or incipient weathering of the top of the unit before deposition of overlying units.

Two bulk-rock samples of Otowi Member contain 7 to 9% phenocrysts of quartz and sanidine 0.5 to 2 mm in diameter (Table II, Fig. 2). Clinopyroxene, plagioclase, and hornblende are present in trace amounts; the plagioclase and hornblende may be xenocrysts. Accessory minerals include magnetite, zircon, and an as-yet-unidentified rare-earth silicate. In thin section, the rare-earth accessory mineral is stubby and has the weak-to-moderate pleochroism characteristic of allanite; however, other grains are lath-like and completely absorb light length-wise like perrierite or chevkinite.

The upper part of the Otowi Member contains 2 to 5% chocolate-brown to black lithics derived from intermediate-composition lava flows. These lithics are 0.3 to 3 cm in diameter and consist primarily of aphanitic dacite. Phenocryst-rich dacites derived from the Tschicoma Formation form a subordinate lithic assemblage.

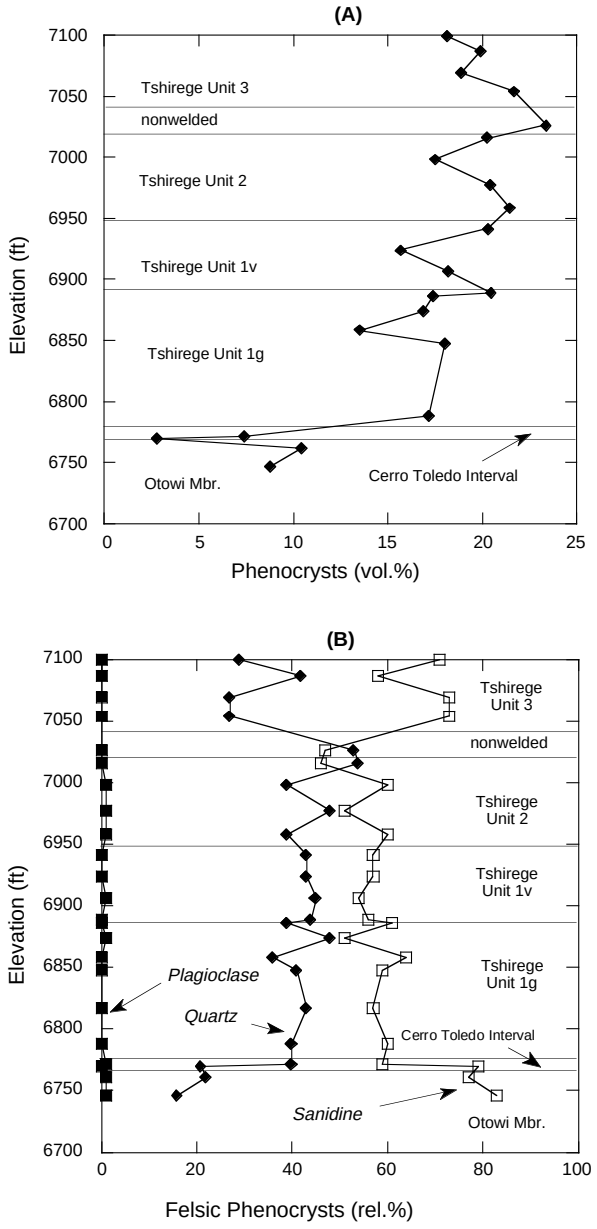

Fig. 2. Variation diagrams of phenocryst abundances in thin section for samples collected in stratigraphic section OU-1106-STRAT2. (A) Variations in total phenocryst abundances are shown on a void-free basis but are not corrected for porosity variations in the tuffs. (B) Variations in the relative proportions of the felsic phenocrysts.

Cerro Toledo Interval

The Cerro Toledo interval is an informal name given to a sequence of epiclastic sediments and tephras of mixed provenance that lie between the two members of the Bandelier Tuff. This unit contains deposits normally assigned to the Cerro Toledo Rhyolite (Smith *et al.*, 1970), including well-stratified tuffaceous sandstones and siltstones as well as primary ash-fall and pumice-fall deposits. The Cerro Toledo interval at TA-21 also contains intercalated deposits not normally assigned to the Cerro Toledo Rhyolite; these include poorly sorted sand, gravel, cobble, and boulder deposits derived from lava flows of the Tschicoma Formation. The Cerro Toledo interval is ~3 m thick at OU-1106-STRAT1 and OU-1106-STRAT2 and 9 m thick at OU-1106-STRAT3. In LADP-4, the Cerro Toledo interval is 12 m thick. These deposits also crop out in Los Alamos Canyon at TA-41 west of TA-21, in DP Canyon east of DP Spring, and in Pueblo Canyon north of TA-21. The distribution is widespread throughout the area; however, predicting the presence and thickness of these deposits is problematic because of the nature of fluvial systems.

Rhyolitic tuffaceous sediments and tephras are the dominant lithologies found in the Cerro Toledo interval at the three stratigraphic sections examined in this study. The tuffaceous sediments are the reworked equivalents of Cerro Toledo Rhyolite tephras erupted from the Cerro Toledo and Rabbit Mountain rhyolite domes located in the Sierra de los Valles. Because of their poorly consolidated nature and the steep topography on which they were deposited, these tephras were quickly eroded from the highlands to the west, transported by east-flowing stream systems, and deposited within a lowland area that is now the site of the Pajarito Plateau. These reworked tephras are subdivided into subunits on Plate 2 based on bedding characteristics, composition of clasts, and mode of deposition. Normally, these subunits pinch out laterally and can not be correlated over wide areas. Individual subunits are 5 to 175 cm thick and generally have well-defined stratification imparted by grading and sorting of ash- to block-sized clasts. Bedding characteristics include graded bedding, cross

TABLE II

MODAL PETROGRAPHY OF TUFFS AT TA-21

Field Number	OU-1106-STRAT2-1	OU-1106-STRAT2-2	OU-1106-STRAT2-3	OU-1106-STRAT2-4	OU-1106-STRAT2-5	OU-1106-STRAT2-6	OU-1106-STRAT2-7	OU-1106-STRAT2-9
Site Identification	160	161	162	163	164	165	166	200
Stratigraphic Unit	Otowi Mbr.	Otowi Mbr.	Cerro Toledo Interval	Cerro Toledo Interval	Tshirege Mbr. (1g)	Tshirege Mbr. (1g)[d]	Tshirege Mbr. (1g)	Tshirege Mbr. (1g)
Lithology[a]	nwt	nwt	b	b	nwt	Single Hb. pumice	nwt	nwt
Major Alteration[b]	Gl	Gl	Gl	Gl	Gl	Gl	Gl	Gl
Minor Alteration[b]	--	--	--	--	--	--	--	--
Matrix Materials (vol. %)[c]								
Ash, shards, pumice	85.9	87.5	94.1	86.9	80.6	59.1	96.5	79.6
Lithics (silicic volcanics)	3.6	0.6	1.5	2.0	0.8	--	0.8	1.2
Lithics (intermediate lavas)	1.2	0.1	1.4	1.0	0.05	0.1	--	0.2
Lithics (other)	0.1 (granitic)	0.1 (granitic)	--	--	0.1 (granitic)	--	--	--
Granophyric pumice	--	--	--	--	--	--	--	--
Perlitic glass fragments	0.5	0.3	0.4	2.4	1.0	--	0.2	1.1
Phenocrysts (vol. %)[c]								
Quartz	1.4	2.2	0.6	3.0	6.7	0	1.1	7.2
Alkali Feldspar	7.2	8.0	2.1	4.3	10.0	3.1	1.4	10.5
Plagioclase	0.04 (3)	0.1 (2)	--	0.05 (2)	0.1 (1)	31.8	--	0.04 (2)
Biotite	--	--	0 (1)	--	--	0 (1)	--	0 (2)
Hornblende	0 (3)	--	--	--	0 (7)	4.9	--	0 (5)
Orthopyroxene	--	--	--	--	--	0 (3)	--	--
Clinopyroxene	0.1 (16)	0.04 (11)	0 (2)	0.05 (9)	0.2 (18)	0.6	0.04 (6)	0.2 (15)
Fayalite	--	--	--	--	--	--	--	--
Other (Psuedo-morphs ect.)	--	--	--	--	--	0.4 (sanidine over-growths on plagioclase)	--	--
Accessory Minerals (counts)[c]								
Fe-Ti Oxides	2 (39)	1 (17)	0 (2)	3 (9)	2 (32)	2 (13)	0 (6)	1 (12)
Perrierite/Chevkinite/Allanite	--	0 (1)	0 (2)	0 (1)	--	--	--	--
Zircon	0 (3)	0 (6)	0 (1)	0 (3)	0 (1)	0 (1)	--	--
Sphene	--	--	--	--	--	--	--	--
Total Counts	2799	2475	5132	6057	2779	2982	4765	2414
Voids (counts)	415	421	1507	1676	189	826	2104	167
Remarks	Thin hematite rims around magnetite	Thin hematite rims around magnetite				Hematite after magnetite		
Phenocryst Summary								
% Phenocrysts (Void free)	8.7	10.3	2.7	7.4	17.0	40.8	2.5	17.9
Quartz as % of Felsic Phenos.	16	22	21	40	40	0	43	41
Sanidine as % of Felsic Phenos.	83	77	79	59	60	9	57	59
Plagioclase as % of Felsic Phenos.	1	1	0	1	0	91	0	0

[a] *Lithology: nwt = nonwelded ash-flow tuff; pwt = partially-welded ash-flow tuff; mwt = moderately-welded ash-flow tuff; b= bedded tuff, includes pumice falls and stratified reworked deposits.*

[b] *Alteration: Gl = none, original volcanic glass preserved; D = high-temperature devitrification; VP = vapor-phase alteration.*

[c] *Matrix materials and phenocrysts are presented as volume percent concentrations on a void-free basis. Accessory minerals are shown as the number of grains counted in the point count. The number in parentheses is a visual countof all grains of a component observed in a thin section.*

[d] *This thin section contains highly vesiculated pumice, some of which were plucked during sample preparation. The low phenocryst content is an artifact of sample and preparation, and it is not representative of the Tshirege Member.*

TABLE II

MODAL PETROGRAPHY OF TUFFS AT TA-21 (CONT)

Field Number	OU-1106-STRAT2-10	OU-1106-STRAT2-11	OU-1106-STRAT2-12	OU-1106-STRAT2-13	OU-1106-STRAT2-14	OU-1106-STRAT2-15	OU-1106-STRAT2-16	OU-1106-STRAT2-17
Site Identification	201	202	203	204	205	206	432	438
Stratigraphic Unit	Tshirege Mbr. (1g)	Tshirege Mbr. (1g)	Tshirege Mbr. (1g)	Tshirege (1g)	Tshirege Mbr. (1v)	Tshirege Mbr. (1v)	Tshirege Mbr. (1v)	Tshirege Mbr. (2)
Lithology[a]	nwt	nwt	nwt	nwt	nwt	nwt	nwt	pwt
Major Alteration[b]	Gl	Gl	Gl	D	D	D	VP, D	VP, D
Minor Alteration[b]	--	--	D	Gl	--	VP	--	--
Matrix Materials (vol. %) [c]								
Ash, shards, pumice	83.8	80.7	87.4	77.1	81.2	66.8	64.7	63.6
Lithics (silicic volcanics)	2.1	0.5	1.2	1.6	0.5	14.3	0.4	0.4
Lithics (intermediate lavas)	0.2	0.2	1	0.3	0.1	0.6	0.7	0.7
Lithics (other)	--	--	--	--	--	--	--	0.04 (granophyre)
Granophyric pumice	--	--	--	--	--	2.4	13.9	13.7
Perlitic glass fragments	0.3	1.6	1.2	0.5	--	--	--	--
Phenocrysts (vol. %) [c]								
Quartz	4.8	7.9	7.0	8.8	8.1	6.8	8.5	8.2
Alkali Feldspar	8.6	8.4	11.0	11.1	9.7	8.8	11.3	12.6
Plagioclase	0.04 (1)	0.2 (3)	0 (2)	0.04 (3)	0.1 (8)	--	0 (5)	0.1
Biotite	0 (1)	0 (1)	--	--	--	--	0 (5)	--
Hornblende	0.04 (5)	0 (3)	0.1 (3)	0 (1)	0.04 (8)	0.04 (5)	0.04 (3)	0.1 (6)
Orthopyroxene	--	--	--	--	--	--	--	--
Clinopyroxene	0 (15)	0.1 (15)	0.2 (17)	0.3 (9)	0.1 (4)	--	--	0.2 (4)
Fayalite	--	0.1 (1)	--	0.1 (2)	0.1 (2)	0 (1)	0.04 (1)	--
Other (Psuedo-morphs ect.)	--	0.1 (aggregates of secondary opaques)	0.1 (aggregates of secondary opaques)	0.1 (aggregates of secondary opaques)	--	--	0.3 cpx?	0.2 fayalite?
Accessory Minerals (counts) [c]								
Fe-Ti Oxides	2 (30)	2 (23)	2 (31)	1(28)	1(45)	1 (45)	1 (23)	3
Perrierite/Allanite	--	0 (1)	--	--	--	0 (1)	0 (1)	--
Zircon	--	--	0 (4)	0 (2)	0 (3)	0 (5)	0 (6)	0 (4)
Sphene	--	--	--	--	--	--	--	--
Total Counts	2701	2781	2785	2868	2855	2384	2374	2929
Voids (counts)	362	543	361	317	372	169	109	126
Remarks		Thin hematite rims around magnetite; pumices glassy but shardy matrix partly devitrified	Thin hematite rims around magnetite; pumices glassy but shardy matrix partly devitrified	Hematite rims around magnetite ; pumices partly glassy; shardy matrix devitrified	Hematite after magnetite	Hematite after magnetite	Hematite after magnetite	Hematite after magnetite
Phenocryst Summary								
% Phenocrysts (Void free)	13.4	16.8	17.4	20.4	18.1	15.6	20.2	21.4
Quartz as % of Felsic Phenos.	36	48	39	44	45	43	43	39
Sanidine as % of Felsic Phenos.	64	51	61	56	54	57	57	60
Plagioclase as % of Felsic Phenos.	0	1	0	0	1	0	0	1

[a] *Lithology: nwt = nonwelded ash-flow tuff; pwt = partially-welded ash-flow tuff; mwt = moderately-welded ash-flow tuff; b= bedded tuff, includes pumice falls and stratified reworked deposits.*

[b] *Alteration: Gl = none, original volcanic glass preserved; D = high-temperature devitrification; VP = vapor-phase alteration.*

[c] *Matrix materials and phenocrysts are presented as volume percent concentrations on a void-free basis. Accessory minerals are shown as the number of grains counted in the point count. The number in parentheses is a visual count of all grains of a component observed in a thin section.*

TABLE II

MODAL PETROGRAPHY OF TUFFS AT TA-21 (CONT)

Field Number	OU-1106-STRAT2-18	OU-1106-STRAT2-19	OU-1106-STRAT2-20	OU-1106-STRAT2-21	OU-1106-STRAT2-22	OU-1106-STRAT2-23	OU-1106-STRAT2-24	OU-1106-STRAT2-25
Site Identification	439	440	440	440	440	440	440	440
Stratigraphic Unit	Tshirege Mbr. (2)	Tshirege Mbr. (2)	Tshirege Mbr. (2)	Tshirege Mbr. (nw)	Tshirege Mbr. (3)	Tshirege Mbr. (3)	Tshirege Mbr. (3)	Tshirege Mbr. (3)
Lithology[a]	mwt	mwt	mwt	nwt	nwt	nwt	pwt	pwt
Major Alteration[b]	VP, D	VP, D	VP, D	VP, D	VP, D	VP, D	VP, D	VP, D
Minor Alteration[b]	--	--	--	--	--	--	--	--
Matrix Materials (vol. %) [c]								
Ash, shards, pumice	70.8	71.3	70.5	67.4	73.3	76.4	74.7	69.3
Lithics (silicic volcanics)	0.2	2.9	0.1	0.4	0.4	0.6	0.7	0.4
Lithics (intermediate lavas)	--	0.03	--	0.5	--	0.6	0.6	0.3
Lithics (other)	--	--	--	--	0.1 metamorphic	0.03 plutonic/meta.	--	--
Granophyric pumice	8.5	8.3	9.4			3.6	4.3	4.5
Perlitic glass fragments	--	--	--	--	--	--	--	--
Phenocrysts (vol. %) [c]								
Quartz	9.7	6.7	10.6	12.0	5.8	5.0	8.1	5.0
Alkali Feldspar	10.3	10.4	9.1	10.7	15.8	13.4	11.1	12.1
Plagioclase	0.2 (5)	0.2 (4)	0.1 (2)	0.1 (2)	0.03 (1)	0.03 (2)	0.1 (3)	0.1 (3)
Biotite	0 (2)	--	0.1 (6)	--	--	--	--	--
Hornblende	0.03 (6)	0.03 (8)	0.1 (2)	0.1(4)	0.03 (9)	0 (5)	0.1 (5)	0.03 (5)
Orthopyroxene	--	--	--	0 (2)?	--	0.3 (12)	--	--
Clinopyroxene	0 (2)	--	--	--	0.03	--	0.4 (21)	0.4 (30)
Fayalite	--	--	--	--	--	--	--	--
Other (Psuedo-morphs ect.)	0.1 (5) fayalite?	0.1 fayalite?	0.2 fayalite?	0.2 fayalite?	--	0.03 (4) cpx?	--	--
Accessory Minerals (counts) [c]								
Fe-Ti Oxides	2	2	2	2	1	1	3	6
Perrierite/Chevkinite/Allanite	--	0 (3)	--	--	0 (6)	0 (3)	0	0 (4)
Zircon	0 (13)	0 (10)	0 (6)	0 (10)	0 (4)	0 (8)	0 (8)	0 (8)
Sphene	--	--	0 (several grains)	--	0 (10)	0 (19)	--	--
Total Counts	3278	3275	2558	3349	3093	2933	3331	3157
Voids (counts)	61	67	13	283	210	107	121	193
Remarks	Hematite after magnetite	Hematite after magnetite	Hematite after magnetite	Hematite after magnetite	Hematite after magnetite	Hematite after magnetite	Hematite after magnetite	Hematite after magnetite
Phenocryst Summary								
% Phenocrysts (Void free)	20.3	17.4	20.2	23.1	21.7	18.8	19.8	18.1
Quartz as % of Felsic Phenos.	48	39	54	53	27	27	42	29
Sanidine as % of Felsic Phenos.	51	60	46	47	73	73	58	71
Plagioclase as % of Felsic Phenos.	1	1	0	0	0	0	0	0

[a] *Lithology: nwt = nonwelded ash-flow tuff; pwt = partially-welded ash-flow tuff; mwt = moderately-welded ash-flow tuff; b= bedded tuff, includes pumice falls and stratified reworked deposits.*

[b] *Alteration: Gl = none, original volcanic glass preserved; D = high-temperature devitrification; VP = vapor-phase alteration.*

[c] *Matrix materials and phenocrysts are presented as volume percent concentrations on a void-free basis. Accessory minerals are shown as the number of grains counted in the point count. The number in parentheses is a visual count of all grains of a component observed in a thin section.*

bedding, and planar bedding (Fig. 1 of Goff, Sec. II, this report). Orange oxidation and clay-rich horizons suggest that at least two periods of soil development are recorded within the Cerro Toledo deposits. These soils are clay-rich and may act as barriers to the downward movement of vadose zone groundwater.

Some of the epiclastic tuffaceous deposits contain both crystal-poor and crystal-rich varieties of pumice. The ashy matrix of these deposits is commonly crystal-rich and contains subhedral sanidine and quartz up to 2 mm in diameter. The mixed pumice populations and the crystal-rich nature of the matrix suggest that these reworked tuffs were derived from both the Cerro Toledo Rhyolite and the underlying Otowi Member.

The tuffaceous portion of the Cerro Toledo interval also contains primary fall deposits. In the lower part of the unit, fall deposits contain <3% phenocrysts of <0.2-mm sanidine and quartz (Table II, Fig. 2). These crystal-poor tephras are equivalent to the Cerro Toledo Rhyolite described by Heiken *et al.* (1986). Primary pumice falls in the upper part of the Cerro Toledo interval contain >7% phenocrysts of >1-mm sanidine and quartz. The petrographic characteristics are similar to those found in the overlying Tshirege Member. However, a clay-rich soil horizon at the top of the Cerro Toledo sequence suggests that these deposits were exposed at the surface for a substantial period of time before deposition of the overlying Tshirege Member. The primary pumice falls in the Cerro Toledo interval may be useful time-stratigraphic markers for correlating deposits over widespread areas of the Pajarito Plateau, but additional work is required to establish correlations between individual tephras. The pumice falls tend to form the most porous and permeable horizons within the Cerro Toledo interval, and locally they may provide important pathways for moisture transport in the vadose zone.

A subordinate lithology within the Cerro Toledo interval includes clast-supported gravel, cobble, and boulder deposits made up of porphyritic dacite derived from the Tschicoma Formation. These dacitic epiclastic deposits are interbedded with the tuffaceous rocks. The coarse dacitic deposits are typically 0.25 to 1.2 m thick, and they generally occur as overlapping lenticular paleochannels up to 1 m deep. In some places, cobbles of densely welded, crystal-rich Otowi ignimbrite are also present. At OU-1106-STRAT1, cobbles and boulders derived from Tschicoma lava flows occur in a matrix of reworked pumice and ash, filling a paleochannel that cut 0.8 m into the underlying Otowi Member. At OU-1106-STRAT3, a paleochannel in the middle of the Cerro Toledo interval contains Tschicoma boulders up to 1 m in diameter.

It is important to note that the proportion of tuffaceous to dacitic detritus making up deposits at this stratigraphic horizon varies from location to location across the Pajarito Plateau. Whereas Cerro Toledo deposits described in this report are dominantly tuffaceous in character, rocks at this stratigraphic horizon in lower DP Canyon (Goff, Sec. II, this report) and in the subsurface at TA-55 (Gardner *et al.* 1993) consist predominantly of coarse dacitic detritus derived from the Tschicoma Formation and include only subordinant amounts of interbedded tuffaceous detritus. The coarse dacitic deposits in the Cerro Toledo horizon are similar to those found in the Puye Formation, a volcanic fanglomerate that lies beneath the Otowi Member. The similarity of Cerro Toledo deposits to those of the Puye Formation and the mixed provenance of the detritus within these deposits indicates that Puye-like alluvial fans continued to develop on the east side of the Jemez Mountains after deposition of the Otowi Member and during the period of Cerro Toledo volcanic activity.

Tshirege Member

The Tshirege Member is a multiple-flow ash-flow sheet that forms the prominent cliffs at TA-21. It is a compound cooling unit whose physical properties vary vertically and laterally. Variations in physical properties result from zonal patterns of welding and crystallization determined by emplacement temperature, thickness, gas content, and composition (Smith, 1960a,b). The thickness of this unit ranges from 89 to 98 m in the three sections measured. All but the uppermost unit (unit 4) of the Tshirege Member occur at TA-21.

Previous workers identified mappable subunits in the Tshirege Member based on a combination of surface-weathering patterns, welding features, and crystallization characteristics (Baltz *et al.*, 1963; Weir and Purtymun, 1962; Crowe *et al.*, 1978; Vaniman and Wohletz, 1990, 1991). Figure 3 correlates the stratigraphic units used by these earlier workers. A certain amount of confusion has resulted from inconsistent use of unit names for the Tshirege Member. In part, this confusion occurs because different criteria were used by different workers to identify the units. But equally important, the differences in nomenclature arose because the internal stratigraphy of the Tshirege Member varies laterally as a function of distance from the caldera source.

This paper generally follows the stratigraphic nomenclature of Vaniman and Wohletz (1990,1991) to describe subunits of the Tshirege Member because their geologic map overlaps the western end of TA-21. However, we do deviate from their nomenclature in two respects. First, we include their nonwelded unit below unit 2 as part of unit 1v because all tuffs below unit 2 are nonwelded. Second, we define unit 1v as a lower resistant orange-

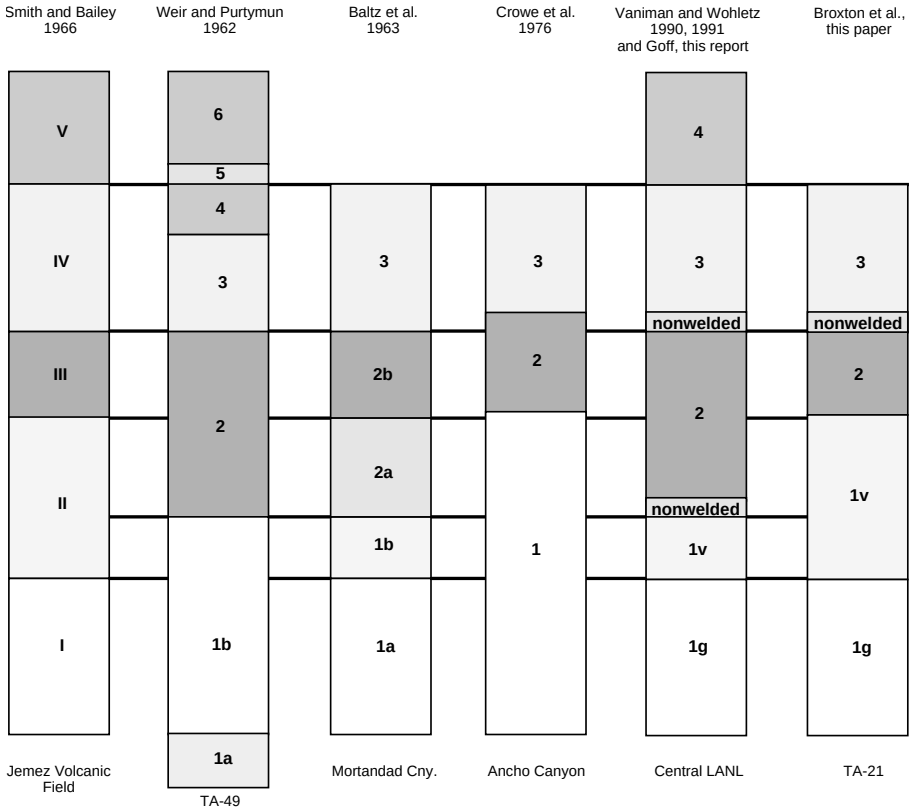

Fig. 3. Stratigraphic nomenclature for the Tshirege Member as used in this report correlated to that of other investigators working on the Pajarito Plateau.

brown colonnade tuff overlain by an upper slope-forming light-colored nonwelded tuff. Vaniman and Wohletz (1990, 1991) considered the upper-slope-forming, light-colored nonwelded tuff as part of unit 2. We believe the Tshirege nomenclature used in this report better reflects the presence of three distinct cooling units in this compound cooling unit at this location. Earth scientists for the ER program are presently conducting stratigraphic studies on the Pajarito Plateau to resolve differences between the different systems of stratigraphic nomenclature used by Los Alamos ER investigators.

Tsankawi Pumice Bed. The Tsankawi Pumice Bed is the basal pumice fall of the Tshirege Member (see Fig. 2, Goff, Sec. II, this report). This pumice bed is 73 to 95 cm thick where exposed and consists of two subunits, each of which has normally graded bedding. The lower subunit is 60 to 74 cm thick and contains equant, angular to subangular clast-supported pumice lapilli up to 6-cm diameter. Pumices are typically fibrous with a vitreous luster. Coarse ash and abundant phenocrysts make up the matrix. A 2- to 7-cm-thick ash bed made up of fragmented pumice, ash, and crystals overlies the lower pumice bed. The upper pumice bed is 13 to 14 cm thick and consists of clast-supported pumice lapilli that grade upwards into a coarse ash bed at the top of the unit.

Pumices in the Tsankawi Pumice Bed are rhyolitic in composition and contain ~5% phenocrysts. Phenocrysts consist of 0.2- to 2-mm sanidine and quartz. There is also a small (<5%) population of medium-gray, dense, finely vesiculated dacitic hornblende-bearing pumice in the Tsankawi Pumice Bed. In addition to hornblende, these finely vesiculated pumices contain clinopyroxene and small subhedral grains of plagioclase. These hornblende-bearing pumices are a diagnostic feature of the Tsankawi Pumice Bed and overlying ash-flow units (Bailey *et al.*, 1969). Lithics make up 1 to 2 % of these pumice beds and consist of dark-gray to dark-red clasts derived from porphyritic dacite. Lithics are 0.5 to 4 cm in diameter.

Tshirege Unit 1g. Unit 1g is the lowermost unit in the thick ignimbrite deposit of the Tshirege Member. This 22- to 32-m-thick unit is poorly indurated but commonly forms near-vertical cliffs because a prominent resistant bench occurs at the top of the unit, forming a protective cap over softer, underlying tuffs.

Fresh tuff surfaces are light-gray to white at the base of the unit but gradually become light pink-orange 9 to 12 m above the base. This color change becomes more pronounced upsection and coincides with the tuffs becoming more resistant to erosion. The uppermost part of unit 1g is a resistant, cliff-forming tuff, the top of which forms a nearly-flat-lying bench up to several meters wide locally. The hardness of these uppermost tuffs may be the result of incipient welding or incipient devitrification near the top of the unit. The bench at the top of the unit marks the base of the vapor-phase notch (Crowe *et al.*, 1978) which is discussed in more detail below. Outcrop surfaces in unit 1g typically weather to a pale-orange color. Weathered cliff faces have a distinctive swiss-cheese appearance because large holes penetrate case-hardened cliff faces and expose the soft underlying tuffs to wind and water erosion.

Unit 1g is a nonwelded, poorly sorted, vitric ignimbrite. It consists of light-gray, vitreous, crystal-rich pumice lapilli supported by a matrix of coarse ash, shards, pumice fragments, and abundant sanidine and quartz phenocrysts. As observed in thin section, delicate glass shards are clear and perfectly preserved and show no evidence of secondary alteration. Glass in the shards is tan to brown in tuffs just below the vapor-phase notch. Pumice lapilli typically make up 30 to 50% of the rock. These lapilli are commonly equant and fibrous, and they are 2 to 5 cm in diameter. Locally, pumice clasts are up to

14 cm in diameter. Most pumices are rhyolitic in composition, but dacitic hornblende-bearing pumices also occur in small amounts.

A distinctive pumice-poor surge deposit forms the base of this unit. This surge bed is 10 to 25 cm thick and contains undulating, laminated, dune-like beds. These surge deposits consist of coarse ash and abundant broken crystals. Individual beds in this unit are 0.5 to 9 cm thick. Some of the surge beds have low-angle cross beds in which laminations are 1 to 30 mm thick and have normal grading. The undulating tops for some of these surge deposits have wavelengths of up to 4 m. The surge deposit is overlain by a thick ignimbrite that makes up the remainder of the unit. The lower 0.3 to 0.7 m of this ignimbrite is an ash-rich tuff that grades upwards into the main body of the deposit, which consists of nonstratified tuff containing abundant pumice lapilli and blocks. This ignimbrite was probably deposited by the passage of a single, large ash flow.

Phenocrysts make up 12 to 16% of unit 1g (Table II, Fig. 2). Sanidine and quartz make up >98% of the phenocryst assemblage, and the maximum size is 2 to 3 mm. Clinopyroxene, hornblende, and fayalite are the dominant ferromagnesian minerals; magnetite, zircon, and perrierite/chevkinite/allanite are accessory minerals. Most of the hornblende and plagioclase identified during point counts of bulk rock samples are associated with a dacitic hornblende-bearing pumice similar to that found in the Tsankawi Pumice Bed. The remainder of the hornblende and plagioclase occurs in the tuff matrix and probably was derived from disaggregation of hornblende-bearing pumice during emplacement. One particularly large hornblende-bearing pumice was thin-sectioned and point-counted (Table II; sample OU-1106-STRAT2-6). Phenocrysts, making up 41% of this pumice, consist of hornblende, plagioclase, clinopyroxene, orthopyroxene, and minor sanidine; accessory minerals include magnetite and zircon.

Lithics are typically sparse (<1%) in unit 1g. Lithic clasts are usually reddish-brown-to-black porphyritic dacite and crystal-poor, devitrified welded tuffs. Rare granitic lithics also occur in these tuffs. Most lithics are 0.2 to 5 cm in diameter.

Tshirege Unit 1v. Unit 1v forms a combination of cliff-like and sloping outcrops that separates the resistant bench at the top of unit 1g from the near-vertical cliff of unit 2 (see Fig. 3 of Goff; Sec. II, this report). The base of unit 1v is a resistant orange-brown colonnade tuff that overlies the bench at the top of unit 1g. This colonnade tuff forms a 1- to 3-m-thick cliff that has distinctive columnar jointing. These features suggest the colonnade tuff may be slightly welded, although pumices show no discernable compaction at hand-specimen scale. The colonnade tuff is overlain by slope-forming tuffs that make up the bulk of unit 1v. These slope-forming tuffs form a distinctive white band of outcrops sandwiched between the darker colored outcrops of the colonnade tuff and unit 2. The light-colored tuffs lack discernable bedding or parting features at TA-21, but these features are present in other locations and indicate the presence of multiple flow units. The upper contact of unit 1v corresponds to the abrupt transition from light-colored, nonwelded, slope-forming tuffs to the darker, partially welded, cliff-forming tuffs of unit 2. At locations east of TA-21 (for example, at TA-54), thin but well-defined surge beds mark the contact between units 1v and 2. These surge beds are absent at TA-21. Unit 1v thickens eastward from 16 to 20 m at TA-21.

Unit 1v is a nonwelded, poorly sorted, devitrified ignimbrite. It consists of tubular, crystal-rich pumice lapilli supported by a light-gray-to-white ashy matrix of shards, pumice fragments, and abundant phenocrysts. Relict shards occur in a cryptocrystalline groundmass. Pumice lapilli typically make up 30 to 50% of the rock and are 0.2 to

6 cm in diameter. Pumices are chocolate-brown to dark purple-gray in the lower colonnade tuff and grade upwards into a light-gray to medium-gray color in the overlying white tuffs. Pumice color variations correspond with mineralogical changes that accompany increasing vapor-phase alteration upsection. Cristobalite is the dominant secondary silica mineral in the colonnade tuff whereas tridymite is more common in the white tuffs. Pumice lapilli typically have a sugary texture as a result of more intense vapor-phase crystallization in the upper part of the unit. Much of the original vesicular structure of pumices is preserved in hand samples. However, on the microscopic scale, most of the fine structure in pumices is destroyed by devitrification and vapor-phase crystallization. Overlapping spherulites, octahedral cristobalite, and lath-like tridymite (in the upper part of the unit) replace the original volcanic glass in the pumices. The colonnade tuff has a pock-marked appearance because of the selective weathering of soft pumice from the enclosing, more resistant matrix.

The vapor-phase notch at the base of this unit is a thin, horizontal zone of preferential weathering that forms a widespread mappable marker horizon throughout the Pajarito Plateau. There is no depositional break associated with the vapor-phase notch at TA-21 or at other localities. The abrupt transition from vitric tuffs below the notch to devitrified tuffs above suggests that this feature is

TABLE III

LITHOLOGIC CHARACTERISTICS OF THE VAPOR-PHASE NOTCH IN STRATIGRAPHIC SECTION OU-1106-STRAT2 AT TA-21

	Tuffs Immediately Below Notch	Tuffs in the Vapor-Phase Notch	Tuffs Immediately Above Notch
Pumice	Original glass in pumice disappears rapidly upward; pumices make up ~50% of rock; size 0.2 to 9 cm.	Original volcanic glass mostly destroyed by devitrification; sugary texture; size 0.2 to 4 cm.	Devitrified relict pumice makes up ~50% rock; sugary texture; 0.2 to 6 cm; no visible compaction but may be slightly welded.
Matrix	Small fragments of vitric pumice; pale, peach-colored, crystal-rich, devitrified ashy matrix.	White, fine-grain, devitrified ash, relict small pumice fragments, and phenocrysts; most original textures destroyed.	Fine-grain, devitrified, crystal-rich ash, relict small pumice fragments; texture of small pumice fragments well preserved.
Lithics	Dark-gray and -brown porphyritic and aphanitic lavas; ~3% of rock; size 0.5 to 6 cm.	Light-gray lavas, and black obsidian, ~3% of rock; size 0.5 to 2 cm.	Light-gray lavas; abundance varies vertically from 1 to 5%; size 0.5 to 5 cm.
Color on Fresh Surfaces	Pale pink to orange grading up to dark orange.	Light-gray with pink hue; wispy areas of dark orange.	White and pink matrix; chocolate-brown and dark-gray pumices.
Weathering Characteristics	Grades up from white, poorly indurated tuffs that form rounded outcrops to orange, resistant bench; large "pot" holes, where case-hardened surface penetrated by erosion; pumice more resistant to erosion than matrix; lacks fractures.	Soft, horizontal, preferentially eroded recess in rock defined by alignment of 1.5-m-tall flattened caves; sometimes forms bench several meters wide; fractures from above terminate abruptly in this zone.	Colonnade, resistant tuff; orange-brown outcrops; distinctive "pockmarked" surfaces from selective erosion of soft, altered pumice.

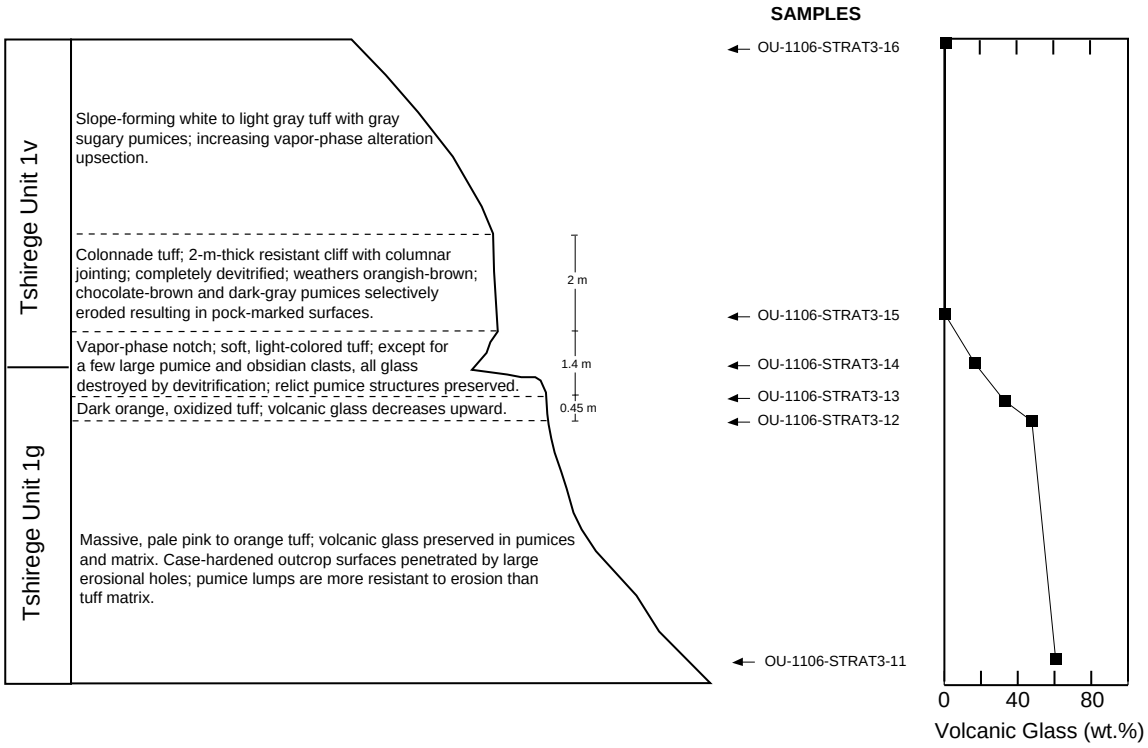

Fig. 4. Detail of lithologic changes across the vapor-phase notch in stratigraphic section OU-1106-STRAT3 at TA-21. The vapor-phase notch marks the rapid transition from vitric tuffs below to devitrified and vapor-phase altered tuffs above. Volcanic glass is the most abundant constituent in tuffs of unit 1g, but disappears abruptly upsection over a 2 m interval within the vapor-phase notch. The contact between units 1g and 1v is arbitrary chosen as the first occurrence of volcanic glass as one moves downsection through the vapor-phase notch interval.

the base of the devitrification that occurred in the hot interior of the cooling ash-flow sheet after emplacement. Initially, primary volcanic glass was deposited within all parts of the Tshirege Member, but high heat retention and outgassing of volatiles caused all of the glass above the vapor-phase notch to crystallize to alkali feldspar and silica polymorphs. Table III and Fig. 4 summarize the principal lithological and mineralogical characteristics of the vapor-phase notch.

Phenocryst assemblages and abundances are similar to those in unit 1g (Table II, Fig. 2). Ferromagnesian phenocrysts show increasing degrees of oxidation up section. Fayalite is more common than in unit 1g. Lithic clasts make up 1 to 5% of the tuff near the base of the unit but decrease to <1% in the upper part. Most lithics are 0.5 to 5 cm in diameter and are similar to those described for unit 1g. Near-vertical fractures penetrate the tuffs in unit 1v. These fractures appear to be downward extensions of prominent fractures in unit 2. Some of the fractures penetrate across the vapor-phase notch before dying out in the softer tuffs of unit 1g.

Tshirege Unit 2. Unit 2 is the 25- to 27-m-thick, vertical cliff-forming unit in the Tshirege Member at TA-21. The first appearance of unconsolidated nonwelded tuffs on the broad bench on top of unit 2 defines its upper contact. This unit forms a distinctive, medium-brown, vertical cliff that stands out in marked contrast to the slope-forming, lighter colored tuffs above and below (see Fig. 3 of Goff; Sec II, this report). This unit is the zone of greatest welding in the Tshirege Member at TA-21, and its thickness decreases from 21 to 10 m eastward.

Unit 2 is a poorly sorted, vapor-phase-altered ignimbrite. The tuffs consist of relatively sparse, crystal-rich pumice lapilli supported by an ashy matrix of shards, pumice fragments, and abundant phenocrysts. The compaction of pyroclasts in the tuff increases upsection and is greatest in the upper part of the unit. The tuff matrix is light pinkish-tan to light-purplish-gray, and the degree of coloration increases with increased welding. Pumice lapilli are medium-gray to grayish-brown in color and have aspect ratios of 1.5:1 to 2:1 (partially welded) near the base of the unit and 5:1 to 10:1 (moderately to densely welded) near the top of the unit.

Pumices are generally smaller (commonly < 2 cm) and relatively sparse (5 to 30% of the rock) compared to those found in lower units. Horizontal pumice swarms contain lapilli from 5 to 14 cm in length locally. These pumice swarms suggest that unit 2 is made up of several ignimbrite deposits.

Devitrification and vapor-phase crystallization destroyed most of the original vitroclastic textures in these tuffs. Relict shards with axiolitic textures occur in a cryptocrystalline to microcrystalline groundmass. Pumices were particularly susceptible to vapor-phase alteration and typically have a granophyric texture in thin section. Hand specimens of pumice appear sugary in texture because of the deposition of coarse (up to 0.3-mm) crystals of tridymite and sanidine. Vapor-phase alteration also has resulted in both the deposition of thin mantles of alkali feldspar around sanidine phenocrysts and the oxidation of ferromagnesian phenocrysts.

The phenocryst assemblages are similar to those in units 1g and 1v, but the phenocryst abundances (17 to 20%) are slightly greater—in part as a result of the lower porosities of these more compacted tuffs (Table II, Fig. 2). Hornblende-bearing pumices similar to those described for unit 1g occur in small amounts (<5%) throughout the unit. Lithic clasts are rare (<1%) and mostly consist of devitrified rhyolitic volcanic rocks. Most lithics are <3 cm in diameter.

Well-developed fractures are characteristic of this unit. Most fractures are nearly vertical and trend N-S to N70W. Some horizontal and low-angle fractures are also present. Fracture spacing is commonly 0.2 to 2 m in the upper, more densely welded portion of the tuff. Fracture apertures range from 1 mm to 4 cm. Many fractures have at least two generations of fracture-filling material. Calcite is the oldest material deposited and it commonly forms a lining up to 0.5 mm thick on the fracture walls. The centers of fractures are filled with brown clays and detritus washed into the fractures from the surface. Additional, more detailed information about fractures in unit 2 is given in the section by Wohletz (Sec. III, this report).

Nonwelded Tuff. Nonwelded tuff underlies the broad, gently sloping bench developed on top of unit 2. These nonwelded tuffs form white, soft outcrops that weather into low, rounded mounds. Talus from the overlying cliffs of unit 3 commonly covers outcrops of the nonwelded tuffs. The contact with unit 3 is gradational and is arbitrarily defined as the break in slope at the base of the uppermost cliff at TA-21. The thickness of the nonwelded unit varies from 10 m in the western part of TA-21 to 5 m in the east.

The nonwelded tuff is a pumice-poor, vapor-phase-altered ignimbrite. It consists dominantly of a white-to-light-gray, ashy matrix of shards, pumice fragments, and abundant phenocrysts. Relict shards have axiolitic textures and the groundmass is cryptocrystalline to microcrystalline. Pumice clasts are sparse (~5%) and have a sugary texture. The light-gray pumice clasts are difficult to distinguish from the light-colored tuff matrix. Pumice clasts are generally equant and range from 1 to 3 cm; rare, isolated pumices are up to 14 cm in length. Vapor-phase alteration of

these tuffs is extensive and has resulted in deposition of tridymite and sanidine in pumices, feathery overgrowths of alkali feldspar around sanidine phenocrysts, and oxidation of most ferromagnesian phenocrysts.

The phenocryst assemblage in the nonwelded unit is similar to that described for the lower units of the Tshirege Member (Table II, Fig. 2). Hornblende-bearing pumices also occur in these tuffs. One notable characteristic of these deposits is that phenocrysts are unusually abundant (21%), given the nonwelded, porous nature of these tuffs. When phenocryst abundances are corrected for porosity effects, the nonwelded unit (~35% phenocrysts) is significantly more crystal-rich than unit 2. At present, it is uncertain whether the nonwelded unit represents the nonwelded top of unit 2 or the base of unit 3. The upward increase in phenocryst contents and the abrupt change from welded tuff to nonwelded tuff suggest that the contact between the nonwelded unit and unit 2 is a partial cooling break that marks a brief hiatus in ash flow eruptions. If this is correct, the nonwelded unit is the lower part of a cooling unit that includes unit 3.

Lithic clasts are rare (<1%) and consist of light-gray, crystal-poor rhyolite and dark-gray porphyritic dacite. These clasts are typically subangular and equant. Most lithics are <4 cm in diameter.

Fractures propagate through this unit despite its nonwelded and poorly indurated nature. Calcite is the oldest fracture-filling material and commonly is deposited on fracture surfaces. The centers of fractures are commonly filled by a mixture of calcite and surface-derived detritus. Fracture apertures range from 2 to 4 cm.

Tshirege Unit 3. Unit 3 is the 16- to 18-m-thick bedrock unit that hosts the subsurface SWMUs at TA-21. Although less steep than unit 2, unit 3 is the prominent cliff-forming unit that forms the caprock of DP Mesa (see Fig. 3 of Goff, Sec. II, this report). Surface exposures are weathered to tan or orangish-tan, but fresh tuff surfaces are light gray.

Unit 3 is a nonwelded to partially welded, vapor-phase-altered ignimbrite. The tuff contains 10 to 20% crystal-rich pumice lapilli in an ashy matrix made up of shards, pumice fragments, and abundant phenocrysts. Local pumice swarms occur in the tuff and contain up to 30% pumice lapilli. Compaction of pyroclasts in the unit is slight and decreases noticeably eastward from STRAT3 to STRAT1. The matrix is white to light gray in the nonwelded tuffs and light gray with a pinkish cast in the partially welded tuffs. The preservation of relict pumices is generally good. Pumices commonly are 1 to 4 cm long and, rarely, up to 10 cm long. They are typically gray to brown and have a sugary appearance. Granophyric intergrowths of sanidine and tridymite and overlapping microcrystalline sheaves of spherulites replace the interiors of pumices. Shards are generally axiolitic and occur in a phenocryst-rich, cryptocrystalline-to-microcrystalline groundmass. Sanidine phenocrysts commonly have feathery overgrowths of alkali feldspar deposited by high-temperature vapors following emplacement of the tuffs. Ferromagnesian phenocrysts show variable degrees of oxidation resulting from vapor-phase alteration.

Phenocrysts make up 18 to 20% of these porous tuffs. Estimates of porosity-free phenocryst abundances range from 35 to 40%, reflecting an overall increase in phenocrysts from unit 1g to unit 3. Sanidine and quartz make up most of the phenocrysts, but the ratio of sanidine to quartz is greater than in underlying units (Table II, Fig. 2). The maximum size of phenocrysts is 2 to 3.5 mm. Clinopyroxene and hornblende are the dominant ferromagnesian minerals; fayalite is absent in these tuffs. Magnetite, zircon, perrierite/chevkinite/allanite, and sphene are accessory minerals. The sphene is present as

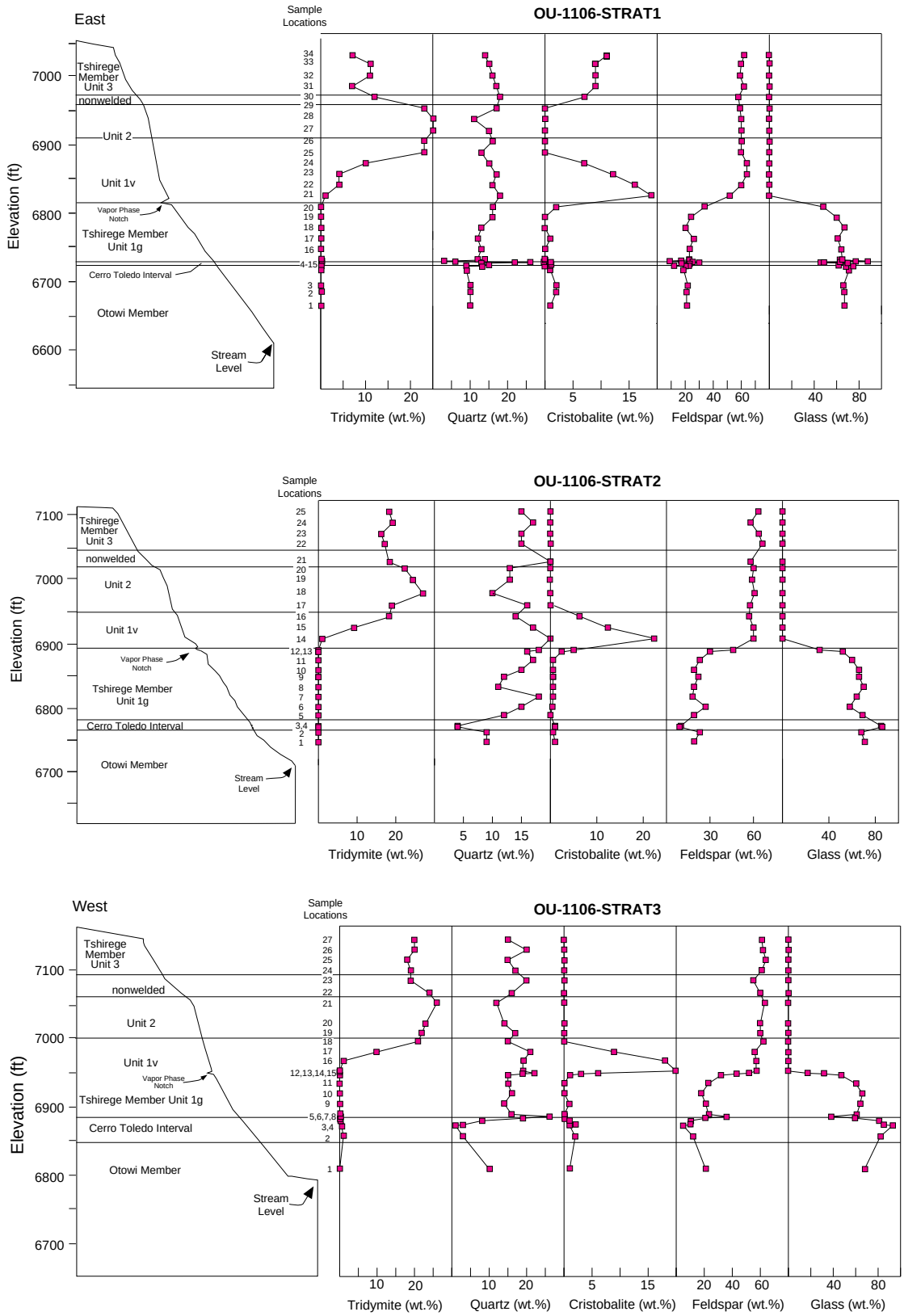

Fig. 5. Variation diagrams showing the mineralogy of tuffs in stratigraphic sections at TA-21. Canyon wall profile from FIMAD topographic base; 3x vertical exaggeration. Vapor-phase notch is also exaggerated.

TABLE IV

X-RAY DIFFRACTION ANALYSES OF TUFFS AT TA-21 [a]

Stratigraphic Section #1 (Easternmost Section)

Sample Field Number	Elevation (ft)	Unit [b]	Smectite	Tridymite	Quartz	Cristo-balite	Feldspar	Glass	Hornblende	Mica	Hematite	Magnetite	Kaolinite	Gypsum	Calcite	∑ Crystalline Phases
OU-1106-STRAT1-34	7036.2	Qbt-3	--	7 ± 1	14 ± 1	11 ± 1	62 ± 9	--	--	--	1 ± 1	--	--	--	--	95 ± 9
OU-1106-STRAT1-33	7023.4	Qbt-3	--	11 ± 1	15 ± 1	9 ± 4	60 ± 8	--	--	Tr	2 ± 1	--	--	--	--	97 ± 9
OU-1106-STRAT1-32	7006.4	Qbt-3	--	11 ± 1	16 ± 1	9 ± 4	59 ± 8	--	--	--	1 ± 1	--	--	--	--	96 ± 9
OU-1106-STRAT1-31	6990.1	Qbt-3	--	7 ± 1	17 ± 1	9 ± 4	62 ± 9	--	--	--	1 ± 1	--	--	--	--	96 ± 10
OU-1106-STRAT1-30	6974.2	Qbt-nw	--	12 ± 1	18 ± 1	7 ± 3	58 ± 8	--	--	--	1 ± 1	--	--	--	--	96 ± 9
OU-1106-STRAT1-29	6957.5	Qbt-2	--	23 ± 2	17 ± 1	--	59 ± 8	--	--	--	1 ± 1	--	--	--	--	100 ± 8
OU-1106-STRAT1-28	6941.3	Qbt-2	--	25 ± 2	11 ± 1	--	60 ± 8	--	--	--	Tr	--	--	--	--	96 ± 8
OU-1106-STRAT1-27	6924.1	Qbt-2	Tr	25 ± 2	15 ± 1	--	60 ± 8	--	--	--	1 ± 1	--	--	--	--	101 ± 8
OU-1106-STRAT1-26	6908.5	Qbt-1v	1 ± 1	23 ± 2	16 ± 1	--	60 ± 8	--	--	--	1 ± 1	--	--	--	2 ± 1	103 ± 8
OU-1106-STRAT1-25	6891.5	Qbt-1v	--	23 ± 2	13 ± 1	--	60 ± 8	--	Tr	--	1 ± 1	--	--	--	--	97 ± 8
OU-1106-STRAT1-24	6875.5	Qbt-1v	--	10 ± 1	15 ± 1	7 ± 3	64 ± 9	--	1 ± 1	Tr	2 ± 1	--	--	--	--	99 ± 10
OU-1106-STRAT1-23	6858.8	Qbt-1v	Tr	4 ± 1	17 ± 1	12 ± 1	64 ± 9	--	Tr	--	1 ± 1	--	--	--	--	98 ± 9
OU-1106-STRAT1-22	6843.3	Qbt-1v	Tr	4 ± 1	16 ± 1	16 ± 1	60 ± 8	--	Tr	--	Tr	--	--	--	--	96 ± 8
OU-1106-STRAT1-21	6827.1	Qbt-1v	--	1 ± 1	18 ± 1	19 ± 1	52 ± 7	--	Tr	--	Tr	--	--	--	--	90 ± 7
OU-1106-STRAT1-20	6810.4	Qbt-1g	--	--	16 ± 1	2 ± 1	34 ± 5	48 ± 5	Tr	--	Tr	--	--	--	--	52 ± 5
OU-1106-STRAT1-19	6794.9	Qbt-1g	Tr	--	16 ± 1	Tr	24 ± 3	60 ± 3	--	--	Tr	--	--	--	--	40 ± 3
OU-1106-STRAT1-18	6779.2	Qbt-1g	--	--	13 ± 1	Tr	20 ± 3	67 ± 3	--	--	--	--	--	--	--	33 ± 3
OU-1106-STRAT1-17	6763.2	Qbt-1g	--	--	12 ± 1	1 ± 1	26 ± 4	61 ± 4	--	--	--	--	--	--	--	39 ± 4
OU-1106-STRAT1-16	6747.4	Qbt-1g	--	--	13 ± 1	--	23 ± 3	64 ± 3	--	--	--	--	--	--	--	36 ± 3
OU-1106-STRAT1-15	6732.3	Qbt-1g	--	--	12 ± 1	--	23 ± 3	65 ± 3	--	--	--	--	--	--	--	35 ± 3
OU-1106-STRAT1-14	6731.3	Qbt-1g	--	--	14 ± 1	--	23 ± 3	63 ± 3	--	--	--	--	--	--	--	37 ± 3
OU-1106-STRAT1-13	6729.5	Qbt-1g	--	--	3 ± 1	--	9 ± 1	88 ± 1	--	--	--	--	--	--	--	12 ± 1
OU-1106-STRAT1-12	6729.2	Qbt-1g	--	--	6 ± 1	--	17 ± 2	77 ± 2	--	--	--	--	--	--	--	23 ± 2
OU-1106-STRAT1-11	6727.5	Qbt-1g	Tr	--	26 ± 2	--	25 ± 4	49 ± 4	Tr	Tr	--	--	--	--	--	51 ± 4
OU-1106-STRAT1-10	6727.3	Qct	1 ± 1	--	22 ± 2	1 ± 1	30 ± 4	46 ± 4	--	Tr	--	--	Tr	--	--	54 ± 5
OU-1106-STRAT1-9	6726.4	Qct	Tr	--	13 ± 1	--	17 ± 2	70 ± 2	--	--	--	--	--	Tr?	--	30 ± 2
OU-1106-STRAT1-8	6726.1	Qct	Tr	--	13 ± 1	Tr	24 ± 3	63 ± 3	--	--	--	--	Tr	--	--	37 ± 3
OU-1106-STRAT1-7	6723.7	Qct	Tr	--	15 ± 1	Tr	23 ± 3	62 ± 3	--	--	--	--	--	--	--	38 ± 3
OU-1106-STRAT1-6	6722.3	Qct	Tr	--	13 ± 1	--	12 ± 2	75 ± 2	--	--	--	--	--	--	--	25 ± 2
OU-1106-STRAT1-5	6722	Qbo	Tr	--	9 ± 1	1 ± 1	21 ± 3	69 ± 3	--	--	Tr	--	--	--	--	31 ± 3
OU-1106-STRAT1-4	6715.8	Qbo	--	--	9 ± 1	1 ± 1	19 ± 3	71 ± 3	--	--	Tr	--	--	--	--	29 ± 3
OU-1106-STRAT1-3	6692.7	Qbo	Tr	--	10 ± 1	2 ± 1	22 ± 3	66 ± 3	--	--	--	--	--	--	--	34 ± 3
OU-1106-STRAT1-2	6683.4	Qbo	Tr	--	10 ± 1	2 ± 1	21 ± 3	67 ± 3	Tr	--	--	--	--	--	--	33 ± 3
OU-1106-STRAT1-1	6662.9	Qbo	1 ± 1	--	10 ± 1	1 ± 1	21 ± 3	67 ± 3	--	--	--	--	--	--	--	33 ± 3

[a] *Mineral abundances reported as weight percent; uncertainties are two standard deviation estimates of analytical precision; -- indicates mineral not detected; Tr = trace abundance (<0.5 wt. %).*

[b] *Stratigraphic Unit - Qbo = Otowi Member of the Bandelier Tuff; Qct = Cerro Toledo interval; Qbt-1g = Tshirege unit 1g; Qbt-1v = Tshirege unit 1v; Qbt-2 = Tshirege unit 2; Qbt-nw = nonwelded tuff; Qbt-3 = Tshirege unit 3.*

TABLE IV (CONT)

X-RAY DIFFRACTION ANALYSES OF TUFFS AT TA-21

Stratigraphic Section #2 (Central DP Mesa)

Sample Field Number	Elevation (ft)	Unit [b]	Smectite	Tridymite	Quartz	Cristo-balite	Feldspar	Glass	Hornblende	Mica	Hematite	Magnetite	Kaolinite	Gypsum	Calcite	Σ Crystalline Phases
OU-1106-STRAT2-25	7103.8	Qbt-3	Tr	18 ±1	15 ±1	--	64 ± 9	--	--	--	1 ±1	--	--	--	--	98 ± 9
OU-1106-STRAT2-24	7086.7	Qbt-3	Tr	19 ±1	17 ±1	--	58 ± 8	--	--	--	1 ±1	--	--	--	--	95 ± 8
OU-1106-STRAT2-23	7069.3	Qbt-3	--	16 ±1	15 ±1	--	63 ± 9	--	--	--	1 ±1	--	--	--	--	95 ± 9
OU-1106-STRAT2-22	7053.8	Qbt-3	--	17 ±1	15 ±1	--	66 ± 9	--	Tr	--	1 ±1	--	--	--	--	99 ± 9
OU-1106-STRAT2-21	7025.9	Qbt-nw	Tr	18 ±1	20 ±2	--	58 ± 8	--	Tr	--	1 ±1	--	--	--	--	97 ± 8
OU-1106-STRAT2-20	7015.8	Qbt-2	--	22 ±2	13 ±1	--	60 ± 8	--	--	--	1 ±1	--	--	--	--	96 ± 8
OU-1106-STRAT2-19	6998	Qbt-2	Tr	24 ±2	13 ±1	--	59 ± 8	--	--	--	1 ±1	--	Tr	--	--	97 ± 8
OU-1106-STRAT2-18	6977.1	Qbt-2	--	27 ±2	10 ±1	--	61 ± 9	--	--	--	Tr	--	--	--	--	98 ± 9
OU-1106-STRAT2-17	6958.2	Qbt-2	--	19 ±1	16 ±1	--	58 ± 8	--	Tr	--	1 ±1	--	--	--	Tr	94 ± 8
OU-1106-STRAT2-16	6941.2	Qbt-1v	--	18 ±1	14 ±1	5 ±2	57 ± 8	--	Tr	Tr	1 ±1	--	--	--	--	95 ± 8
OU-1106-STRAT2-15	6923.7	Qbt-1v	--	9 ±1	17 ±1	10 ±1	60 ± 8	--	Tr	Tr	--	--	--	--	--	96 ± 8
OU-1106-STRAT2-14	6906.6	Qbt-1v	Tr	1 ±1	20 ±2	18 ±1	60 ± 8	--	--	Tr	--	--	--	--	--	99 ± 8
OU-1106-STRAT2-13	6889	Qbt-1v	--	--	18 ±1	4 ±1	46 ± 6	32 ± 6	Tr	--	Tr	--	--	--	--	68 ± 6
OU-1106-STRAT2-12 (pumice)	6886.5	Qbt-1g	Tr	--	7 ±1	1 ±1	20 ± 3	71 ± 3	--	--	1± 1	--	--	--	--	29 ± 3
OU-1106-STRAT2-12 (matrix)	6886.5	Qbt-1g	Tr	--	16 ±1	2 ±1	30 ± 4	52 ± 4	--	--	Tr	--	--	--	--	48 ± 4
OU-1106-STRAT2-11	6873.5	Qbt-1g	--	--	17 ±1	Tr	23 ± 3	60 ± 3	Tr	--	Tr	--	--	--	--	40 ± 3
OU-1106-STRAT2-10	6858.1	Qbt-1g	--	--	15 ±1	Tr	19 ± 3	66 ± 3	Tr	--	Tr	--	--	--	--	34 ± 3
OU-1106-STRAT2-9 (pumice)	6847.4	Qbt-1g	--	--	13 ±1	Tr	12 ± 2	75 ± 2	--	--	Tr	--	--	--	--	25 ± 2
OU-1106-STRAT2-9 (matrix)	6847.4	Qbt-1g	--	--	12 ±1	Tr	22 ± 3	66 ± 3	--	--	Tr	--	--	--	--	34 ± 3
OU-1106-STRAT2-8	6831.8	Qbt-1g	--	--	11 ±1	Tr	19 ± 3	70 ± 3	--	--	--	--	--	--	--	30 ± 3
OU-1106-STRAT2-7	6816.6	Qbt-1g	Tr	--	18 ±1	Tr	18 ± 3	64 ± 3	--	--	--	--	--	--	--	36 ± 3
OU-1106-STRAT2-6	6800.9	Qbt-1g	--	--	15 ±1	Tr	27 ± 4	58 ± 4	Tr	--	Tr	--	--	--	--	42 ± 4
OU-1106-STRAT2-5	6788	Qbt-1g	Tr	--	12 ±1	1 --	19 ± 3	69 ± 3	Tr	--	--	--	--	--	--	31 ± 3
OU-1106-STRAT2-4	6771.2	Qct	Tr	--	4 ±1	±1	10 ± 1	85 ± 1	--	--	--	--	--	--	--	15 ± 2
OU-1106-STRAT2-3	6769.7	Qct	Tr	--	4 ±1	1 ±1	9 ± 1	86 ± 1	--	--	--	--	--	--	--	14 ± 2
OU-1106-STRAT2-2	6761.3	Qbo	Tr	--	9 ±1	Tr	23 ± 3	68 ± 3	--	--	--	--	--	--	--	32 ± 3
OU-1106-STRAT2-1	6746.4	Qbo	Tr	--	9 ±1	1 ±1	19 ± 3	71 ± 3	--	--	--	--	--	--	--	29 ± 1

TABLE IV (cont)

X-Ray Diffraction analyses of Tuffs at TA-21

Stratigraphic Section #3 (Westernmost Section)

Sample Field Number	Elevation (ft)	Unit [b]	Smectite	Tridymite	Quartz	Cristo-balite	Feldspar	Glass	Hornblende	Mica	Hematite	Magnetite	Kaolinite	Gypsum	Calcite	∑ Crystalline Phases
OU-1106-STRAT3-27	7150.8	Qbt-3	--	20 ± 2	15 ± 1	--	61 ± 9	--	--	--	1 ± 1	--	--	--	--	97 ± 9
OU-1106-STRAT3-26	7133.9	Qbt-3	--	20 ± 2	20 ± 2	--	62 ± 9	--	--	--	1 ± 1	--	--	--	--	103 ± 9
OU-1106-STRAT3-25	7117.7	Qbt-3	--	18 ± 1	15 ± 1	--	64 ± 9	--	--	--	1 ± 1	--	--	--	--	98 ± 9
OU-1106-STRAT3-24	7100.8	Qbt-3	--	19 ± 1	17 ± 1	--	61 ± 9	--	Tr	--	1 ± 1	--	--	--	--	98 ± 9
OU-1106-STRAT3-23	7084.5	Qbt-nw	--	19 ± 1	20 ± 2	--	55 ± 8	--	--	--	1 ± 1	--	--	--	--	95 ± 8
OU-1106-STRAT3-22	7063.7	Qbt-nw	--	24 ± 2	16 ± 1	--	60 ± 8	--	--	--	--	--	--	--	--	100 ± 8
OU-1106-STRAT3-21	7048.2	Qbt-2	--	26 ± 2	12 ± 1	--	63 ± 9	--	--	--	Tr	--	--	--	--	101 ± 9
OU-1106-STRAT3-20	7014.6	Qbt-2	Tr	23 ± 2	14 ± 1	--	60 ± 8	--	--	--	1 ± 1	--	--	--	--	98 ± 8
OU-1106-STRAT3-19	6999.0	Qbt-2	--	22 ± 2	17 ± 1	--	60 ± 8	--	--	--	--	--	--	--	--	99 ± 8
OU-1106-STRAT3-18	6985.8	Qbt-1v	1 ± 1	21 ± 2	15 ± 1	--	62 ± 9	--	--	--	--	--	--	--	--	99 ± 9
OU-1106-STRAT3-17	6968.8	Qbt-1v	--	10 ± 1	21 ± 2	9 ± 3	56 ± 8	--	--	--	--	--	--	--	--	96 ± 9
OU-1106-STRAT3-16	6954.3	Qbt-1v	--	1 ± 1	19 ± 1	18 ± 1	57 ± 8	--	Tr	Tr	--	--	--	--	--	95 ± 8
OU-1106-STRAT3-15	6937.9	Qbt-1v	--	--	19 ± 1	20 ± 2	57 ± 8	--	--	--	Tr	--	--	--	--	96 ± 8
OU-1106-STRAT3-14	6934.3	Qbt-1v	--	--	22 ± 2	6 ± 2	52 ± 7	17 ± 7	--	--	Tr	--	3 ± 1	--	--	83 ± 8
OU-1106-STRAT3-13	6933.2	Qbt-1g	--	--	19 ± 1	3 ± 1	43 ± 6	32 ± 6	--	--	Tr	--	3 ± 1	--	--	68 ± 6
OU-1106-STRAT3-12	6931.1	Qbt-1g	--	--	15 ± 1	1 ± 1	32 ± 4	47 ± 4	--	--	Tr	--	5 ± 1	--	--	53 ± 4
OU-1106-STRAT3-11	6917.5	Qbt-1g	--	--	15 ± 1	Tr	23 ± 3	60 ± 3	1 ± 1	--	Tr	--	1 ± 1	--	--	40 ± 3
OU-1106-STRAT3-10	6901.5	Qbt-1g	--	--	16 ± 1	Tr	18 ± 3	66 ± 3	--	--	Tr	--	--	Tr	--	34 ± 3
OU-1106-STRAT3-9	6885.0	Qbt-1g	--	--	14 ± 1	1 ± 1	21 ± 3	64 ± 3	--	--	--	--	--	--	--	36 ± 3
OU-1106-STRAT3-8	6867.7	Qbt-1g	--	--	16 ± 1	--	23 ± 3	61 ± 3	--	--	--	--	--	--	--	39 ± 3
OU-1106-STRAT3-7	6864.2	Qbt-1g	--	--	26 ± 2	--	36 ± 5	-?-	Tr	Tr	--	--	--	--	--	62 ± 5
OU-1106-STRAT3-6	6861.4	Qct	--	--	19 ± 1	--	21 ± 3	60 ± 3	--	--	--	--	--	Tr	--	40 ± 3
OU-1106-STRAT3-5	6857.3	Qct	--	--	8 ± 1	1 ± 1	10 ± 1	81 ± 1	--	--	--	--	--	--	--	19 ± 2
OU-1106-STRAT3-4	6850.7	Qct	Tr	Tr	3 ± 1	2 ± 1	10 ± 1	85 ± 1	--	--	--	--	--	--	--	15 ± 2
OU-1106-STRAT3-3	6849.5	Qct	--	Tr	1 ± 1	1 ± 1	5 ± 1	93 ± 1	--	--	--	--	--	--	--	7 ± 2
OU-1106-STRAT3-2	6831.9	Qct	--	1 ± 1	3 ± 1	2 ± 1	12 ± 2	82 ± 2	Tr	--	--	--	--	--	--	18 ± 3
OU-1106-STRAT3-1	6779.1	Qbo	--	--	10 ± 1	1 ± 1	21 ± 3	68 ± 3	--	--	--	--	--	--	--	32 ± 3

tiny (<0.05-mm), wedge-shaped grains in the shardy matrix. Hornblende-bearing pumices also occur in this unit.

Lithic clasts generally make up <1 to 5% of the tuff. Lithics include gray, brown, and black phenocryst-poor devitrified rhyolite, porphyritic dacite, and crystal-rich, moderately to densely welded Otowi Member. Most lithics are 1 to 7 cm in diameter, but a few are as much as 15 cm across. Despite excellent exposures in the stratigraphic sections and other cliff outcrops, there were no occurrences of the boulder deposits that were encountered near the base of unit 3 during construction of the vertical waste shafts at MDA T (Purtymun, 1969).

Mineralogy

Figure 5 shows bulk-tuff mineralogical variations at TA-21 as a function of stratigraphic position. The Bandelier and Cerro Toledo tuffs consist primarily of feldspar + quartz ± cristobalite ± tridymite ± glass (Table IV). Minor constituents include smectite, hornblende, mica, magnetite/maghemite, hematite, calcite, and kaolinite.

Volcanic glass is the major constituent (commonly >60%) of tuffs in the lower half of the stratigraphic section, including the Otowi Member, tuffs of the Cerro Toledo interval, and unit 1g of the Tshirege Member (Table IV and Fig. 5). Glass occurs as pumices and in the shardy matrix. Quartz and feldspar (sanidine) are the two other major constituents of the glassy tuffs; these crystalline phases occur as phenocrysts and as relatively minor devitrification products in the fine ash. The volcanic glass is fresh in thin section, and the absence of significant alteration minerals such as clays and zeolites strongly suggests that these tuffs have had limited contact with groundwater since their deposition. Glass abundances are fairly consistent in the upper Otowi Member and in unit 1g of the Tshirege Member. In the Cerro Toledo interval, the proportion of glass to crystalline phases varies widely because individual depositional units contain varying amounts of glassy pyroclasts, phenocrysts, and devitrified lava detritus (Fig. 5).

Volcanic glass disappears abruptly at the top of unit 1g at the vapor-phase notch (Tables III and IV; Figs. 4 and 5). Glass abundances begin to decline within 5 m of the vapor-phase notch, but most of the glass disappears within 2 m of the notch. It should be noted that, despite extensive colloquial use, the term *vapor-phase notch* is probably a misnomer because the mineral assemblage (feldspar + quartz + minor cristobalite) and textural features (lack of vapor-phase minerals lining pumices and vugs) suggest that glass underwent high-temperature devitrification without significant vapor-phase crystallization at this stratigraphic level.

Unit 1v of the Tshirege Member consists primarily of feldspar + quartz + cristobalite + tridymite. Cristobalite abundances are greatest in the colonnade tuff near the base of the unit and systematically decrease upsection (Fig. 5). Tridymite abundances vary inversely with those of cristobalite. Cristobalite is intergrown with alkali feldspar—mainly as axiolitic and spherulitic growths—and these intergrowths replace the original glassy pyroclasts that make up the tuff. These relations suggest that crystallization of colonnade tuff was largely a result of *in situ* devitrification. Tridymite, on the other hand, commonly occurs with alkali feldspar as discrete crystals and crystal aggregates that were deposited on surfaces of open pores in the tuff. Mostly likely, these occurrences of tridymite and alkali feldspar were deposited by gases rising through the tuff. The distribution of tridymite indicates that vapor-phase alteration increases systematically upsection.

Unit 2 of the Tshirege Member consists of a simple mineral assemblage of feldspar + quartz + tridymite. Tridymite is most abundant (~25%) in the moderately to densely welded tuffs of this unit (Fig. 5). Laths of

tridymite and equant crystals of alkali feldspar line voids in relict pumices and in the tuff matrix. The cores of some pumices are coarsely crystalline and have granophyric textures resulting from intergrowths of sanidine and quartz. Despite its greater degree of welding (and presumably a correspondingly lower permeability), unit 2 contains the highest concentrations of tridymite found in the Tshirege Member. High tridymite concentrations suggest that vapor-phase alteration was more intense in unit 2 than in other parts of the Tshirege Member. The high degree of welding and high tridymite concentrations suggest that ash flows of unit 2 were unusually hot and welded so fast that large amounts of gas was entrapped.

The nonwelded unit and unit 3 of the Tshirege Member have similar mineralogical characteristics. They both contain the assemblage feldspar + quartz + tridymite ± cristobalite.

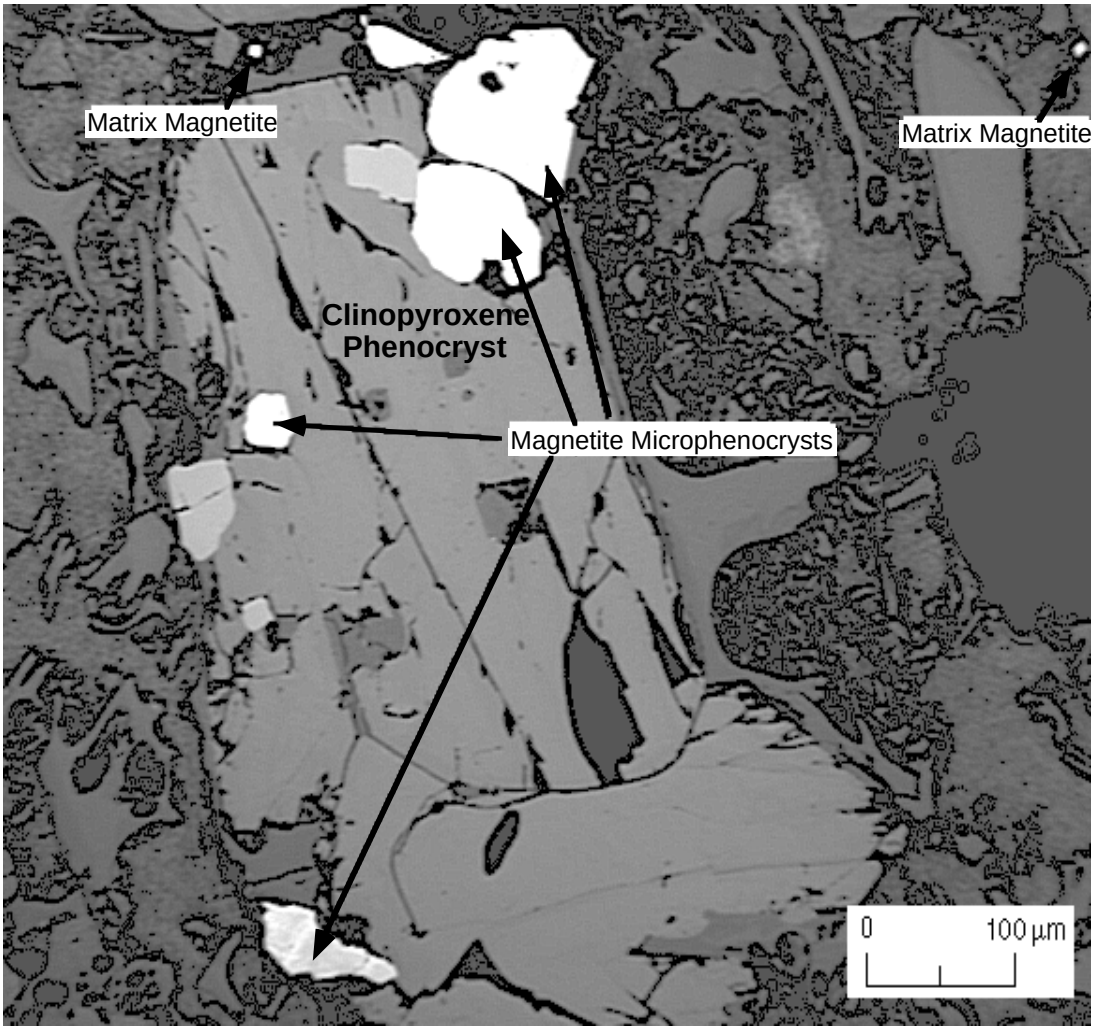

Fig. 6. Photomicrograph of magnetite microphenocrysts enclosed within a clinopyroxene phenocryst. Ilmenite exsolution lamella are visible in the lowermost magnetite grain. Magnetite microphenocrysts make up 60 to 90% of the magnetite in these tuffs. As shown in this photograph, the magnetite microphenocrysts commonly are enclosed within mafic phenocrysts; this limits their availability for mineral/water interaction. More important for mineral/water interaction are the small-matrix magnetite/hematite grains. These matrix magnetites are disseminated throughout the permeable tuff matrix and make up ~95% of the magnetite surface area available for mineral/water interaction. The sample shown here is OU-1106-STRAT3-21 from Tshirege unit 2; it is a reflected-light image.

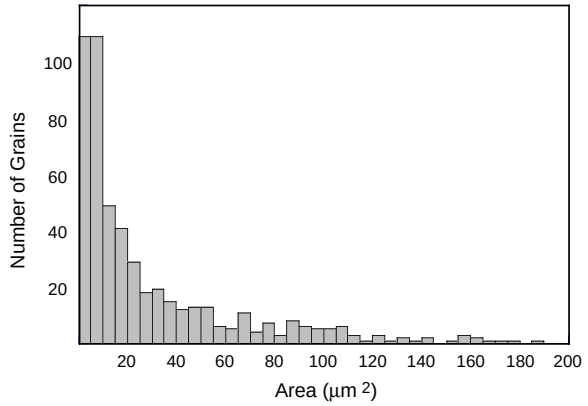

Fig. 7. Histogram of magnetite grain areas in sample 1106-STRAT2-16. Most of the grains have cross sectional areas <75 μm², and they are disseminated in the tuff matix; the remainder of magnetite grains are the relatively large microphenocrysts. Although matrix magnetites represent only 10 to 40% of the magnetite present in the rock, they provide as much as 95% of the surface area available for magnetite/ water interactions. These image analysis data were collected from a thin section using reflected light (200x).

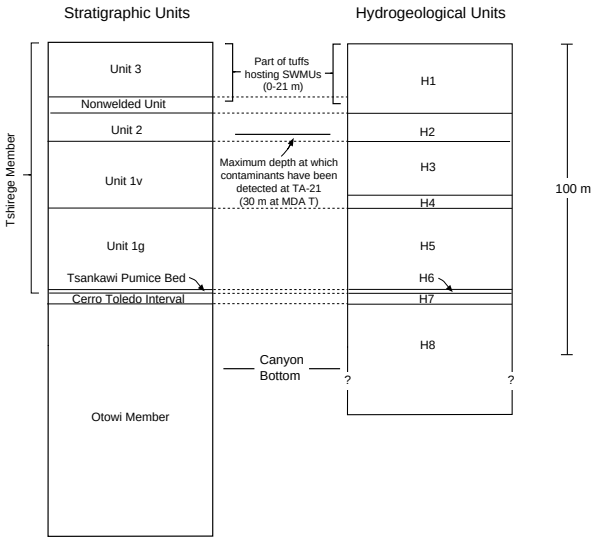

Fig. 8. Relation between stratigraphic units and preliminary proposed hydrogeological units at TA-21. The hydrogeological units generally correspond to the stratigraphic units, except for H1 and H3, which cross stratigraphic boundaries.

Though tridymite is present, its concentrations are notably less than those found in unit 2, suggesting somewhat less intense vapor-phase alteration. Cristobalite is absent in the west and central stratigraphic sections, but it is present in the east section (Table IV and Fig. 5). Tridymite abundance decreases from west to east in these units (Fig. 5). These relations suggest that vapor-phase alteration decreases eastward in the more distal portions of these tuffs.

Smectite and hematite occur in small (<2%) amounts throughout the stratigraphic sequence at TA-21 (Table IV). These two trace minerals are important because they are sorptive of certain radionuclides and could provide important natural barriers to their migration. Smectites are highly selective for cationic radionuclides (Grim, 1968). Magnetite and its alteration products, such as hematite, have an affinity for uranium and actinide species through surface-complexation (Allard and Beall, 1979; Beall and Allard, 1981; Allard *et al.*, 1982; Hsi and Langmuir, 1985; Ho and Miller, 1986). Although these minerals occur in small quantities, they are disseminated throughout the stratigraphic sequence, and their aggregate abundance and surface area available for adsorption are large when integrated over long groundwater flow paths through the tuffs.

Magnetite is present as a microphenocryst in all of the tuffs at TA-21. Its abundance commonly ranges from 0.03 to 0.2%. Magnetite grains are generally unaltered in the vitric tuffs, but some contain exsolution lamellae of ilmenite or its alteration products along 111 crystallographic directions. The magnetite shows no oxidation to maghemite in unit 1g, but varying degrees of oxidation occur in units 2 and 3. Partial to complete replacement of magnetite by hematite also occurs in the crystallized tuffs of the Tshirege Member. Former ilmenite lamellae consist of an aggregate of rutile ± hematite ± anatase (?) ± goethite. Relatively large (>75 μm² in cross section area) microphenocrysts make up only ~15% of the individual magnetite (and hematite pseudomorph) crystals observed in thin

sections (Fig. 6). Yet these few microphenocrysts account for an estimated 60 to 90% of magnetite present. The remainder of the magnetite grains are small (<75 μm^2) and occur as disseminated crystals or aggregates of crystals that are distributed uniformly throughout the matrix (Figs. 6 and 7). These smaller crystals are more important than the relatively large microphenocrysts for radionuclide retardation because they occur in the highly permeable tuff matrix and because their surface areas (based on estimates derived from grain perimeter data) account for ~96% of surface area available for mineral/water interaction.

Relation Between Stratigraphic Units and Hydrogeological Units

Figure 8 presents a preliminary representation of the major hydrogeological units for the upper part of the vadose zone at TA-21. Complete delineation of all hydrogeological units at TA-21 must await characterization of subsurface units and systematic measurements of hydrological properties from all rock units. Previous sections of this report subdivide stratigraphic units according to their mode of deposition and cooling histories. However, physical characteristics (such as permeability, bulk density, and moisture content) as well as chemical properties (such as mineralogy, rock chemistry, and water chemistry) control the movement of groundwater and contaminants through tuff. The hydrogeological zones represented in Fig. 8 are delineated by degree of welding, mineralogy, fracture characteristics, and juxtaposition of contrasting lithologies. Welding characteristics should generally correlate with hydrological properties, which are not yet determined. These hydrogeological units partly correspond with the stratigraphic units described above, but some cross stratigraphic boundaries (Fig. 8).

Hydrogeological unit H1 combines Tshirege unit 3 with the underlying nonwelded unit. Although unit 3 is partially welded near the top of the mesa, the transition into nonwelded tuffs below is gradual. The mineralogy of the nonwelded unit and unit 3 are similar. This hydrogeological unit hosts most of the subsurface SWMUs at TA-21 (Fig. 8)

Hydrogeological unit H2 consists of the moderately to densely welded, highly fractured tuffs of Tshirege unit 2. The contact between H1 and H2 represents an abrupt change in welding characteristics. Although the hydrologic properties of these tuffs have not yet been tested, hydrogeological unit 2 is expected to have significantly lower porosities and permeabilities than unit H1 because of its greater degree of welding. The sharp contrast in lithological properties across this boundary may divert groundwaters laterally where flow occurs in a porous media. This boundary may be especially important at MDA T and MDA U, where contaminants diverted laterally beneath these liquid waste sites could discharge to DP Canyon, which is developed on top of H2. Locally, where conditions favor rapid influx of recharge (for example, in drainages), groundwater flow may be controlled by the network of fractures in unit 2. Hydrogeological unit H2 is the lowest unit in which contaminated transport has been documented at TA-21 (Fig. 8 and Nyhan *et al.*, 1984).

Hydrogeological unit H3 consists of the white, slope-forming nonwelded tuffs of unit 1v. Although these tuffs probably consist of multiple flow units, the individual flows have similar lithological properties and they probably have similar hydrological properties. Because these tuffs are nonwelded, they are probably more permeable than overlying unit H2. The mineralogy of these tuffs in H3 is fairly uniform, except for the abundances of cristobalite and tridymite, which vary as a function of vertical stratigraphic position. Sorption behavior and sorption capacity of these tuffs should be unaffected by the increase in the ratio of tridymite to cristobalite upsection. These tuffs contain fractures but they are not as numerous as in unit H2.

Hydrogeological unit H4 consists of the colonnade tuffs at the base of unit 1v and includes the vapor-phase notch at its base. These tuffs are cliff-forming above the vapor-phase notch and may be incipiently welded. These tuffs have undergone *in situ* devitrification, but there is little evidence of the vapor-phase alteration that is so prevalent in overlying tuffs. Differences in welding and alteration characteristics may affect the pore structure of these rocks and cause them to have different hydrologic properties than those of the tuffs in H3. Moisture profiles from nearby drillholes commonly show increased moisture contents in this interval (for example, see Broxton *et al.*, Sec. VI, this report).

Hydrogeological unit H5 is equivalent to Tshirege unit 1g. This nonwelded ignimbrite is fairly uniform in its lithological properties, and it should be relatively permeable because of its open network of interconnected pores. The presence of abundant—and possibly reactive—glass in H5 contrasts with the devitrified mineral assemblage in H4. The ash-rich tuff at the base of the main ignimbrite and underlying surge deposits are better sorted and more stratified than the overlying massive ignimbrite. However, for now, these tuffs are included in H5 because it is not known if the occurrance of these features is widespread. These tuffs can be subdivided into separate hydrogeological units at a later date if further studies show that they are regionally extensive and that their hydrologic properties differ significantly from those of the remainder of H5.

Hydrogeological unit H6 is equivalent to the Tsankawi Pumice Bed. This pumice-fall deposit is extremely porous and is commonly associated with elevated water content in the unsaturated zone (for example, Broxton *et al.*, Sec. VI, this report). At TA-21, these pumice deposits overlie a soil horizon that may act as a perching layer. This is well illustrated in outcrops exposed in the large alcove just downstream of DP Spring, where seeps are perched within water-saturated Tsankawi Pumice Bed above fine-grain clay-rich soils.

Hydrogeological unit H7 lumps together all of the bedded deposits of the Cerro Toledo interval. These well-stratified deposits contain numerous thin depositional units characterized by a wide range of lithologies. Undoubtedly, these individual depositional units have differing hydrogeological properties. In addition, juxtaposition of lithologies with contrasting grain sizes across depositional boundaries can result in capillary and permeability barriers and cause the lateral diversion of groundwater flow. Nonetheless, these deposits are lumped together at present because their deposition in complex fluvial settings makes correlation of more finely subdivided units impractical.

Hydrogeological unit H8 is equivalent to the upper part of the Otowi Member. This nonwelded ignimbrite has fairly uniform lithological properties and should be fairly porous because of its nonwelded nature. So far only the uppermost part of this ignimbrite has been studied, and H8 may be extended to include more of the Otowi Member after further investigation.

CONCLUSIONS

Heterogeneous tuffs underlie the solid waste management units at TA-21. The physical properties of these tuffs vary both vertically and laterally. Vertical variations provide most of the geologic control for movement of groundwater in the vadose zone. Recognition of tuff heterogeneity is important for developing conceptual models of the site, evaluating transport pathways and processes, and bounding parameters in computer codes used to model groundwater and contaminant transport.

Tuff stratigraphy, with the bedrock geologic map, provides the geologic context for understanding the distribution of rock units and

forms the basis for describing cores and cuttings from future drillholes at TA-21. Depositional and cooling histories control the distribution of the major stratigraphic units whereas physical and chemical properties of the tuffs control the movement of groundwater.

Eight hydrogeological units are identified on a provisional basis (until further hydrologic testing is completed for these rocks). The hydrogeological units have unique lithological and mineralogical properties that probably affect their conductivity to water and gas. Some of these hydrogeological units cross stratigraphic boundaries. Systematic measurements of hydrological properties are necessary to complete the characterization of these units. Additional delineation of hydrogeological units in the subsurface will occur during the drilling program for the site.

The two critical bedrock units for evaluating subsurface contaminant transport at TA-21 are Tshirege unit 3 and the underlying nonwelded tuff unit that makes up hydrogeological unit H1, and Tshirege unit 2, which makes up hydrogeological unit H2. Hydrogeological unit H1 hosts both surface and subsurface SWMUs at TA-21, and its physical properties govern how contaminants are mobilized and transported at their source term. Our study shows that this hydrogeological unit is generally highly porous and contains no bedding features that might divert groundwater to canyon margins. Because of its high porosity and low degree of moisture saturation, hydrogeological unit H1 should provide an effective physical barrier to waste migration because of its ability to imbibe and trap water in the tuff matrix under natural recharge conditions. These tuffs also may provide a mineralogical barrier to contaminant migration in the tuff matrix because of the presence of trace amounts of magetite/hematite and smectite, which are highly sorptive of certain radionuclides. One area of concern is that the favorable barriers in unit H1 could be bypassed by transport through fractures. This is of particular concern at the liquid-waste MDAs, which received large amounts of effluent in addition to the natural recharge. Porous flow through the tuff matrix as well as fracture flow may have occurred beneath some of these MDAs. Preliminary observations about fracture mineralogy indicate that water from the surface has penetrated to at least the level of hydrogeological unit H2 under natural conditions.

Hydrogeological unit H2 is the lowest unit in which contaminants are documented at TA-21 (Nyhan *et al.*, 1984). Although testing of hydrologic properties of tuffs at TA-21 has not yet occurred, hydrogeological unit H2 is expected to have significantly lower porosities and permeabilities than unit H1 because of its greater degree of welding. The contrast in physical properties at the contact between H1 and H2 might provide a barrier to the downward movement of water. Such a barrier could act as a zone of accumulation for downward moving contaminants or it might divert contaminants laterally. The relative impermeability of the tuff matrix and abundance of fractures in unit H2 suggests that the RFI work plan's strategy to use slant drillholes for characterizing as many fractures as possible is warranted for the deeper boreholes being planned to investigate the liquid waste MDAs at TA-21.

ACKNOWLEDGEMENTS

We thank D. Mann and Carlos Montoya for preparing thin sections of these tuffs, many of which were difficult to mount and polish. J. Gardner, J. Wolff, P. Aamodt, C. Brause, K. Bitner, G. Eller, T. Glatzmaier, L. Maassen, J. Nyhan, S. Reneau, J. Smith, and E. Springer provided critical reviews of this report.

REFERENCES

Allard, B. and Beall, G. W., 1979, Sorption of Am on geologic media, J. Environ. Sci. Health A14 (6),.507-518.

Allard, B., Olofsson U., Torstenfelt, B., Kipasti, H., and Anderson, H., 1982, Sorption of actinides in well-defined oxidation states on geologic media, in Scientic Basis for Nuclear Waste Management V, Materials Research Society Symposia Proceedings, L. Lutze, ed. (Materials Research Society, Pittsburg, Pennsylvania), pp. 775-786.

Bailey, R. A., Smith, R. L., and Ross, C. S., 1969, Stratigraphic nomenclature of the volcanic rocks in the Jemez Mountains, New Mexico, US Geol. Survey Bull. 1274-P, 19 pp.

Baltz, E. H., Abrahams, J. H., Sr., and Purtymun, W. D., 1963, Preliminary report on geology and hydrology of Mortandad Canyon near Los Alamos, New Mexico, with reference to disposal of liquid low-level radioactive wastes, US Geological Survey open-file report (Albuquerque, New Mexico), 105 pp.

Beall, G. W. and Allard, B., 1981, Sorption of actinides from aqueous solutions under environmental conditions, in Proceedings of a Symposium on Adsorption from Aqueous Solutions, March 24-27, 1980, American Chemical Society Meeting, Division of Colloid and Surface Chemistry (Houston, Texas), pp. 193-212.

Bish, D. L. and Chipera, S. J., 1988, Problems and solutions in quantitative analysis of complex mixtures by x-ray powder diffraction, in Advances in X-Ray Analysis (Plenum Press, New York, 1988), Vol. 31, pp. 295-308.

Bish, D. L. and Chipera, S. J., 1989, Revised mineralogic summary of Yucca Mountain, Nevada, Los Alamos National Laboratory report LA-11497-MS.

Broxton, D. E., Eller, P. G., and Flores, D., 1995, Preliminary drilling results for boreholes LADP-3 and LADP-4, Sec. VI, this report, Los Alamos National Laboratory, New Mexico.

Chung, F. H., 1974a, Quantitative interpretation of x-ray diffraction patterns of mixtures. I. Matrix-flushing method for quantitative multicomponent analysis, J. App. Crystall. 7, 519-525.

Chung, F. H., 1974b, Quantitative interpretation of x-ray diffraction patterns of mixtures. II. Adiabatic principle of x-ray diffraction analysis of mixtures, J. App. Crystall. 7, 526-531.

Crowe, B., Linn, G., Heiken, G., and Bevier, M., 1978, Stratigraphy of the Bandelier Tuff in the Pajarito Plateau, applications to waste management, Los Alamos National Laboratory report LA-7225-MS, 57 p.

Fisher, R. V. and Schmincke, H.-U.,1984, Pyroclastic Rocks (Springer-Verlag, Berlin), 472 p.

Gardner, J. N., Kolbe, T., and Chang, S., 1993, Geology, drilling, and some hydrologic aspects of Seismic Hazards Program Core Holes, Los Alamos National Laboratory, New Mexico, Los Alamos National Laboratory report LA-12460-MS, 19 p.

Goff, Fraser, 1995, Geologic Map of TA-21, Sec. VI, this report, Los Alamos National Laboratory, New Mexico.

Griggs, R. L., 1964, Geology and groundwater resources of the Los Alamos area, New Mexico, US Geological Survey water-supply paper 1753, 107 p.

Grim, R. E., 1968, Clay Mineralogy, 2nd ed. (McGraw-Hill Book Company, New York), 596 p.

Heiken, G., Goff, F., Stix, J., Tamanyu, S., Shafiqullah, S., Garcia, S., and Hagan, R, 1986, Intracaldera volcanic activity, Toledo caldera and embayment, Jemez Mountains, New Mexico, J. Geophys. Res. 91(B2), 1799-1815.

Ho, C. H. and Miller, N. H., 1986, Adsorption of uranyl species from bicarbonate solution onto hematite particles, J. Colloid Interface Sci. 110, 165-171.

Hsi, C-K and Langmuir, 1985, Adsorption of uranyl onto ferric oxyhydroxides: Application of the surface complexation site-binding model, Geochim. Cosmochim. Acta. 49, 1931-1941.

Izett, G. A. and Obradovich, J. D., 1994, $^{40}Ar/^{39}Ar$ age constraints for the Jaramillo Normal Subchron and the Matuyama-Brunhes geomagnetic boundary, J. Geophys. Res. 99(B2), 2925-2934.

Klug, H. P. and Alexander, L. E., 1974, X-Ray Diffraction Procedures for Polycrystalline and Amorphous Materials (John Wiley & Sons, Inc, New York).

Nyhan, J. W., Drennon, B. J., Abeele, W. V., Trujillo, G., Herrera, W. J., Wheeler, M. L., Booth, J. W., and Purtymun, W. D., 1984, Distribution of radionuclides and water in Bandelier Tuff beneath a former Los Alamos liquid waste disposal site after 33 years, Los Alamos National Laboratory report LA-10159-LLWM, 51 pp.

Peterson, D. W., 1979, Significance of the flattening ofpumice fragments in ash-flow tuffs, Geological Society of America special paper 80, pp. 195-204.

Purtymun, W. D., 1969, Correspondence from W. E. Hale, District Chief, Water Resources Division, US Geological Survey, to C. W. Christenson, H-7 Group Leader, Subject: Geology at Disposal Area Near Bldg. 257, TA-21, April 19, 1969, 2 pp.

Reneau, S., 1995, Geomorphic studies of DP Mesa and vicinity, Sec. VI, this report, Los Alamos National Laboratory, New Mexico.

Smith, R. L., 1960a, Zones and zonal variations in welded ash flows, US Geological Survey professional paper 354-F, pp. 149-159.

Smith, R. L., 1960b, Ash flows, Geol. Soc. Am. Bull. 71, 795-842.

Smith, R. L. and Bailey, 1966, The Bandelier Tuff: a study of ash-flow eruption cycles from zoned magma chambers, Bull. Volcanol. 29, 83-104.

Smith, R. L., Bailey, R. A., and Ross, C. S., 1970, Geologic map of the Jemez Mountains, New Mexico, US Geological Survey Map I-571, scale 1:1250000.

Stoker, A. K., McLin, S. G., Purtymun, W. D., Maes, M. N., and Hammock, B. G., 1992, Water supply at Los Alamos during 1989, Los Alamos National Laboratory report LA-12276-PR, 51 p.

Vaniman, D. and Wohletz, K., 1990, Results of geological mapping/fracture studies, TA-55 area, Los Alamos National Laboratory Seismic Hazards memorandum EES1-SH90-17.

Vaniman, D. and Wohletz, K., 1991, Revisions to report EES1-SH90-17, Los Alamos National Laboratory seismic hazards memorandum EES1-SH91-12.

Weir, J. E. and Purtymun, W. D., 1962, Geology and hydrology of Technical Area 49, Frijoles Mesa, Los Alamos County, New Mexico, US Geological Survey adminstrative release report, Albuquerque, New Mexico, 225 pp.

Wohletz, K., 1995, Measurement and analysis of rock fractures in the Tshirege Member of the Bandelier Tuff along Los Canyon adjacent to TA-21, 1995, Sec. II, this report, Los Alamos National Laboratory, New Mexico.

GEOMORPHIC STUDIES AT DP MESA AND VICINITY

by

S. L. Reneau

A geomorphic characterization of TA-21 was undertaken primarily to provide site-specific data on surficial processes that pertain to the potential erosion and deposition of contaminants. An additional objective was to define the geomorphic setting of the DP Spring, a perennial spring that contains contaminants probably originating from TA-21. These studies support RCRA RFI work at OU 1106 for the ER Program.

Sediment deposition areas downslope of MDAs at TA-21 include the narrow grassy floor of BV Canyon south of MDAs B and V and a broader grassy flat within DP Canyon north of MDAs A, T, and U. The floor of DP Canyon includes alluvium and slopewash of widely varying age, and these sediments record alternating cycles of sediment deposition and erosion extending back at least 27,000 years. The most recent cycle occurred in historic time, and up to 6 ft of sediment was deposited and subsequently partially eroded since major development began in the drainage basin. These historic sediments constitute a significant potential storage area for contaminants within DP Canyon, including plutonium, which has been documented previously in DP Canyon sediments.

Cliff retreat processes and rates apparently vary dramatically between cliffs bordering Los Alamos Canyon and those bordering the shallow tributary canyons at TA-21 (including DP Canyon). Partially detached landslide blocks along Los Alamos Canyon demonstrate that individual mass-wasting events can extend 75 ft or more from the mesa edge, and the unweathered appearance of many cliff faces also suggests relatively frequent failures. In contrast, retreat of cliffs bordering the tributary canyons probably involves failure of smaller fracture-bounded blocks; extensive erosional pitting of these cliffs suggests long periods between failures. The occurrence and composition of old alluvial deposits in one shallow tributary canyon at DP Mesa further suggests that these tributaries were largely eroded by streams originating in the Sierra de los Valles before incision of Los Alamos Canyon and that minimal cliff retreat has occurred in these canyons since then. The MDAs at TA-21 are all located along the shallow tributary canyons, and exposure of most of the MDAs through cliff retreat is improbable over periods exceeding 10,000 years. The exception, MDA V, is within 20 to 25 ft of the mesa edge, which is composed of artificial fill that buries a shallow embayment. Failure of this fill and the buried rock slope should be considered possible; such a failure could potentially expose Absorption Bed 3.

DP Spring emerges from an extensive old valley fill in lower DP Canyon (dated at about 37,000 years old) that is perched ~20 ft above the modern valley bottom. This valley fill is confined to areas eroded into nonwelded units of the Bandelier Tuff and probably extends less than 300 ft upcanyon. Because the spring is perennial and surface runoff within DP Canyon is intermittent, the most likely flow path for the springwater may include fractures in units 2 and 1v, with the groundwater emerging from fractures into the upper part of the valley fill and then flowing through the fill to DP Spring.

INTRODUCTION

A geomorphic characterization of TA-21 was undertaken primarily to provide site-specific data on surficial processes that pertain to the potential erosion and deposition of contaminants. An additional objective was to define the geomorphic setting of DP Spring, a perennial spring containing contaminants that probably originated from TA-21.

The developed area at TA-21 is located on DP Mesa; it is bordered by Los Alamos Canyon to the south (350 to 400 ft deep) and DP Canyon to the north (generally 70 to 100 ft deep). Potential sources of contaminants include deep releases (such as from seepage pits and absorption beds), near-surface liquid releases from septic systems, subsurface solid-waste disposal areas, and surface contamination from stack-release fallout and spills. The two primary surficial processes of concern are sediment transport by surface runoff from the site into the adjacent canyons and cliff retreat that could potentially expose MDAs located near the mesa edge. Discharge of waters containing plutonium and other contaminants into DP Canyon occurred in the past, and transport of low concentrations of plutonium in this canyon has been documented previously (Purtymun, 1971, 1974; Purtymun *et al.*, 1990). Because of this known contamination, the geomorphic characteristics of DP Canyon were examined in particular detail.

METHODS

The geomorphic characterization of TA-21 involved a combination of airphoto analysis, field mapping, field investigations of selected sites, and analyses of topographic maps. The entire area was examined on 1:7200-scale, 1991 color airphotos, and features observed on these photos were either plotted directly onto 1:1200-scale Facility for Information Management Analysis and Display (FIMAD) 2-ft contour maps or first plotted on 1:1200-scale orthophotos and then transferred to the 1:1200-scale maps. Much of the area was also examined on the ground—particularly the canyon rims, canyon bottoms, and areas downslope of the MDAs—to field-check features identified on the photos and to examine features not visible on the photos. Geomorphic features examined include drainage channels, recent sediment-storage areas, older sedimentary deposits, cliff faces, partially detached landslide blocks, and areas of artificial fill. Geomorphic maps of parts of TA-21, at a scale of 1:1200, are presented on Plates 5, 6, and 7; additional surficial units are shown on Plate 1 at a scale of 1:4200.

Natural streambank exposures of valley-bottom sediments were examined in DP Canyon and Los Alamos Canyon, and radiocarbon dates were obtained for charcoal samples collected from the sediments in DP Canyon to constrain their age. After drainage channels downslope

of the MDAs were examined and located on the topographic maps, sites for topographically based sediment sampling were identified.

To provide additional data on the process of cliff retreat, two cliff areas immediately south of MDA B were chosen for more detailed investigation. Fracture-bounded blocks were measured and samples of cliff faces were collected for analyses of cosmogenically produced isotopes (see, for example, Poths and Goff, 1990; Lal, 1991; Nishiizumi *et al.*, 1991) to provide constraints on cliff retreat rates.

The analysis of topographic maps was undertaken primarily to provide additional data on canyon widths and, by inference, variations in cliff retreat. Measurements of the distance from the center-line of the modern valley floor to the north and south canyon rims were made using 1:1200-scale FIMAD 2-ft contour maps. These measurements were at frequent enough intervals to include the irregularities of canyon rims, particularly the promontories and the center of embayments.

TA-21 CANYONS

Los Alamos Canyon

Los Alamos Canyon forms the southern boundary of TA-21. This canyon was examined in only a preliminary manner during this study because it will be studied in more detail as part of the Canyons RFI work. DP Canyon, a major tributary to Los Alamos Canyon on the northern side of TA-21, was studied in greater detail. The main sources of contaminants in Los Alamos Canyon adjacent to TA-21 are probably at TA-2 and TA-41, which are located on the canyon bottom upstream of TA-21.

Los Alamos Canyon is one of the deepest canyons within the boundaries of LANL, and is >400 ft deep adjacent to TA-21. The primary landforms in the canyon are (1) steep cliffs of Bandelier Tuff (see mapping units described in Goff, Sec. II, this report), (2) extensive slopes mantled with colluvium derived from the tuff, and (3) a wide, fairly flat valley floor. The cliffs are developed in units 3, 2, and 1v of the Tshirege Member of the Bandelier Tuff; unit 2 exhibits the steepest, most continuous cliffs. Colluvium mantles nonwelded tuff in the lower part of the Tshirege Member (unit 1g), the Otowi Member of the Bandelier Tuff, and the intervening Cerro Toledo interval (see Goff, Sec. II, this report and Broxton *et al.*, Sec. IV, this report for description of bedrock units). The age of the colluvium is unknown, but probably ranges in age from historic (modern rockfall) to at least tens of thousands of years. The latter inference is drawn from observations that the colluvium locally buries older alluvial terrace deposits of Los Alamos Canyon, whose age probably exceeds 10,000 years, without the presence of an intervening buried soil to provide evidence for a significant gap in time. One buried alluvial deposit below TA-21 occurs ~23 ft above the stream channel (stream elevation ~6654 ft); its elevation above the channel is similar to that of a deposit in lower DP Canyon dated at ~37,000 years old. The sediments underlying the wide valley floor are inferred to be Holocene in age, deposited within the last 10,000 years. This inference is based on their similarity to sediments <6500 years old studied in other valley bottoms on the Pajarito Plateau (Gardner *et al.*, 1990; Reneau *et al.*, 1993).

BV Canyon

An unnamed, shallow, hanging valley on the south margin of TA-21 is incised within Tshirege unit 3 and the underlying nonwelded unit. This valley is herein informally called "BV Canyon" because it is located below MDAs B and V. The floor of the canyon is perched above the cliff-forming welded tuff of Tshirege unit 2. Relatively little sediment is stored in this canyon, and the sediment is largely confined to a narrow (6- to 33-ft-wide) grassy strip along the canyon bottom.The channel itself is discontinuous, and the flow often spreads out over the grassy valley

bottom. These areas of unchannelized flow are likely spots for modern sediment deposition. At the lip of the hanging valley, south of MDA V, the flow drops over a waterfall into Los Alamos Canyon and generally infiltrates an extensive bouldery colluvial deposit without reaching the main channel.

DP Canyon

The geomorphic characteristics of DP Canyon, on the north margin of TA-21, are strongly influenced by lithologic variations within the Bandelier Tuff (Fig. 1), and the canyon can be divided into four segments that reflect these bedrock variations.

The uppermost segment of DP Canyon, cut into the resistant part of Tshirege unit 3, is relatively steep and narrow, and the canyon bottom is generally choked with boulders derived from the adjacent canyon walls.

The next segment of DP Canyon, cut through the weaker, lower part of Tshirege unit 3 and the underlying Tshirege nonwelded unit, is relatively flat and wide. It contains extensive deposits of sediment derived from both the upper part of DP Canyon and the adjacent canyon walls. The low gradient of this segment is related to a base-level control immediately downstream, where the resistant Tshirege unit 2 is located. Historic outfalls from TA-21 discharged into this part of the canyon, and runoff from three of the five MDAs at TA-21 also flows into this segment.

The third segment of DP Canyon is incised into the resistant Tshirege unit 2 to form a steeper, narrow, rock-bound inner canyon. Little sediment is stored in this segment; instead, sediment is generally carried by runoff downstream past this segment.

The fourth segment, the steepest part of DP Canyon, is cut into Tshirege units 1v and 1g, the Cerro Toledo deposits, and the Otowi Member. The canyon bottom is generally choked with boulders and includes numerous small sediment-deposition areas. DP Spring, a perennial spring, emerges in the upper part of this segment and runoff is generally present for some distance downstream. This runoff does not usually reach the main Los Alamos Canyon stream channel; instead, it infiltrates the alluvium of lower DP Canyon.

Deposits of sediment within DP Canyon provide valuable data on both the episodic nature of sediment transport within the canyon and the canyon's development since deposition of the Tshirege Member of the Bandelier Tuff at 1.22 Ma (million years ago; age from Izett and Obradovich, 1994). The following report sections discuss the older alluvium of DP Canyon, the valley fill of lower DP Canyon, the late Pleistocene and Holocene sediments of upper DP Canyon, and historic alluvium in upper DP Canyon.

Older Alluvium of DP Canyon

Deposits of stream-rounded cobbles and boulders occur on the south side of lower D P Canyon, both on a bench developed within the Tshirege nonwelded unit (above the resistant cliff-forming unit 2) and within a short tributary to DP Canyon off the eastern end of DP Mesa (Plate 3). At the western exposure of the older alluvium, the deposits include consolidated, stratified sand and gravels that were deposited against a vertical, stream-polished wall of Tshirege unit 3. Clasts in the older alluvium are as large as 3 ft in diameter and include a mixture of ~20% Tschicoma Formation dacite derived from the Sierra de los Valles and 80% welded Bandelier Tuff eroded from a stratigraphically higher cooling unit not present at TA-21. Similar gravels are now being deposited only in the major canyons that originate in the Sierra de los Valles (such as Los Alamos Canyon), although the high percentage of welded Bandelier Tuff is unusual.

The nature and location of these older alluvial deposits indicate that incision of the main canyons on this part of the Pajarito Plateau did not occur immediately after deposition of

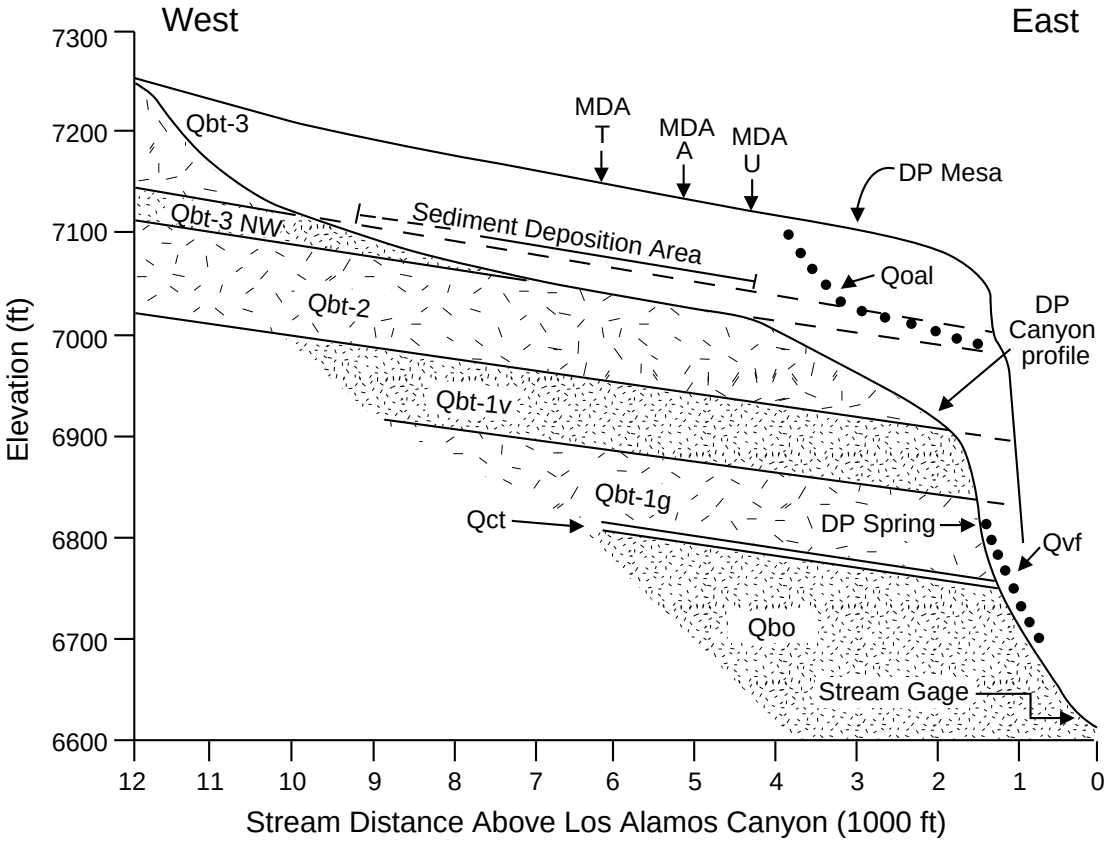

Fig. 1. Longitudinal profile of DP Canyon, showing relation of stream profile to lithologic variations and location of post-Bandelier Tuff sediment deposits. See Plates 1 and 5 for explanation of geologic unit symbols.

the Tshirege Member of the Bandelier Tuff at 1.22 Ma. Following Tshirege deposition, the streams originating in the Sierra de los Valles may have had a braided pattern as they traversed parts of the Plateau (such as DP Mesa) that now only receive local runoff (Fig. 2). Eventual incision of the main canyons was probably driven by headward erosion from the Rio Grande. The steep profile of the older alluvium in the DP Canyon tributary (Fig. 1) probably reflects deposition during this period of headward erosion of the canyons and consolidation of the drainages. It is possible that other shallow canyons on this part of the Pajarito Plateau (such as upper DP Canyon and BV Canyon) were similarly occupied by streams draining the Sierra de los Valles (Fig. 2); however, no deposits from such streams were found in this study.

An additional implication of these older alluvial deposits is that very little modification of some small tributary canyons has occurred since the time of major drainage consolidation. The upper part of the DP Canyon tributary is plugged with older alluvium, and no net incision of the head of this canyon or headward erosion has occurred since its deposition—implying incision of this canyon was largely the result of runoff from the Sierra de los Valles. However, local runoff has been sufficient to incise the lower part of this tributary canyon 10 to 20 ft below the gravels. The modern canyon walls are also very close to the older alluvial deposits; the tops of steep Tshirege unit 3 slopes to the south are only 50 to 130 ft from the alluvium (average ~100 ft). If the alluvium was originally deposited

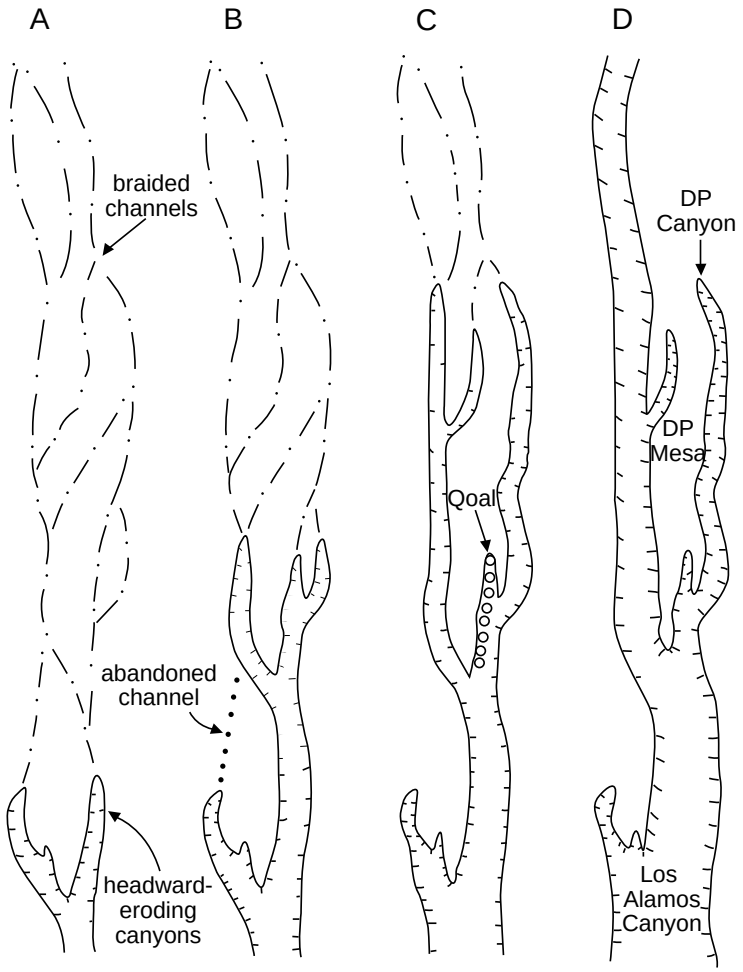

Fig. 2. Hypothetical evolution of Los Alamos Canyon drainage system. (A) Drainage channels are braided and not incised over western Pajarito Plateau. Headward erosion of canyons progresses westward from Rio Grande along braided channels. (B) Some channels are abandoned as headward erosion proceeds. (C) Older alluvium of DP Canyon (Qoal) is left along abandoned channel as incised canyons erode farther west. (D) Modern Los Alamos Canyon has widened significantly through cliff retreat, but the shallow tributary canyons have widened little.

against vertical cliffs of Tshirege unit 3, a maximum of 50 to 130 ft of retreat could have occurred since that time.

The age of the older alluvial deposits is not known, so measurements of maximum wall retreat can not be used to make precise estimates of long-term retreat rates. If this stream course was abandoned close to 1.22 Ma (the age of the Tshirege Member of the Bandelier Tuff), the average maximum retreat rate would have been 0.11 ft/ky (ky = 1000 years), and if the course was abandoned at 0.5 Ma, the average maximum retreat rate would have been 0.26 ft/ky.

Valley Fill of Lower DP Canyon

Remnants of a formerly extensive valley fill occur on both sides of lower DP Canyon (Plate 3 and Fig. 3). The base of the fill is ~20 ft above the modern channel. This valley fill consists of lenses of stratified sand and rounded stream gravels interbedded with and buried by coarse colluvium that contains

angular boulders of Bandelier Tuff from the adjacent canyon walls. DP Spring emerges from a layer of rounded stream gravels resting on a bevelled tuff surface of Tshirege unit 1g (Fig. 4). Downstream, a radiocarbon date of ~37 ka (thousand years before present) was obtained from charcoal contained within a sandy lens in the valley fill (Fig. 3, Table I) and provides an estimated average stream incision rate of 0.56 ft/ky.

The width of the valley fill suggests a period of relative stability for the stream channel, during which the channel was able to cut laterally. Since that time, the channel has incised the former valley floor, and at present the valley floor is less than one-fourth as wide as it was (Fig. 3). Many of the tuff boulders that choke the bottom of lower DP Canyon today may be derived from the older valley fill.

Occurrence of the valley fill is coincident with the presence of easily eroded, nonwelded units of the Bandelier Tuff and the Cerro Toledo interval (Fig. 1); thus it appears that the stream cuts laterally only where there is nonwelded tuff. Nonwelded units are not exposed in the valley walls upstream of DP Spring, and it is unlikely that the valley fill extends very far upstream past the limit of Tshirege unit 1g exposures. Similarly, the perched groundwater that emerges at DP Spring probably discharges into the fill from the tuff a short distance upstream (within <300 ft).

Late Pleistocene and Holocene Sediments of Upper DP Canyon

Extensive deposits of alluvium and colluvium (including slopewash) occur in the upper part of DP Canyon above the area where the

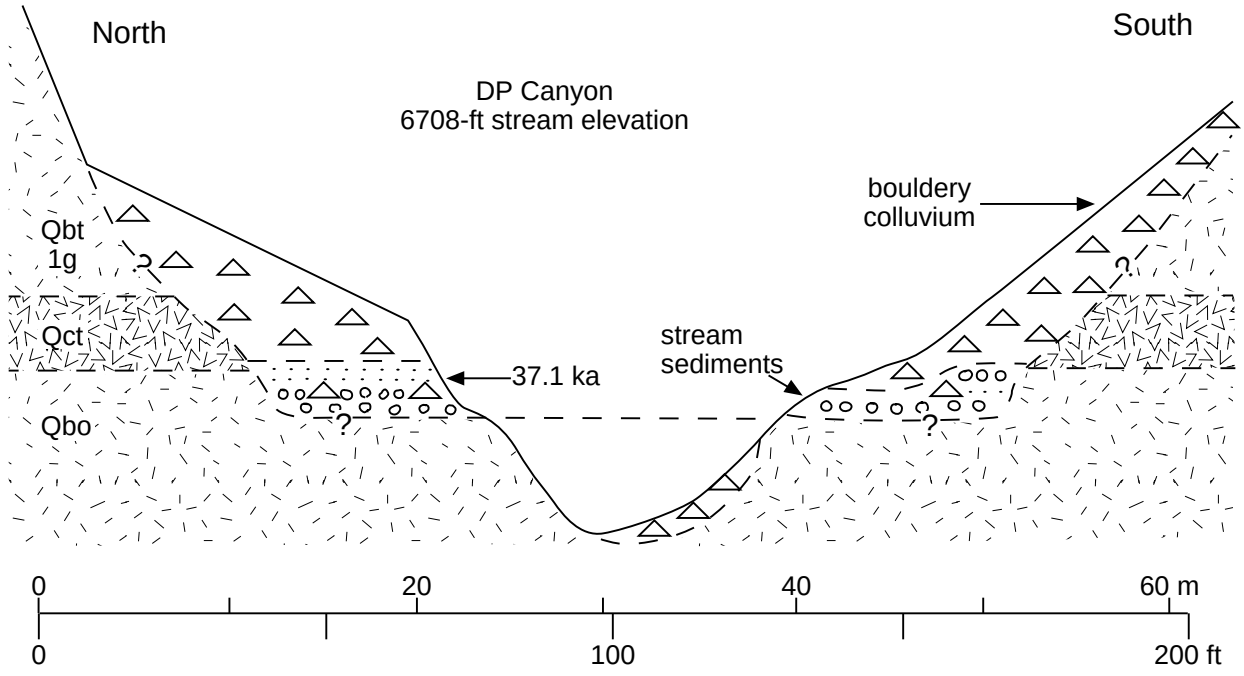

Fig. 3. Schematic cross section of radiocarbon sample site within valley-fill deposits of lower DP Canyon. Radiocarbon age in thousands of years before present (ka); there is no vertical exaggeration. See Plate 1 for explanation of geologic unit symbols.

canyon incises resistant Tshirege unit 2 (see Plate 4). Examination of these deposits along the stream channel indicates that deposits of multiple ages are present and that the canyon bottom has undergone many cycles of aggradation (raising of the stream bed through sediment deposition), subsequent incision, and partial erosion of these sediments. To provide some constraint on age of deposition and on the timing of former periods of aggradation in the canyon, five radiocarbon dates were obtained on charcoal fragments contained within the deposits at three sites. However, this limited number of dates is probably insufficient to fully document the cycles of sediment erosion and deposition of the deposits.

The radiocarbon dates confirm a long history of erosion and deposition cycles in upper DP Canyon. The oldest dated deposit is a stratified, clay-rich alluvium exposed near the modern stream bed; the deposit yielded a radiocarbon age of 26.7 ka (Figs. 5 and 6, Table I). This alluvium is texturally similar to that exposed at many other sites in the canyon. A fine-textured slopewash deposit that overlies the alluvium at this site provided a radiocarbon age of 21.6 ka, which is stratigraphically consistent with the older date. Upstream, a deposit of sandy and gravelly alluvium yielded a date of 16.0 ka (Fig. 6 and Table I). At this site, the stream channel has incised ~1.8 ft into the Tshirege nonwelded unit since deposition of the alluvium at an average rate

TABLE I
RADIOCARBON DATES FROM DP CANYON

Sample Number [a]	^{14}C Date (yr bp) [b]	Calibrated Age [c]	Stream Elevation (ft)	Height Above Channel (m)	Depth Below Surface (m)	Notes
Beta-58056 CAMS-4574	21,630±110	too old for calibration	7046	1.2	1.05	slopewash
Beta-58057 CAMS-4575	26,680±80	too old for calibration	7046	0.2	1.9	old alluvium
Beta-58058 CAMS-4576	15,980±80	18860 cal BP (18512-19259 cal bp) 16910 cal BC (16562-17309 cal bp)	7067	1.5	1.0	old alluvium
Beta-58059 CAMS-4577	5450±70	6280 cal BP (5923-6496 cal bp) 4330 cal BC (3973-4546 cal bc)	7035	0.8	1.4	slopewash; 0.2 m above old alluvium
Beta-58060 CAMS-4578	2010±80	1940 cal BP (1560-2343 cal bp) 10 cal AD (390 cal AD-393 cal bc)	7035	1.35	0.45	slopewash
Beta-58061 CAMS-4579	37,070±630	too old for calibration	6708	8.75	0.55 [d]	terrace; 6.4-m-high strath

[a] Samples prepared at radiocarbon laboratory of Beta Analytic, Inc., Miami, Florida (Beta sample number); analyses run at the Lawrence Livermore National Laboratory accelerator mass spectrometry facility (CAMS sample number).

[b] Calibrated ages obtained using computer program CALIB 3.0 (Stuiver and Reimer, 1993). Ages in parentheses are in the 2σ range using an error multiplier of 2.0.

[c] Analyses are radiocarbon years "before present" (before 1950 AD), uncorrected for atmospheric variations in $^{14}C/^{12}C$ ratios.

[d] Depth below top of alluvium, buried beneath bouldery colluvium.

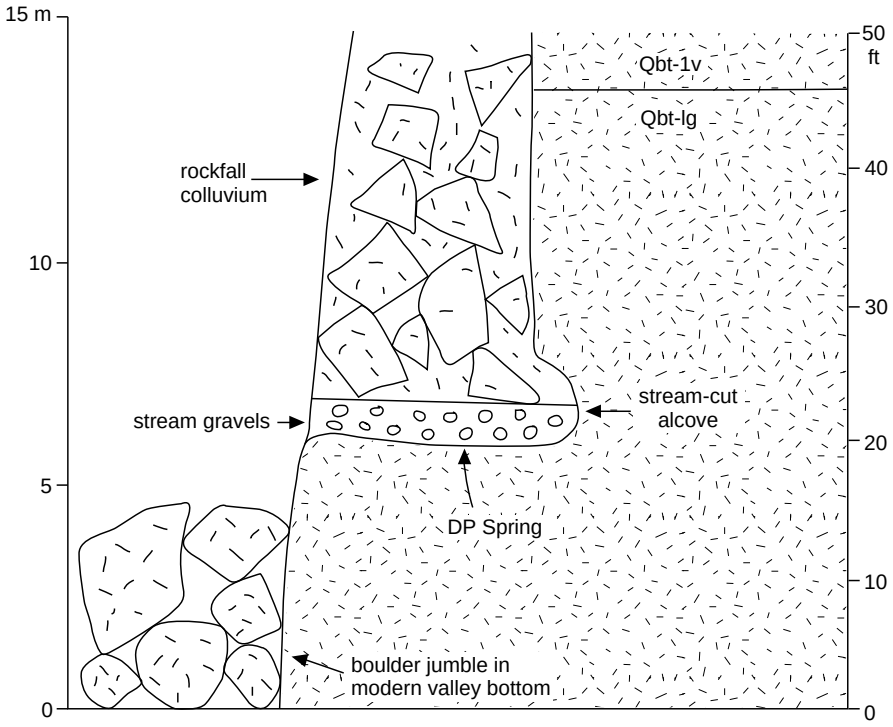

Fig. 4. Sketch of DP Spring looking northwest, showing stream-channel deposits in the valley-fill deposits of lower DP Canyon. See Plate 1 for explanation of geologic unit symbols.

of ~0.10 ft/ky. Downstream, two stratigraphically consistent dates of 2.0 and 5.4 ka were obtained from an extensive slopewash deposit that overlies an older alluvial deposit (Figs. 5 and 6, Table I). This slopewash deposit was graded to a level above the modern floodplain and may have been deposited during a period of channel aggradation that extended from before 5.4 ka to after 2.0 ka.

The long-term cycles of stream aggradation and degradation may be driven partly by climatically induced changes in runoff and/or sediment yield. Streams commonly aggrade their beds during periods of increased sediment supply, (derived from accelerated erosion of the surrounding basin) or during periods of decreased stream flow. Similarly, streams may degrade their beds during periods of increased flooding or when the sediment supply is reduced significantly.

In addition to providing data on the periods of stream aggradation and degradation, the radiocarbon dates confirm that the stream bed in upper DP Canyon has been near its present elevation for at least 26,000 years and possibly considerably longer. In many places, the modern channel rests on tuff bedrock that was exhumed after the overlying deposits were stripped, and in other locations the bedrock surface is buried. Only in the upper reaches, where the channel gradient steepens, has the stream been able to incise significantly into tuff (that is, the 16.0-ka site; Fig. 6), and the calculated incision rate of 0.10 ft/ky is considerably lower than the 0.56 ft/ky-rate estimated in lower DP Canyon.

Historic Alluvium of Upper DP Canyon

Extensive deposits of alluvium that post-date significant historic development in the basin (post-1943 AD) are exposed along the channel

in upper DP Canyon. The historic age of these deposits is shown by the presence of various man-made materials as well as exotic, rounded quartzite gravels that are commonly imported for road construction. The historic deposits are often ~3 ft thick in stream-bank exposures, but deposits up to 7 ft thick were observed. They commonly underlie a well-developed terrace surface that borders the modern channel (Figs. 5, 6, and 7). Since this terrace surface was abandoned, lowering of the channel has led to incision of gullies along several tributary channels (Figs. 5 and 7).

The extensive sedimentation that occurred in upper DP Canyon in historic time and the subsequent incision of the channel through these deposits may have been caused by land-use changes in the basin since widespread development began in the 1940s. Specifically, the historic deposits suggest the erosion of large volumes of material from developed areas adjacent to the canyon; their subsequent incision may have been caused by a reduction in sediment supply and/or an increase in runoff in the basin. At present, ~50% of the upper basin is covered by impermeable surfaces such as roads, parking lots, and buildings, and major increases in runoff associated with such widespread development is well documented in many areas (Dunne and Leopold, 1978).

The presence of the thick historic deposits complicates the identification and quantification of contaminants in DP Canyon. If significant amounts of contaminants were transported from TA-21 into upper DP Canyon during the period of channel aggradation, they may be locally buried under several feet of sediment or eroded from the modern stream banks. Alternatively, contaminants transported into upper DP Canyon before or after the period of channel aggradation may have been largely flushed downstream into lower DP Canyon or Los Alamos Canyon.

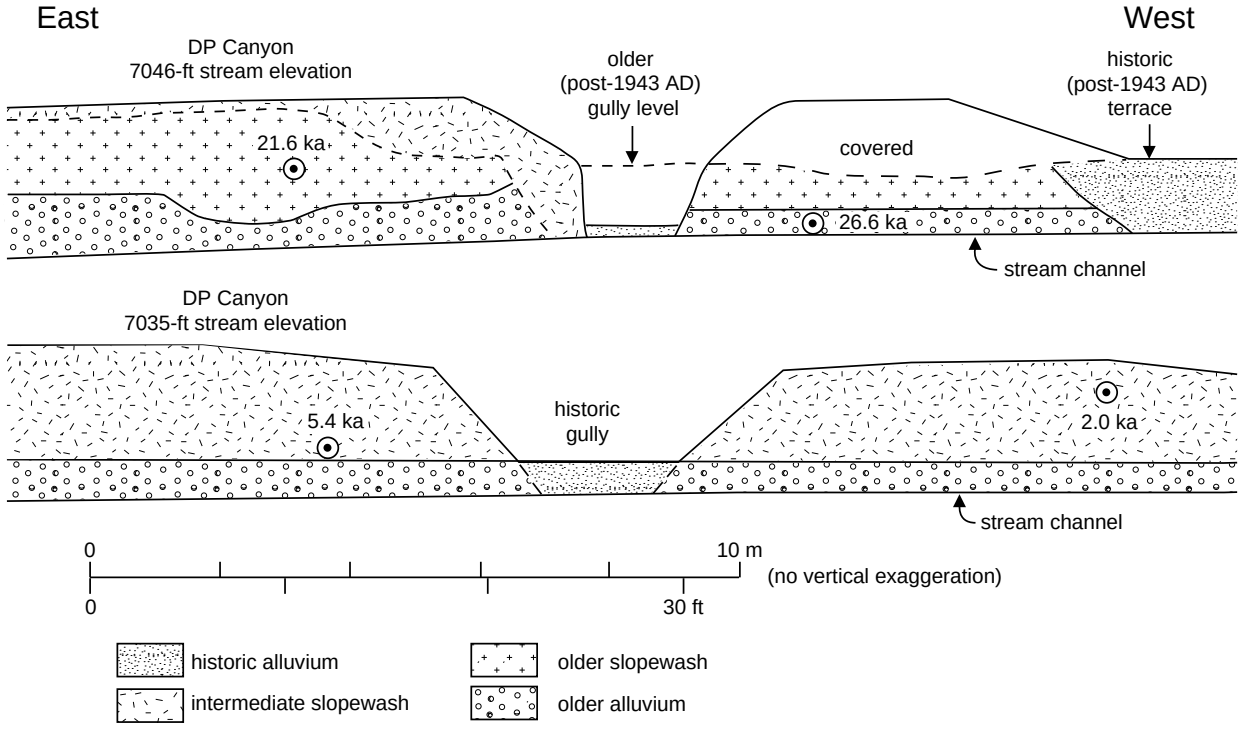

Fig. 5. Sketches of radiocarbon sample sites in upper DP Canyon.

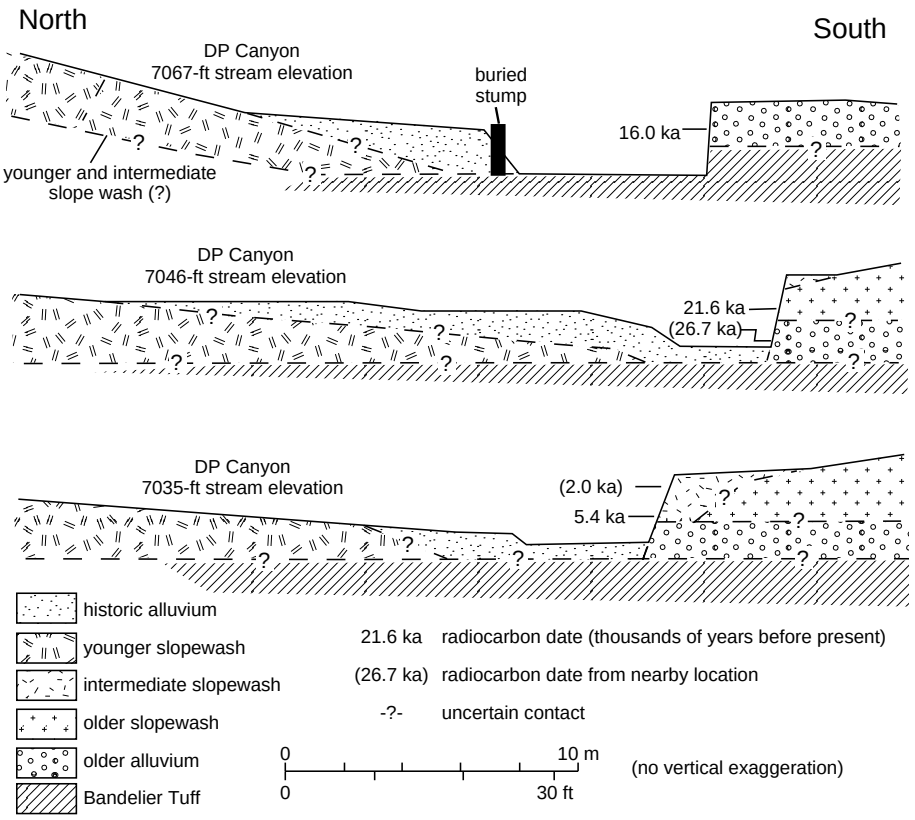

Fig. 6. Simplified cross sections across upper DP Canyon floor show generalized stratigraphy and location of radiocarbon dates.

CLIFF RETREAT

Knowledge of cliff-retreat rates at TA-21 would make it possible to estimate the length of time that MDAs near cliff edges will be stable. However, cliff-retreat rates are difficult to acquire, which limits the confidence of such stability estimates. At TA-21, several different approaches have provided insight into the processes and rates of cliff retreat, including (1) field mapping of landslides and field observations of cliff-retreat processes at TA-21, (2) analysis of cosmogenically produced ^{21}Ne in cliffs, (3) analysis of variations in canyon width, as measured from topographic maps, and (4) interpretation of long-term (post-1.22 Ma) canyon evolution.

Field Observations of Landslides and Rockfall

The retreat of the mesa edges at TA-21 occurs by a combination of small rockfalls from cliffs, detachment of rocks from slopes, and larger, deep-seated landslides. The character of the mesa edges differs significantly between north- and south-facing slopes and between slopes bordering Los Alamos Canyon and those bordering the shallower tributary canyons (DP and BV Canyons). These variations provide evidence for significant spatial differences in mass-wasting processes.

Fig. 7. Photograph of DP Canyon looking upstream at a radiocarbon sample site (7046-ft stream elevation). Surface to the right is an historic terrace ~3.3 ft above the channel. Radiocarbon dates of 21.6 and 26.7 ka were obtained from older deposits in stream banks to the left. An historic gully is visible to the left.

The most common type of mass wasting from the cliffs bordering DP Mesa is rockfall consisting of single- or multiple-fracture-bounded blocks of tuff. The youngest of these observed at TA-21 occurs within Tshirege unit 3, along the north rim of Los Alamos Canyon west of BV Canyon. For a distance of ~17 ft along the rim, the cliff face failed on steeply dipping fractures, resulting in ~10 ft of cliff retreat at this location. Both the cliff face behind the rockfall and the associated tuff boulders downslope expose unweathered, grey tuff, indicating a very young age. Rockfalls can also occur on the forested north-facing canyon walls. For example, an ~10-ft-diameter boulder dislodged from Tshirege unit 2 on the south wall of Los Alamos Canyon near TA-21 in the summer of 1992 and rolled and bounced down the slope to the valley bottom.

Rockfalls are frequent enough along the north rim of Los Alamos Canyon that Tshirege unit 3 is characterized by almost continuous cliffs where fracture-bounded blocks of tuff have dislodged (Fig. 8). In contrast, the north rims of DP and BV Canyons, formed in the same rock unit, possess discontinuous cliffs that typically have been exposed long enough that the original fracture-bounded rock surfaces have been deeply pitted and modified by secondary spalling (Figs. 9 and 10). In addition, the top of Tshirege unit 3 has been rounded extensively by erosion of the mesa edge along the side canyons, sharply contrasting with the abrupt cliff top that characterizes this unit along Los Alamos Canyon. These contrasting characteristics provide evidence for much slower cliff-retreat rates along the north walls of DP and BV Canyons than along the north wall of Los Alamos Canyon.

Measurements of the thickness of fracture-bounded blocks in the Tshirege unit 3 cliffs along BV Canyon suggest that individual rockfalls are typically small (an average thickness of 4 ft and median thickness of 3 ft, as shown in Fig. 11). These blocks are much smaller than the average spacing of primary fractures in the Bandelier Tuff, as measured by Vaniman and Wohletz (1990) and Wohletz (Sec. III, this report) because of the development of secondary fractures parallel to the cliff faces. The closest that the cliff embayments along BV Canyon approach MDA B is 60 ft, which would require the failure of 15 average-size blocks before waste pits could be exposed. Even if failure occurred by the largest block measured (16 ft), four failures would be required before exposure of the waste.

Along the rim of Los Alamos Canyon, several large, partially detached landslide blocks provide evidence for mass-wasting on a scale much larger than is seen along DP and BV Canyons. One landslide near the eastern end of DP Mesa (Plate 3 and Fig. 12) extends 330 to 500 ft along the mesa edge and reaches a width of 35 to 50 ft. The main block of the landslide has dropped ~3 ft below the mesa, and a 120-ft-long, 13- to 23-ft-wide, 3-ft-deep graben separates part of the landslide from the mesa. The outer edge of this landslide is broken into many smaller blocks that have dropped farther below the mesa, suggesting that the landslide was originally wider. One of these blocks clearly involves the Tshirege unit 2 cliff as well as the Tshirege unit 3 cliff. This evidence demonstrates that the failure involves multiple units of the Bandelier Tuff, including both the more-resistant cliff-forming units and intervening nonwelded units. The lower extent of this landslide is not known because it is covered by colluvium below the Tshirege unit 2 cliff, but Tshirege unit 1v and possibly underlying nonwelded units are likely to have been involved.

A second, partially detached landslide block, ~230 ft long and 75 ft wide, occurs at TA-21 northwest of Building 21-155. It has dropped the Tshirege unit 3 cliff 7 to 16 ft below the mesa. An additional, ~130-ft-long, 55-ft-wide landslide involving Tshirege unit 3 is present along the north rim of Los Alamos Canyon east of TA-21 and the Main Gate, dropping the Tshirege unit 3 cliff 3 to 8 ft. A failure ~265 ft long and 50 to 60 ft wide involving Tshirege unit 2 on the north wall of Los Alamos Canyon above TA-2 was mapped previously by Vaniman and Wohletz (1990). This failure dropped an intact block of tuff ~13 ft. Evidence for complete failure of a large section of Tshirege unit 2 cliff is provided by a large deposit of angular tuff boulders that clogs the drainage below the BV canyon hanging valley south of MDA V (Plate 5). The fact that the cliff above this location appears exceptionally fresh and uniform provides additional evidence for a large-scale cliff failure (Fig. 13).

The presence of the partially detached landslides demonstrates that the north wall of Los Alamos Canyon can fail in blocks much larger than those seen along either DP or BV Canyons, causing the mesa edge to retreat up to 75 ft; failures of at least this size can be expected in the future. Triggering of landslides by earthquakes is well documented (Keefer, 1984; Keefer and Wilson, 1989), and seismic shaking may thus be an important triggering mechanism for large-scale landslides along Los Alamos Canyon.

The reason for the large landslides along the margin of Los Alamos Canyon—in contrast to the small rockfalls within DP and BV Canyons—is probably related to the greater relief in Los Alamos Canyon. Observations of the cliff faces in embayments in Los Alamos Canyon and lower DP Canyon indicate that curved fracture surfaces can develop adjacent to the cliffs within the nonwelded parts of the Bandelier Tuff, much like the curved failure surfaces commonly developed in landslides (Fig. 14). These curved surfaces allow cliff failures to involve the predominantly unfractured, nonwelded tuff as well as the fractured cliff-forming units and allow a larger section of cliff to be involved in individual failures.

Fig. 8. Photograph of Tshirege unit 3 cliff along Los Alamos Canyon west of BV Canyon. Nearly continuous, near-vertical cliffs have been produced by repeated rockfalls.

Cosmogenic ^{21}Ne Analyses

When exposed rock surfaces are bombarded by cosmic rays, various stable and radioactive isotopes are produced in the rock. The concentrations of these isotopes progressively increase over time, making it possible to estimate exposure ages and/or erosion rates of the rock surfaces (see for example, Poths and Goff, 1990; Lal, 1991; Nishiizumi *et al.*, 1991). Samples collected from cliff faces along BV Canyon below MDA B were analyzed for concentrations of cosmogenically produced ^{21}Ne to provide constraints on the exposure history of these cliffs and to allow additional insights into cliff-retreat rates.

Preliminary estimates of the apparent exposure ages of three BV Canyon samples, provided by J. Poths (personal communication, 1994), are presented in Table II. Several simplifying assumptions (see below) were made to convert the measured ^{21}Ne concentrations into apparent exposure ages, and future modifications of these estimates will be necessary.

(1) A ^{21}Ne production rate one-half of that on a horizontal rock surface, which is appropriate for a vertical cliff. Because the sampled cliffs were less than vertical, actual production rates would be somewhat higher and the apparent exposure age somewhat lower.

Fig. 9. Photograph of Tshirege unit 3 cliffs along BV Canyon south of MDA B. Cliffs are discontinuous and the original rockfall surfaces have been highly modified.

Fig. 10. Photograph of Tshirege unit 3 cliff along BV Canyon south of MDA B; deep pits have been eroded into the cliff face (rock hammer provides scale).

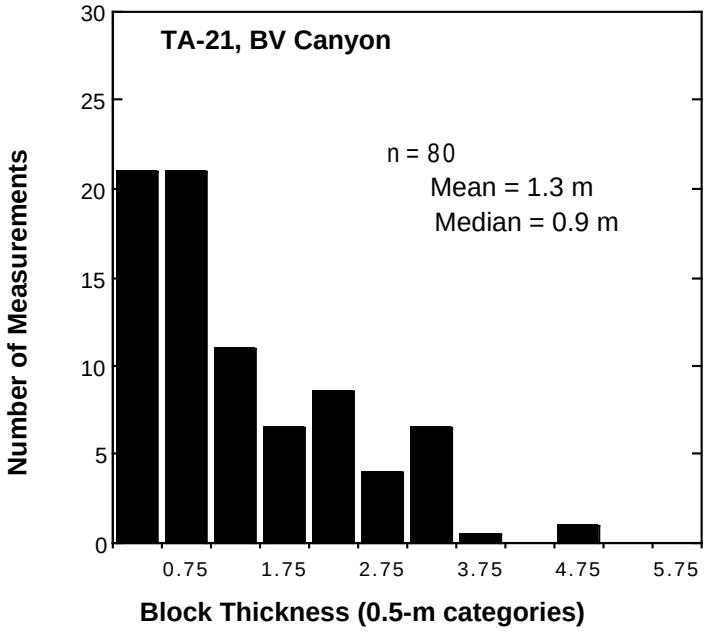

Fig. 11. Histogram of thickness of blocks along cliff faces south of MDA B, measured perpendicular to the cliffs. Measurements of the distance from the cliff face back to next fracture, made every 3.3 ft in two embayments along the edge of the canyon, represent the approximate thickness of individual rockfall blocks. Measurements include both blocks bounded by primary cooling fractures and those bounded by secondary fractures produced by spalling.

Fig. 12. Photograph of partially detached landslide block near east end of DP Mesa, along north rim of Los Alamos Canyon. Graben at head of landslide in foreground is about 3.3 ft deep and 16.4 ft wide. Landslide has moved to right, towards Los Alamos Canyon.

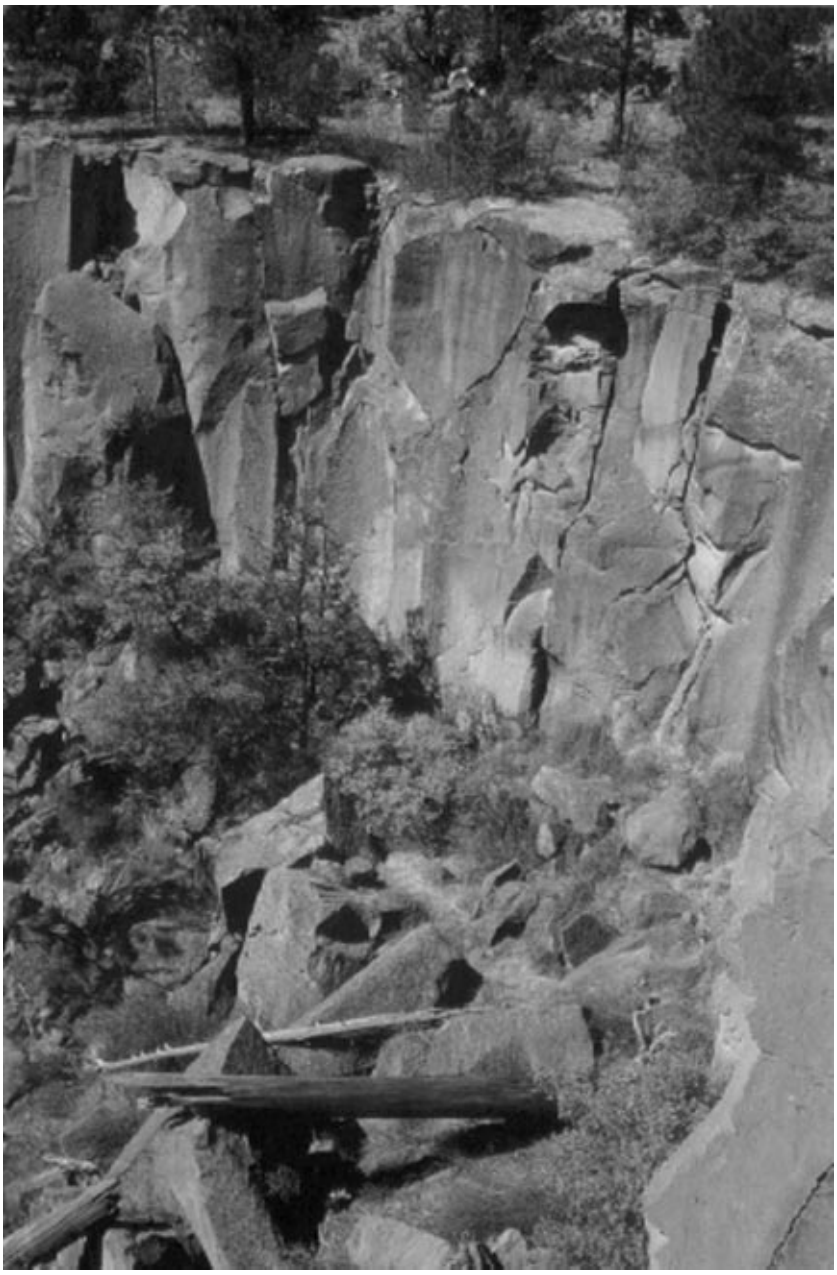

Fig. 13. Photograph of Tshirege unit 2 cliff south of MDA V at a site of relatively young cliff failure. Cliff appears to be exceptionally unweathered and angular rockfall boulders are present at cliff base.

(2) ^{21}Ne is produced only from cosmic rays bombarding the cliff face, not from cosmic rays penetrating the upper subhorizontal rock surface. Because the BV Canyon cliffs are relatively short (typically 6 to 8 ft high) and the tuff has a relatively low density that allows the cosmic rays to penetrate deeply, this assumption is probably not completely valid, and actual exposure ages would be less than estimated.

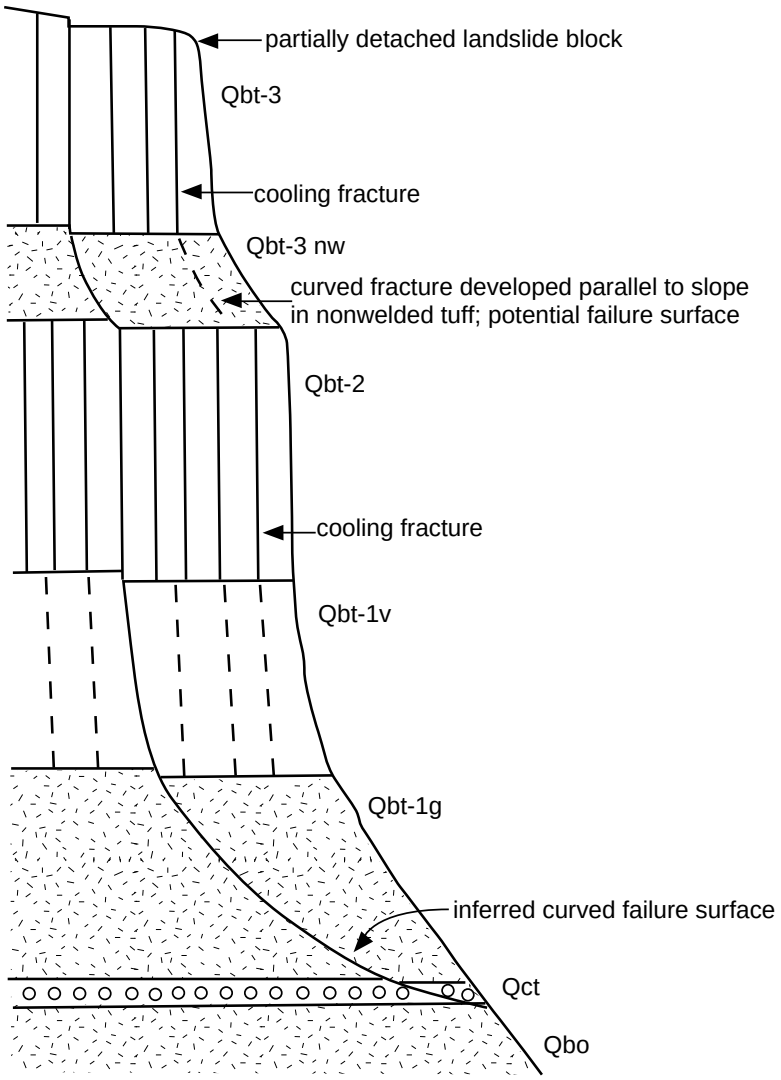

Fig. 14. Sketch showing inferred characteristics of large failures along the south edge of DP Mesa that borders Los Alamos Canyon. Landslides involving both welded and nonwelded units link primary cooling fractures in welded units. See Plate 1 for explanation of geologic unit symbols.

(3) The rockfall that exposed the sampled cliff was large enough to remove all tuff that previously contained ^{21}Ne—thus completely "resetting the clock." Because of the small size of the typical block along BV Canyon (3 to 4 feet; see Fig. 11), complete resetting may not have occurred; again, this tends to result in overestimated exposure ages.

(4) The sampled cliff was not shielded from cosmic rays by neighboring cliffs or the opposite canyon wall. Because of the irregularities of the canyon walls, this assumption is probably not completely valid, which results in somewhat lower actual ^{21}Ne production rates and leads to underestimates of exposure ages.

TABLE II
COSMOGENIC ^{21}NE ANALYSES FROM BV CANYON[a]

Sample Number	^{21}Ne Concentration (10^5 atoms/g)	Apparent Exposure Age (ka)
21-SLR-1	6.9 ± 1.4	19 ± 4
21-SLR-2	4.8 ± 1.1	14 ± 3
21-SLR-3	4.7 ± 1.0	13 ± 3

[a] Preliminary analyses by J. Poths, Los Alamos National Laboratory. Calculated exposure ages use a ^{21}Ne production rate of 35 atoms/g/yr for the latitude and altitude of Los Alamos and a vertical exposure; stated errors represent 1 standard deviation of the analytical uncertainties. Other uncertainties not encompassed by these errors are discussed in text.

Because of the above uncertainties, the apparent exposure ages in Table II should be used cautiously, although errors introduced by the simplifying assumptions would generally result in overestimates of exposure age. Two points are notable. First, the analyses and accompanying uncertainties suggest that typical ages for the last rockfall at the sample sites are less than 15,000 to 20,000 years, and therefore active cliff retreat occurred in BV Canyon within the latest Pleistocene and Holocene. Second, the apparent exposure ages are very similar, despite the fact that the sampled cliffs varied significantly in weathering characteristics and thus in inferred age. In the field, samples 21-SLR-1 and 21-SLR-2 appeared older than sample 21-SLR-3, yet the estimated ages are identical within the analytical uncertainty. This suggests that the measured ^{21}Ne concentrations may have resulted mainly from vertical penetration of cosmic rays through overlying rock. Alternatively, individual rockfall failures may be small enough along these cliffs to prevent complete resetting of the clock; this suggests that the ^{21}Ne concentrations may be better interpreted as a long-term erosion rate. Additional research is required to resolve these uncertainties and allow more confident interpretation of the results.

Topographic Analysis

Measurements of the width of Los Alamos, DP, and BV Canyons were made from 1:1200-scale FIMAD maps with 2-ft contours to evaluate spatial variations that may provide insight into cliff-retreat variations. Canyon width was measured perpendicular to a centerline down each canyon and from the break-in-slope on the resistant part of Tshirege unit 3 on the edges of the adjacent mesas. The measurement locations were chosen to ensure the maximum amount of variability, including both embayments where the canyons are widest and promontories where they are narrowest.

Measurements of canyon widths on the Pajarito Plateau have previously been used to calculate long-term cliff-retreat rates (Purtymun and Kennedy, 1971). The calculations assume that initial incision of the canyons occurred very soon after emplacement of the 1.22-Ma Tshirege Member of the Bandelier Tuff and that since that time cliff retreat rates have been constant. However, as discussed earlier, incision of the drainages through each cooling unit of the Bandelier Tuff could have occurred significantly after 1.22 Ma during progressive headward erosion of the

canyons. A significant part of canyon widening may have occurred during their early development. In addition, short- and long-term rates of cliff retreat could be related to other variables such as canyon depth, climate, and seismic activity, which would result in variable rates of cliff retreat over time.

All three canyons examined in the vicinity of TA-21 generally become narrower and shallower upcanyon (Fig. 15). These relationships are consistent with the headward development of the canyons over time, such that canyon incision began later upcanyon than downcanyon. Thus, local measurements of canyon width will only provide minimum values of cliff-retreat rate averaged over the past 1.22 Ma; the highest values would be calculated downcanyon, where the canyons are widest. East of TA-21 near the eastern limit of Tshirege unit 3 (the upper cliff-former at TA-21), the canyon reaches 1750 ft in width, providing a minimum-limiting average cliff-retreat rate of 0.72 ft/ky averaged over 1.22 Ma. Farther downstream, canyon width between the Tshirege unit 2 cliffs reaches 2600 ft west of State Route 4, providing a minimum-limiting average cliff-retreat rate of 1.07 ft/ky.

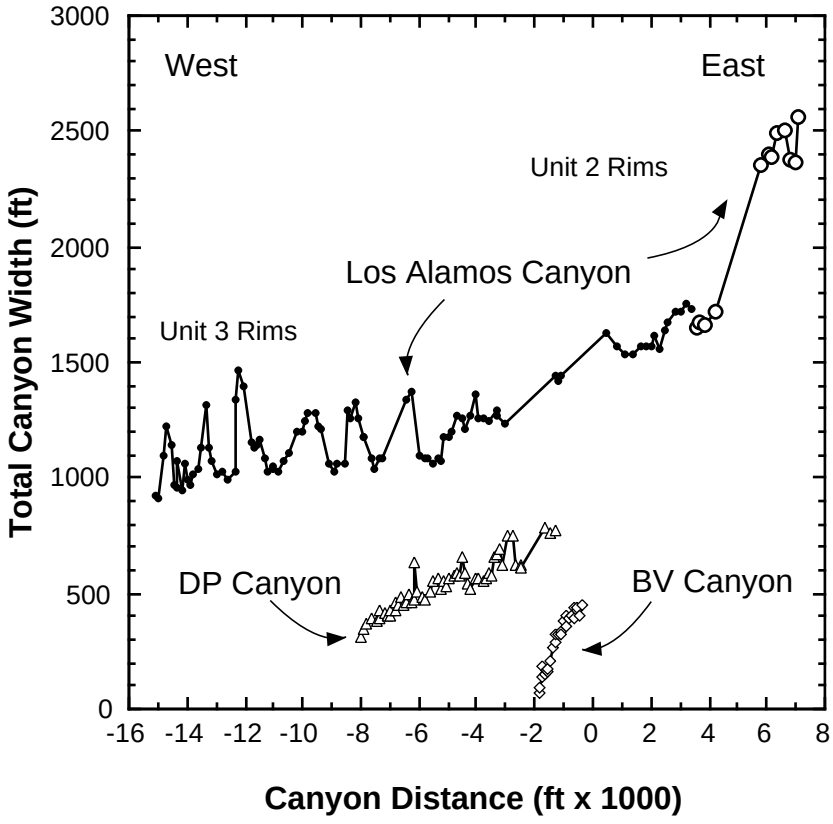

Fig. 15. Plots of total canyon width* vs *distance along Los Alamos, DP, and BV Canyons. Edge of canyon is defined as the break in slope at top of cliff or steep slope developed on resistant unit of Bandelier Tuff. Edge of canyon for DP, BV, and western part of Los Alamos Canyons is in Tshirege unit 3, and the edge of canyon in eastern part of Los Alamos Canyon is in Tshirege unit 2. Measurements made from FIMAD 1:1200-scale maps with 2-ft contour intervals. All canyons decrease in width to the west. Canyon distance uses junction of Los Alamos and DP Canyons as "0" point.

There may be local variability in average cliff-retreat rates that is associated with variations in fracture density. Significant local variations in canyon width occur along Los Alamos Canyon, and the wide parts often correspond with areas of increased fracture density along projected fault zones (Fig. 16). These include the Guaje Mountain fault zone (GMFZ) and two traces of the Rendija Canyon fault zone (RCFZ) west of TA-21, as mapped by Vaniman and Wohletz (1990). At TA-21, increased canyon width occurs near MDA V (Fig. 16), where exceptionally high fracture density has been documented (see Wohletz, Sec. III, this report). Two additional areas of higher cliff-retreat rates are suggested by increases in canyon width between MDA V and the GMFZ and between the RCFZ and the GMFZ at TA-41. The local increases in canyon width suggest that cliff-retreat rates in areas of more highly fractured tuff are 20 to 50% higher than in nearby cliffs.

A comparison was made of the distance from the approximate centerline of the valley bottoms to each canyon rim to evaluate evidence for any significant canyon asymmetry that would suggest greater retreat rates for either the north- or south-facing slopes. Specifically, if either rim was consistently a greater distance from the valley bottom, it would suggest that rim was retreating faster because of a difference in aspect. The term *valley bottom* used in this report is generally equivalent to the area of Quaternary alluvium (Qal), as mapped by Goff (Sec. II, this report).

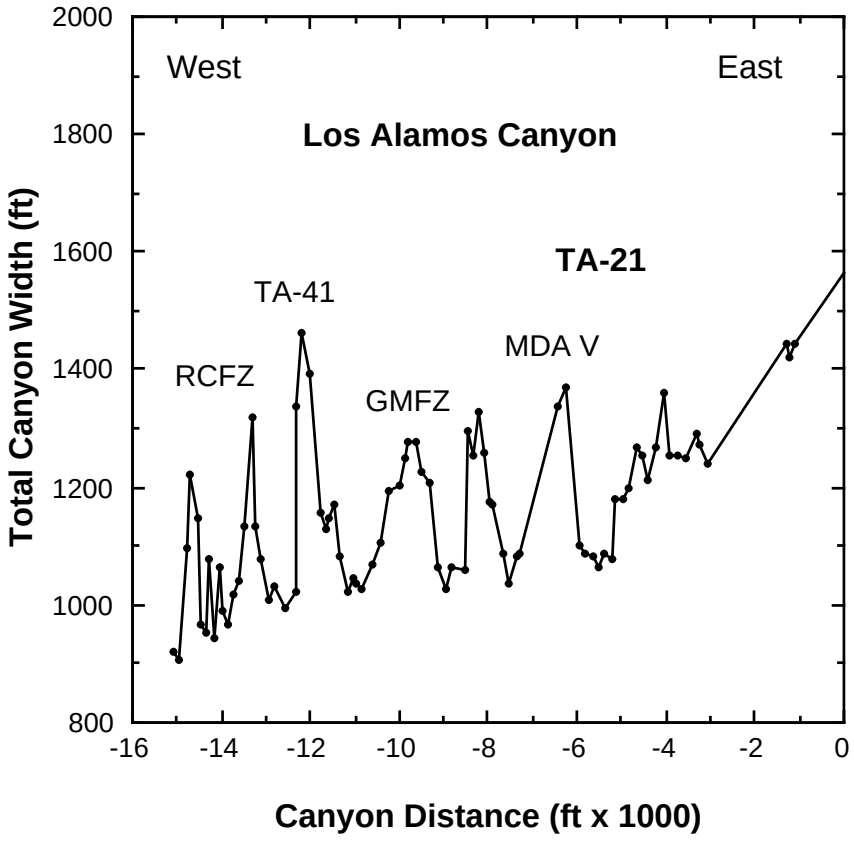

Fig. 16. Plot of total canyon width in Los Alamos Canyon near TA-21. Wide parts of canyon generally correspond to projected fault zones; GMFZ = Guaje Mountain fault zone and RCFZ = Rendija Canyon fault zone (from Vaniman and Wohletz, 1990). Canyon distance uses junction of Los Alamos and DP Canyons as "0" point.

Topographic measurements indicate that although significant asymmetry is present in places (Fig. 17), it is not systematic and most of the canyon lengths are roughly symmetric. In the western part of both Los Alamos Canyon and BV Canyon, the rims are roughly equidistant from the valley bottom, suggesting approximately uniform retreat rates. Canyons with significant asymmetry generally correlate with the presence of extensive valley fills on one side of the canyon, which provides evidence for lateral stream migration. These asymmetric reaches include the western part of DP Canyon (shown on Fig. 17), where deposits of older alluvium and slopewash occur on the southern side of the valley (Plate 4), and the eastern part of Los Alamos Canyon, where wide stream terraces are present ~100 ft above stream level south of the channel.

Measurements from topographic maps thus suggest that, despite differences in vegetation and the extent of cliffs between north- and south-facing canyon walls, there is no strong evidence for significant, systematic differences in the retreat rates of opposite canyon walls in the vicinity of TA-21. Estimates of cliff-retreat rates obtained from one canyon wall may therefore be generally applicable to the opposing wall.

Long-Term Canyon Evolution

Inferences about the long-term (post-1.22-Ma) evolution of the canyons adjacent to TA-21—based on the field mapping and analyses of topographic maps—have important implications for the timing and rates of cliff retreat. The occurrence of older alluvial deposits within the small tributary canyon to DP Canyon and along the margins of lower DP Canyon provides strong evidence that the tributary canyon was largely cut by a stream originating in the Sierra de los Valles and that little widening of this canyon has occurred since the old stream channel was abandoned. The

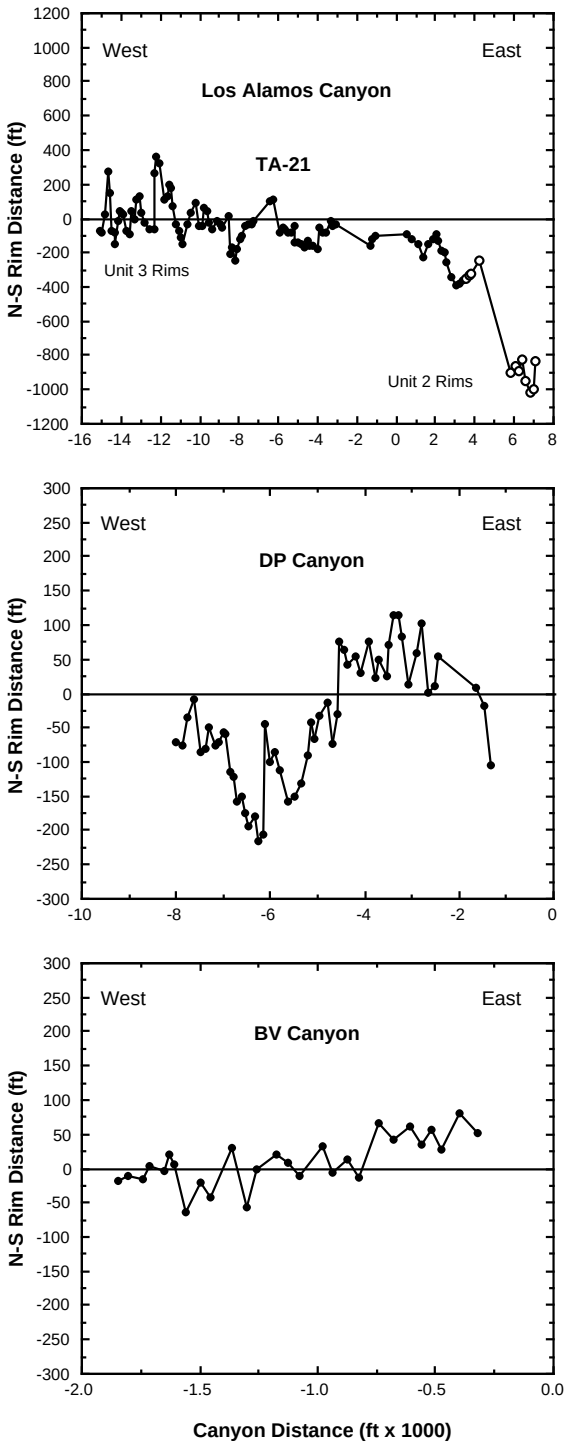

Fig. 17. Plots of differences between distance to north and south rims from approximate centerline of late Quaternary valley floor show canyon asymmetry. A positive value indicates that the north rim is farther than the south rim from the canyon floor. Western parts of both BV and Los Alamos Canyons are roughly symmetric, suggesting that retreat rates of the north and south rims are similar. Other parts of the canyons are asymmetric.

similarity between this small tributary canyon and DP and BV Canyons further suggests that DP and BV Canyons were also formed largely by streams originating in the Sierra de los Valles (Fig. 2). The age of these older stream channels that flowed over the mesas near TA-21 is unknown, but they may exceed 1 Ma.

These observations imply that minimal retreat of the cliffs adjacent to DP and BV Canyons has occurred since integration of the mesa-top channels (presumably along the present course of Los Alamos Canyon) and that the most significant canyon widening occurred during periods of lateral migration of the stream channel against the canyon walls. The significant increase in the width of Los Alamos Canyon downstream of DP Canyon (Fig. 8), which is associated with an extensive stream terrace ~100 ft above the channel that extends east to State Route 4, also suggests that the widening of Los Alamos Canyon in this reach was strongly related to lateral cutting by the stream when the terrace gravels were being deposited.

Precise cliff-retreat rates cannot be determined because the time when the earlier channels were abandoned is not known and the canyon width at that time is also not known. However, average long-term rates can be constrained by making reasonable assumptions about the age of the channels. Assuming ages of 0.5 to 1.22 Ma for the older alluvium of DP Canyon and using a maximum distance of 130 ft from these gravels to the Tshirege unit 3 canyon rim will provide maximum-limiting cliff-retreat rates of 0.11 to 0.26 ft/ky. If the 4.3-ft average block thickness measured along BV Canyon below MDA B (Fig. 7) is used, this is equivalent to removal of one block every 16,000 to 33,000 years on average. As coarse as these estimates are, they emphasize that rockfalls at any point along the tributary canyons are probably very infrequent.

GEOMORPHIC EVALUATION OF TA-21 MDAs

MDA B and MDA V

Sediment Transport and Deposition

MDA B and MDA V are both located on the south side of DP Mesa. All surface drainage from MDA B and the majority of the drainage from MDA V is to the south into BV Canyon (Plate 5).

Most runoff from MDA B is first channeled along the dirt road bounding the MDA on the south and later discharges off the south side of the road onto the rocky sloping mesa. Most of this runoff occurs at discrete locations, generally feeding into natural, shallow mesa-top drainages and flowing downslope over the Tshirege unit 3 cliffs into BV Canyon (Plate 5). The distinct drainages south from the MDA B dirt road occupy only some of the natural drainages on the mesa, and many of the natural drainages are bypassed by the road-related drainage system. These drainages mainly occur below the western, paved part of MDA B, implying that the present source for much of the runoff is the paved surface. Runoff from the main drainages can be traced over the gently sloping upper mesa southward to the steep rocky slopes and cliffs of Tshirege unit 3. This runoff is in part braided and takes multiple, meandering courses between fracture-bounded blocks of tuff. Bandelier Tuff bedrock is exposed along much of the drainage courses above the cliffs and few sediment-storage sites exist. Thus there are relatively few sites for infiltration of significant runoff into sediment or storage of contaminants, although some infiltration of runoff into fractures in the bedrock probably occurs.

Additional runoff, probably of much smaller volume, leaves the dirt road and diffuses rapidly onto the mesa; recognizable drainages cannot be traced far. The diffuse runoff south of the MDA B dirt road generally can only be

traced a few feet over the mesa surface and most of the water may infiltrate into the mesa-top soils. Also, the present locations of this diffuse runoff are strongly influenced by subtle features such as low berms along the road. These features are probably ephemeral, so that the location of diffuse runoff shifts over time. Much of the runoff may infiltrate into the shallow soil or into fractures on the rocky slope before reaching BV Canyon. Any contaminants that may have been transported by surface runoff away from MDA B are unlikely to have been concentrated on the slope. It is more likely that they would have been dispersed on the slope or transported down into BV Canyon.

The axis of BV Canyon contains many sites of potential sediment deposition—and, therefore, sites of potential deposition of contaminants. The bottom of BV Canyon, generally a grassy flat in the lower reaches, grades into patches of grass among rockfall boulders upstream. The canyon floor lacks a distinct channel for the lower 600 ft above the waterfall and has a discontinuous channel upstream. Notably, for the lower 1200 ft above the waterfall, the valley floor alternates between narrow, confined reaches (5 to 10 ft wide) and wider, unconfined reaches (20 to 30 ft wide). At present, the areas immediately downstream of confined reaches are the most significant sites of sediment deposition in BV Canyon. At these sites, runoff spreads and shallows over unchanneled grassy flats, losing its capacity to transport sediment. The presence of a grassy bed, which increases roughness, should also tend to slow the flow and encourage sediment deposition.

Four sites of sediment deposition in BV Canyon that are potential sediment sampling sites are shown on Plate 5. Two of these are sites of significant flow expansion, roughly 600 and 1200 ft above the waterfall at the lip of the hanging valley, where rapid shallowing of the flow should encourage sediment deposition. The third site is in a confined reach near the downslope end of the hanging valley, downstream of all side channels from both MDA B and the west side of MDA V. The fourth site is roughly 1700 ft above the waterfall, where a recent rockfall—burying most of a vintage car's hood—partially blocked the canyon and created a sediment trap.

Future sediment samples from BV Canyon should probably be obtained in transects across the valley flat because runoff spreads over these areas and likely would disperse any contaminants. Samples should also be acquired over a depth interval such as 0 to 6 in. because these are likely sites for burial of sediments and any associated contaminants.

Present surface runoff away from the perimeter of MDA V is generally diffuse and spreads over the mesa surface in unchanneled flow. Distinct surface channels are present only near the southeast corner of MDA V; surface runoff flows over the mesa and then drops over the steep, rocky Tshirege unit 3 slopes immediately east of the BV Canyon waterfall. There are no major sediment deposition areas associated with this runoff. Some of the diffuse runoff also concentrates in the shallow drainage west of MDA V, which drains into BV Canyon.

Cliff Retreat

The available data on cliff-retreat processes at TA-21 indicate that exposure of buried waste by cliff retreat south of MDA B is improbable within a time frame of 10,000 years or more. As discussed earlier, extensive pitting and erosional modification of the south-facing cliffs bordering the shallow tributaries to Los Alamos Canyon (BV and DP Canyons) suggest that failures are much less frequent here than on the south-facing cliffs bordering Los Alamos Canyon. In addition, the minimal retreat that could have occurred for cliffs adjacent to the older alluvial deposits provides evidence for maximum average retreat rates of 0.11 to 0.26 ft/ky, or 1.1 to 2.6 ft/10,000 yr. Using average rates can be misleading, however, because retreat probably occurs in discrete rockfall events.

The largest measured block south of MDA B is ~16 ft thick measured perpendicular to the cliff face (Fig. 11), and local retreat of this scale could presumably occur at any time—especially during earthquakes. Nevertheless, the closest the cliffs of BV Canyon approach MDA B is ~60 ft at the southeast end; thus exposure of the wastes by cliff retreat is extremely unlikely within a period of 10,000 years and could conceivably require in excess of 100,000 years.

The risk of exposure of buried wastes by cliff retreat at MDA V is more difficult to evaluate. The original cliff adjacent to MDA V probably was deeply embayed, as is the case further west along BV Canyon. Field and airphoto examination indicates that the head of an embayment was buried by artificial fill at the southwest corner of the MDA. The southwest corner of Absorption Bed 3 at MDA V may approach within 20 to 25 ft of the steep edge of this artificial fill (bed location from Fig. 16.7-2, TA-21 RFI Work Plan) and is possibly within several feet of the edge of the original cliff. The stability of the artificial fill is unknown, but the fill slope has a gradient of ~0.85 (40°), and noncompacted fill as probably occurs at this site is often unstable at such steep slopes. Failure of the fill slope and the buried edge of the former cliff during a triggering event like an earthquake or intense rainstorm should be considered possible with the consequent exposure of the southwest corner of Absorption Bed 3. Also, an increase in the width of Los Alamos Canyon near MDA V (Fig. 16) suggests locally higher cliff-retreat rates here, which are possibly associated with the increase in fracture density reported by Wohletz (Sec. III, this report).

MDAs A, T, and U

Sediment Transport and Deposition

MDAs A, T, and U are located on the north edge of DP Mesa and drain north into DP Canyon. It is known that radioactive contaminants, including plutonium, have been transported down DP Canyon in small concentrations (Purtymun, 1971, 1974; Purtymun *et al.*, 1990). The source of these contaminants is thought to be primarily outfalls from TA-21. It is possible that contaminants also have been derived partly from surface erosion at the MDAs and from air emissions at TA-21.

Surface drainage from all three MDAs is channeled along the access road adjoining TA-21 to the north and feeds into culverts that discharge below the road. The surface runoff from the three MDAs flows down the steep Tshirege unit 3 slopes before spreading over gentle, grassy slopes developed on alluvium and slopewash in the bottom of DP Canyon (Plate 4). These gentle slopes are likely sites of deposition for much of the sediment carried by the surface runoff and are appropriate sites for sediment sampling to determine whether significant amounts of contaminants have been deposited downslope of the MDAs. In addition, small areas of sediment deposition are present below MDAs A and U in narrow troughs in the tuff below the road (Plate 4). These are also appropriate sites for sediment sampling.

The bottom of DP Canyon is underlain in part by sediment that was deposited since development began in the watershed, as discussed earlier; the evidence for the young age is provided by the presence of exotic material within the sediments. This historic sediment can reach 7 ft in thickness upstream of the MDAs, although thicknesses of ~3 ft are more common in the reach affected by the MDAs and outfalls. Previous sampling of sediment in upper DP Canyon has been restricted to the presently active channel (Purtymun, 1971). It is possible that contaminants were deposited in the valley bottom sediments as they aggraded during historic time. There are natural streambank exposures of the historic sediments down-channel from the MDAs, immediately above where the channel steepens and cuts into Tshirege unit 2 bedrock. These exposures are appropriate sampling sites for determining whether significant amounts of

contaminants are stored in these sediments. One suggested sampling site, at an excellent north-south streambank exposure, is shown on Plate 4. Sampling to span this vertical exposure is recommended—such as in several depth intervals (for example, 0 to 6 in., 6 to 12 in., etc.). If contaminants are found, more detailed sampling of individual stratigraphic layers may be warranted because the contaminants may be concentrated in one or more discrete layers.

Cliff Retreat

Available data on cliff-retreat processes at TA-21 suggest that exposure of buried waste by the retreat of the slopes north of MDAs A, T, and U is unlikely within time frames of 10,000 years or more. No evidence of recent rockfalls was observed along the north-facing walls of DP and BV Canyons and, as discussed earlier, the distribution of the older alluvial deposits provides evidence for extremely slow retreat rates on the slopes bordering the shallow tributary valleys to Los Alamos Canyon (including upper DP Canyon). The northern margins of MDAs A, T, and U are about 200, 65, and 75 ft, respectively, from the break in slope at the top of the steep Tshirege unit 3 slopes and farther than MDA B; thus, exposure by cliff retreat caused by repeated rockfalls is considered unlikely.

The possibility of infrequent, larger scale mass-wasting on the north side of DP Mesa is suggested by the presence of anomalous arcuate troughs and steps north of MDAs A and U (Plate 4). These features are similar to steps and troughs that develop at the heads of large landslides. However, there is no other evidence for landsliding on this scale within the shallow canyons at TA-21, and it seems more reasonable that another mechanism created these features. Specifically, the arcuate steps occur west of and roughly on line with the paleo-stream channel that contains the older alluvial deposits (Plate 3), and the steps may have been carved by similar streams that once flowed over the top of DP Mesa. In addition, even if these steps were created by large-scale landsliding, future failures would most likely involve movement of the already detached blocks north of the MDAs (if they exist) and would not expose buried contaminants.

SUMMARY

The most significant pathway for surface transport of contaminants at TA-21 is erosion by surface runoff. Contaminants that are available for surface transport may be present in sediment previously eroded from MDAs or downslope of outfalls, or may be widely dispersed over the area as a result of air emissions. The most likely sites for deposition and temporary storage of contaminants downslope of the MDAs are shown on Plates 6 and 7. Below MDAs B and V, these sites are within BV Canyon, a shallow, low-gradient tributary to Los Alamos Canyon, where modern sediment deposition occurs on the grassy valley floor. Below MDAs A, T, and U, these sites are on grassy alluvial surfaces on the margins of the main DP Canyon channel and at local sediment-deposition areas upslope. Sediment deposited at each of these sites should be considered in temporary storage. The long-term record of sediment erosion and deposition in DP Canyon indicates that remobilization of this sediment can occur on time scales of years to thousands of years. In addition, the valley floor in DP Canyon has undergone aggradation by deposition of sediment in the last 50 years, and it is possible that contaminants eroded from MDAs or discharged from outfalls are retained within these sediments. The modern channel of DP Canyon has incised these historic sediments, and contaminants within previously deposited sediment may be supplied to the modern channel through bank erosion. Samples from these historic sediments exposed in streambanks in DP Canyon can be used to determine contaminant concentrations and possible contaminant sources for the stream.

All five MDAs at TA-21 are located near the edges of DP Mesa, and eventual exposure of buried contaminants by the retreat of cliffs is possible. Along the cliffs bordering Los Alamos Canyon, partially detached landslide blocks show that failure can occur up to at least 75 ft from the mesa edge. Single failures of this scale should be considered possible along the rim of Los Alamos Canyon, especially during earthquakes. However, the MDAs border shallow tributary canyons to Los Alamos Canyon, where the geomorphic characteristics provide evidence that rockfalls are very infrequent and that MDAs more than 50 ft from the cliffs should be considered stable with respect to mass-wasting for periods exceeding 10,000 years. Four of the five MDAs meet this criteria. The possible exception, MDA V, may have an absorption bed within 20 to 25 ft of the mesa edge. The mesa edge here consists of artificial fill that buries the head of an embayment along the canyon wall. Absorption Bed 3 may be within several feet of the original mesa edge, and exposure of the southwest corner of this bed through failure of the artificial fill or an adjacent buried fracture-bounded block of tuff should be considered possible during an earthquake or intense rainstorm. Local increases in canyon width (Fig. 16) and fracture density (see Wohletz, Section III, this report) near MDA V also suggest the potential for relatively fast rates of cliff retreat here.

DP Spring, which contains low concentrations of tritium, emerges from the base of an old valley fill in lower DP Canyon. This valley fill probably extends less than 300 ft upcanyon from DP Spring and is largely confined to the part of the canyon that is cut into the nonwelded units of the Bandelier Tuff. Because the spring is perennial—in contrast to the intermittent surface flow farther up DP Canyon—the water must have infiltrated into the tuff upstream, either directly from the stream channel or after first infiltrating alluvium. The favored model for the springwater flow path is that water from the alluvium in upper DP Canyon infiltrates the highly fractured Tshirege units 2 and 1v and emerges from the fractures into the upper part of the valley fill in lower DP Canyon. From there, the water flows through the valley fill before emerging at the contact between the valley fill and the Tshirege unit 1g at DP Spring.

ACKNOWLEDGEMENTS

This work was funded by the Los Alamos National Laboratory ER Program as part of site characterization activities for TA-21. The author thanks G. Eller, D. Broxton, and M. Devaurs for their support; J. Poths for cosmogenic ^{21}Ne analyses; D. Anderson, K. Anderson, J. Carney, and K. Reid for field and laboratory assistance; D. Walther for FIMAD map preparation; and D. Broxton, G. Eller, and J. Gardner for helpful review comments.

REFERENCES CITED

Broxton, D.E., Heiken, G., Chipera, S.J., and Byers, F.M., 1995, Stratigraphy, petrography, and mineralogy of Bandelier Tuff and Cerro Toledo deposits, Los Alamos National Laboratory, New Mexico, this report.

Dunne, T. and Leopold, L.B., 1978, Water in environmental planning, W.H. Freeman and Company, San Francisco, 818 pp.

Gardner, J.N., Baldridge, W.S., Gribble, R., Manley, K., Tanaka, K., Geissman, J.W., Gonzalez, M., and Baron, G., 1990, Results from seismic hazards trench #1 (SHT-1) Los Alamos Seismic Hazards Investigations Report EES1-SH90-19, Los Alamos, New Mexico.

Goff, F., 1995, Geological map of TA-21, Los Alamos National Laboratory, New Mexico, Sec. II, this report.

Izett, G.A. and Obradovich, J.D., 1994, $^{40}Ar/^{39}Ar$ age constraints for the Jaramillo Normal Subchron and the Matuyama-Brunhes geomagnetic boundary, *J. Geophys. Res. 99 (B2)*, 2925-2934.

Keefer, D.K., 1984, Landslides caused by earthquakes, *Geol. Soc. Am. Bull. 95,* 406-421.

Keefer, D.K. and Wilson, R.C., 1989, Predicting earthquake-induced landslides, with emphasis on arid and semi-arid environments, in *Landslides in a semi-arid environment, with emphasis on the inland valleys of southern California,* P.M. Sadler and D.M. Morton, eds., *Publ. Inland Geol. Soc. 2,* 118-149.

Lal, D., 1991, Cosmic ray labeling of erosion surfaces: *in situ* nuclide production rates and erosion models, *Earth Planet. Sci. Lett.104,* 424-439.

Nishiizumi, K., Kohl, C.P., Arnold, J.R., Klein, J., Fink, D., and Middleton, R., 1991, Cosmic ray produced ^{10}Be and ^{26}Al in Antarctic rocks: exposure and erosion history, *Earth Planet. Sci. Lett.104,* 440-454.

Poths, J. and Goff, F., 1990, Using cosmogenic noble gases to estimate erosion rates, *EOS, Trans. Am. Geophys. Union 71,* 71.

Purtymun, W.D., 1971, Plutonium in stream channel alluvium in the Los Alamos area, New Mexico, Los Alamos Scientific Laboratory report LA-4561.

Purtymun, W.D., 1974, Storm runoff and transport of radionuclides in DP Canyon, Los Alamos County, New Mexico, Los Alamos Scientific Laboratory report LA-5744.

Purtymun, W.D. and Kennedy, W.R., 1971, Geology and hydrology of Mesita del Buey, Los Alamos Scientific Laboratory report LA-4660.

Purtymun, W.D., Peters, R., and Maes, M.N., 1990, Transport of plutonium in snowmelt run-off, Los Alamos National Laboratory report LA-11795-MS.

Reneau, S.L., Gardner, J.N., Kelson, K.I., and Hemphill-Haley, M.A., 1993, Holocene stream aggradation and degradation, Pajarito Plateau, northern New Mexico, *Geol. Soc. Am. Abst. Prog. 25, no. 5,* 138.

Stuiver, M. and Reimer, P.J., 1993, Extended ^{14}C data base and revised CALIB 3.0 ^{14}C age calibration, *Radiocarbon 35,* 215-230.

Vaniman, D. and Wohletz, K., 1990, Results of geological mapping/fracture studies: TA-55 area, Los Alamos National Laboratory Seismic Hazards Memo EES1-SH90-17 (3 plates).

Wohletz, K., 1995, Measurement and analysis of rock fractures in the Tshirege Member of the Bandelier Tuff along Los Alamos Canyon adjacent to TA-21, this report.

PRELIMINARY DRILLING RESULTS FOR BOREHOLES LADP-3 AND LADP-4

by

D. E. Broxton, P. A. Longmire, P. G. Eller, and D. Flores

This report presents preliminary geologic and hydrologic findings for two geologic characterization boreholes drilled in autumn 1993 as part of TA-21 RFI investigations. LADP-3 was drilled to determine if perched groundwater occurs at depths greater than that of alluvial groundwater in Los Alamos Canyon. LADP-4 was drilled to determine if perched groundwater occurs beneath DP Canyon and to investigate whether subsurface contaminants from the industrialized areas of TA-21 have migrated northward towards DP Canyon.

LADP-3 penetrated a thick sequence of slope-derived colluvium and stream-derived alluvium on the canyon floor before entering bedrock. Bedrock units penetrated by the borehole include the Otowi Member of the Bandelier Tuff (including the Guaje Pumice Bed) and gravels of the Puye Formation. This borehole encountered two perched groundwater zones. The upper zone is part of the canyon's alluvial groundwater and is divided into two distinct zones of saturation. An intermediate-depth perched groundwater zone was encountered at a depth of 325 ft in the Guaje Pumice Bed. Water from this deeper perched zone contains 6.0 $\pm$ 0.16 nCi/ℓ of tritium—which is above regional background for surface water but well below the drinking water standard of 20 nCi/ℓ. Preliminary analyses for low-level ^{137}Cs and Pu isotopes failed to detect these constituents. Mixing calculations suggest that ~70% of the groundwater in the Guaje Pumice Bed is recharge from alluvial groundwater.

LADP-4 penetrated alluvium on the canyon floor and entered the following bedrock units: the Tshirege Member of the Bandelier Tuff (including the Tsankawi Pumice Bed), fluvial sediments of the Cerro Toledo interval, the Otowi Member of the Bandelier Tuff (including the Guaje Pumice Bed), and fluvial sands, gravels, and cobbles of the Puye Formation. Low-level tritium was found in this borehole. Preliminary laboratory analysis yielded 2.15 $\pm$ 0.18 pCi/g tritium in a tuff sample collected from a moist zone associated with the Tshirege unit 1v/1g boundary at a depth of 158.6 to 160.1 ft. This value is above background but well below the screening action level of 820 piC/g. The origin of the tritium is not yet known, but moisture transport from several industrial sites at TA-21 is a possibility.

Additional chemical and radiochemical analyses are being conducted to more fully characterize potential contamination in these two boreholes. Also, hydrologic testing of core samples is underway to characterize the geohydrologic properties of subsurface units at TA-21.

INTRODUCTION

During autumn 1993, two geologic characterization boreholes were drilled at TA-21. Borehole LADP-3 is located in Los Alamos Canyon south of TA-21, and borehole LADP-4 is located in DP Canyon to the north (Fig. 1). These boreholes, described in section 12.5.1.2 of the RFI work plan, were drilled to identify potential transport pathways in the vadose zone and to characterize vertical and lateral variations in the geohydrologic properties of the site. All work was done according to the RFI work plan.

LADP-3 was drilled to determine if perched groundwater occurs at depths greater than that of the alluvial groundwater in Los Alamos Canyon. In addition, geologic and hydrologic data from LADP-3 are being collected in conjunction with data from other nearby boreholes to identify the presence and properties of major hydrogeologic units at TA-21. These data are used to improve conceptual models for the site, identify potential transport pathways, and provide useful planning information for subsequent drilling operations at TA-21.

LADP-4 was drilled to determine if perched groundwater occurs beneath DP Canyon and to investigate whether subsurface contaminants from the industrialized areas of TA-21 have migrated northward towards DP Canyon. In addition, geologic and hydrologic data from LADP-4 is being collected to characterize the major hydrogeologic units at TA-21.

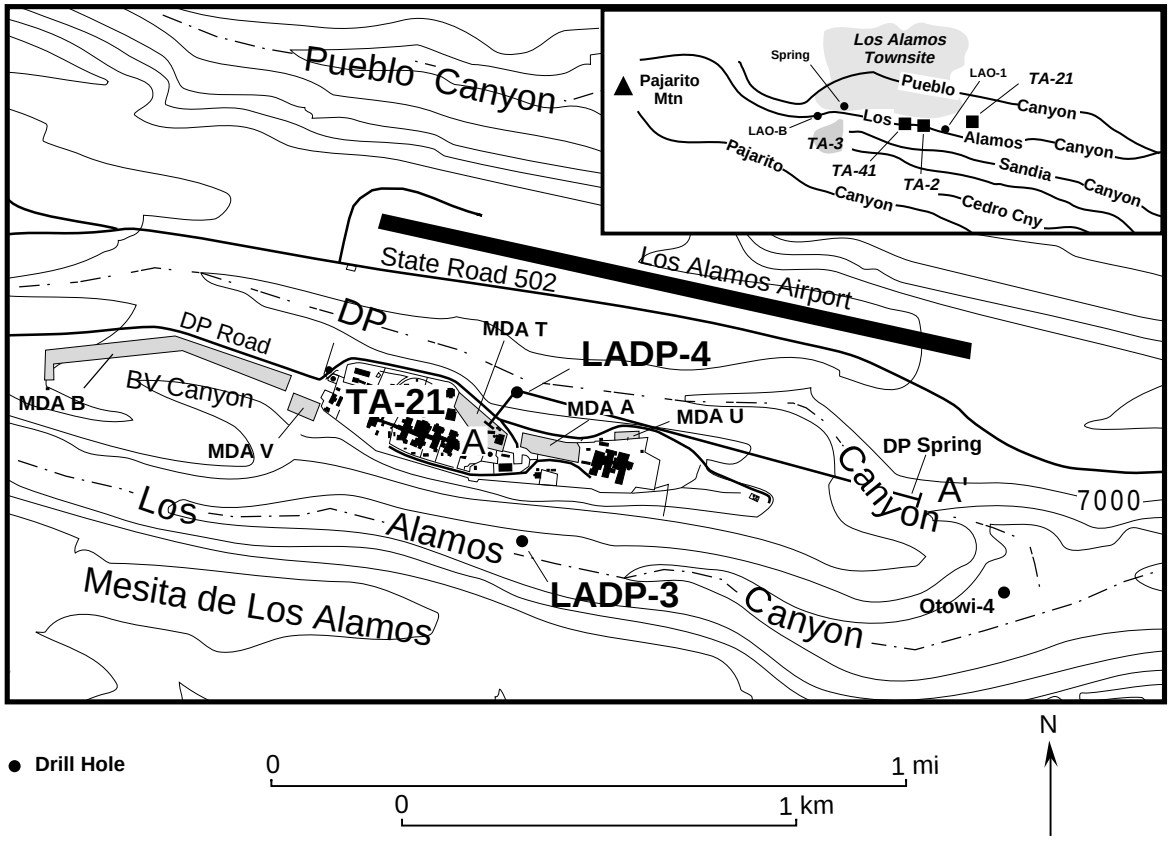

Fig. 1. Map showing locations of boreholes LADP-3 and LADP-4 at TA-21. A-A' is the line of cross section shown in Fig. 15. Inset shows locations of the monitoring wells and DP Spring.

METHODS

LADP-3

Drilling of LADP-3 began November 2, 1993, and was completed on December 17, 1993. Originally, the target depth for LADP-3 was determined by the elevation of the uppermost basalt penetrated by borehole Otowi 4, located ~0.75 miles to the east (Fig. 1), or 490 ft—whichever was encountered first. However, because groundwater was encountered at 325 ft, drilling was terminated at 350 ft after the extent of the perched zone was determined.

LADP-3 was drilled from the surface to 232 ft using an 8.5-in. hollow-stem auger. The borehole was completed to the final depth of 350 ft using air-rotary drilling methods (Fig. 2). Rock coring, using a 4.5-in.-diam rock barrel, alternated with advancement of 5.625-in.-i.d. ODEX casing from 232 to 350 ft. Alluvial and surface groundwater were cased out of the borehole by installing and grouting permanent 8.625-in.-o.d. surface casing to a depth of 90 ft.

Samples for gravimetric moisture and tritium analyses were collected every 5 ft in LADP-3. Four background geochemical and radiochemical samples were also collected. The analytical suite for chemical and radionuclide characterization are described in Table 12.5-III of the RFI work plan. In addition, 36 intact core samples were collected for analysis of hydrogeologic properties. The core was sealed in airtight containers to prevent changes in moisture content and other properties. Water samples were collected from the alluvial groundwater and from the perched zone at 325 ft. Except as noted below, laboratory analyses of cores and water samples are not yet available.

LADP-4

Drilling of LADP-4 began August 30, 1993, and was completed November 7, 1993. Well LADP-4 was drilled to a depth of 800 ft using air-rotary methods (Fig. 3). Surface and near-surface groundwater were cased out of the hole with a 10.75-in.-o.d. surface conductor pipe cemented around the well to a depth of 28 ft. ODEX casing (8.625-in.-o.d.) inside the first pipe lines the hole to a depth of 579 ft. From 579 to 800 ft the ODEX casing telescopes to 6.626-in.-o.d. Continuous core 4.5 in. diameter was collected from the surface to 573-ft depth. Cuttings were collected from 573- to 800-ft depth because the unconsolidated nature of the Puye Formation prevented intact core recovery.

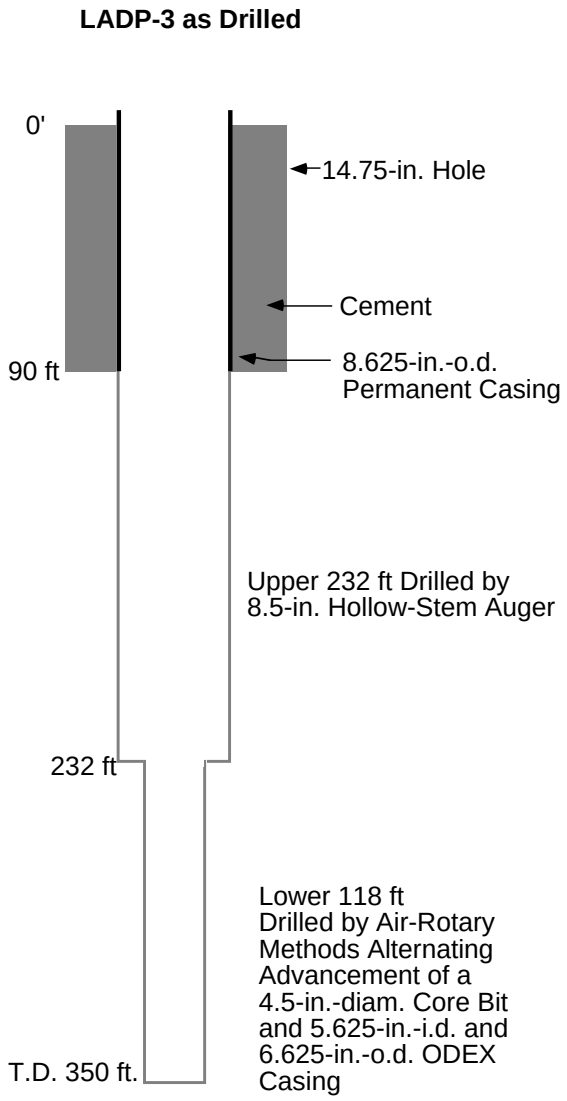

Fig. 2. Construction of LADP-3. (Prepared from data provided by J.C. Newsom and E.D. Davidson, Jr.)

Samples for moisture and tritium analyses were collected every 5 ft for the total depth of LADP-4. Six background geochemical and radiochemical samples also were collected. The analytical suite for chemical and radionuclide characterization is presented in Table 12.5-III of the RFI operable unit work plan. Except as noted below, laboratory analytical results are not yet available. In addition, 25 intact core samples were collected for characterization of hydrogeologic parameters. The core samples were sealed in airtight containers to prevent changes in moisture content and other properties before analysis.

RESULTS

LADP-3

LADP-3 penetrated a thick sequence of slope-derived colluvium and stream-derived alluvium on the canyon floor before entering bedrock. Bedrock units penetrated by the borehole include the Otowi Member of the Bandelier Tuff (including the Guaje Pumice Bed) and gravels of the Puye Formation. Preliminary geologic information for LADP-3 is summarized in Figs. 4 and 5.

Thin sheets of groundwater were encountered at depths of 27 and ~35 ft. These sheets of groundwater occur in stream-deposited alluvium and are at or slightly below the elevation of the main stream channel in Los Alamos

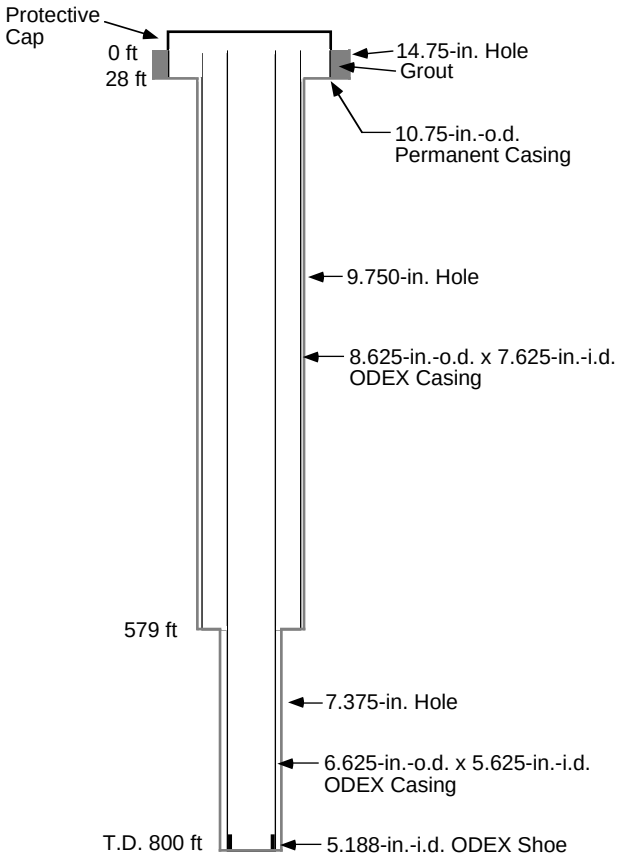

Fig. 3. Construction of LADP-4. (Prepared from data provided by J.C. Newsom and E.D. Davidson, Jr.)

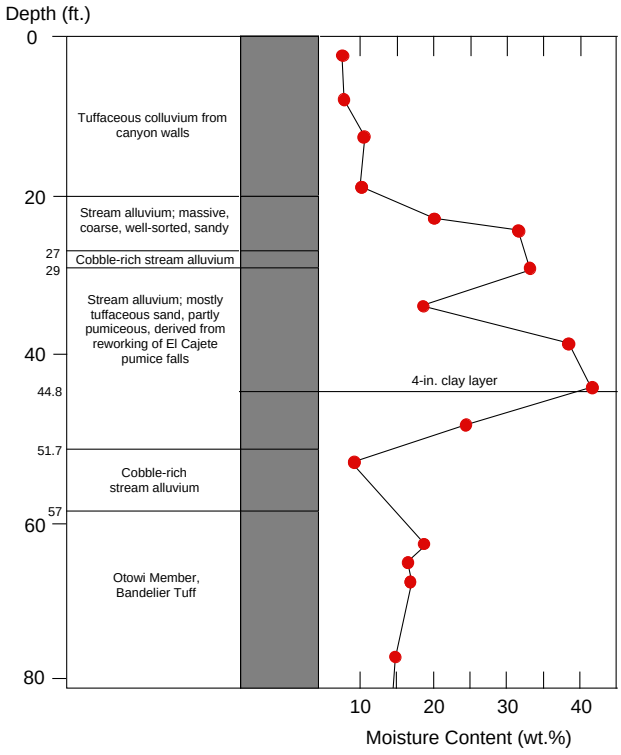

Fig. 4. Preliminary geologic information and variations in moisture content in the alluvial groundwater penetrated by the upper part of LADP-3 in Los Alamos Canyon.

Canyon. Because of their position relative to the canyon floor and the nature of their host deposits, these sheet flows are interpreted as being part of the alluvial groundwater in Los Alamos Canyon. Laboratory analyses of water collected from the alluvial groundwater are not yet available.

Another perched groundwater was encountered at a depth of 325 ft in the lower part of the Guaje Pumice Bed. Borehole operations were temporarily suspended at the base of the Guaje Pumice Bed to evaluate this perched zone. Initially, there was 15 ft standing water in the borehole, but after several days the standing water level dropped to ~5 ft. Drilling operations resumed to determine the nature and extent of the groundwater. A clay layer a few inches thick was found at the top of the Puye Formation. This clay layer might be a paleosoil and may act as a permeability barrier that causes the groundwater to perch in the overlying pumice bed. Drilling stopped at the 350-ft depth within Puye Formation after it was determined that the groundwater is confined to the Guaje Pumice Bed.

Water from the perched groundwater at 325 ft was analyzed for major constituents and tritium (see Table I for a summary of results

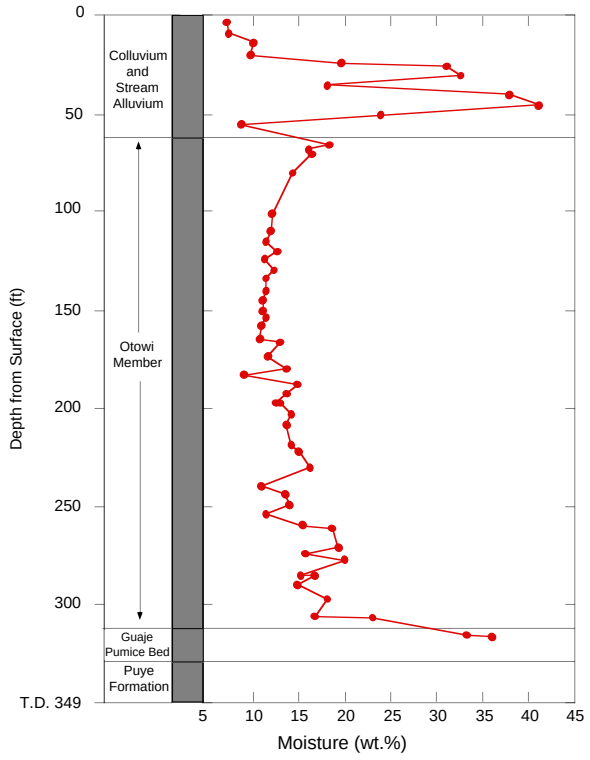

Fig. 5. Preliminary geologic information and variation in moisture content as a function of depth in borehole LADP-3, Los Alamos Canyon.

TABLE I.
CHEMISTRY OF GROUNDWATER SAMPLE PP93-36 AT 325-FT DEPTH IN BOREHOLE LADP-3, LOS ALAMOS CANYON [a]

Ag	<0.0005	Sb	<0.001
Al	0.21 ± 0.03	Se	<0.001
As	<0.001	Si	20.0 ± 0.1
B	0.04 ± 0.01	Sr	0.13 ± 0.01
Ba	0.02 ± 0.01	Zn	0.16 ± 0.01
Br	0.07		
Ca	11.7 ± 0.1	ClO_3	<0.02
Cd	<0.001	CO_3	0
Cl	46.8	HCO_3	65
Co	0.004 ± 0.002	NH_4	0.32
Cr	0.003 ± 0.002	NO_2	0.37
Cs	0.002 ± 0.002	NO_3	1.21
Cu	0.008 ± 0.002	OH	0
F	0.38	PO_4	<0.02
Fe	0.13 ± 0.01	SO_4	12.8
Hg	<0.002	S_2O_3	<0.01
I	<0.01		
K	8.7 ± 0.3	Cation Sum	2.688
Li	0.02 ± 0.01	Anion Sum	2.702
Mg	4.08 ± 0.01		
Mn	0.44 ± 0.01	Total Disolved Sol.	229.3
Mo	0.022 ± 0.002	Cond. (µmho/cm)	302
Na	33.8 ± 0.9		
Ni	0.026 ± 0.002	pH	6.62
Pb	<0.002	^3H (nCi/l) [b]	6.0 ± 0.16
Rb	0.046 ± 0.004	^3H (nCi/l) [c]	5.5 ± 0.7

[a] *Values reported in ppm unless otherwise noted. Analyses (except for tritium) performed by D. Counce of the Geology/Geochemistry Group, Los Alamos National Laboratory.*
[b] *Tritium analyzed at University of Florida.*
[c] *Tritium analyzed at Group CST-9, Los Alamos National Laboratory.*

from these preliminary analyses). This groundwater contains 6.0 ± 0.16 nCi/ℓ of tritium, which is an order of magnitude above background for surface water in Los Alamos Canyon (P. Longmire, unpublished data) but well below the drinking water standard of 20 nCi/ℓ. Preliminary analyses for low-level ^{137}Cs and Pu isotopes failed to detect these constituents. Additional analyses are being conducted to determine if other contaminants are present and to further investigate the possibility of a hydrologic connection between the alluvial groundwater and groundwater in the Guaje Pumice Bed.

Moisture content was determined for 59 core samples in LADP-3. Moisture contents range from 7 to 41%, and the average moisture content is 16%. Moisture distribution as a function of depth is shown in Figs. 4 and 5.

Gravimetric moisture contents up to 40% are associated with the alluvial groundwater near the top of the borehole (Fig. 4). The moisture data reflect the sheet-like occurrence of the groundwater, which occurs in two water-producing zones. The upper zone is associated with a cobble layer at a depth of 27 ft. The lower water-producing zone occurs in a porous, pumice-rich stream alluvium and may be perched above a 4-in. clay layer at a depth of 45 ft.

Moisture contents decrease to 12 to 15% in the bedrock tuffs immediately below the canyon floor. However, moisture contents systematically increase with depth, starting at 170 ft in the middle of the Otowi Member and peak in the upper part of the Guaje Pumice Bed just above the perched groundwater (Fig. 5).

LADP-4

LADP-4 penetrated alluvium on the canyon floor and then entered the following bedrock units: the Tshirege Member of the Bandelier Tuff (including the Tsankawi Pumice Bed), fluvial sediments of the Cerro Toledo interval, the Otowi Member of the Bandelier Tuff (including the Guaje Pumice Bed), and fluvial sands, gravels, and cobbles of the Puye Formation. Figure 6 presents a preliminary geologic log for LADP-4.

The original target depth for LADP-4, 675 ft, was selected in order to penetrate potential perched groundwater zones such as those that occur in the midreach of Pueblo Canyon and near the confluence of Pueblo and Los Alamos Canyons. The borehole also was designed to intersect a basalt flow penetrated by drillhole Otowi 4 in Los Alamos Canyon (Fig. 1). Where present, massive, little-fractured basalt could act as a barrier to the downward migration of groundwater in the vadose zone—causing water to perch. Alternatively, rubble zones at the base of basalt flows are permeable and may divert flow laterally.

Neither basalt nor perched groundwater were encountered in the borehole at its original target depth. The drill hole was deepened to 800 ft to ensure that no basalt flow occurs deeper than originally projected. Drilling was terminated in gravels of the Puye Formation at a depth of 800 ft.

Moisture contents were determined for 139 samples in LADP-4. Moisture in core and cuttings range from 0 to 23%, and the average moisture content is 7%. Figure 7 shows moisture distribution as a function of depth.

Moisture contents are somewhat elevated (~10%) in surface soils and in the upper part of bedrock tuffs in LADP-4. Moisture in the tuff decreases to <5% at a depth of ~136 ft, where a noticeable increase in moisture occurs at the abrupt transition between devitrified tuffs of Tshirege unit 1v and vitric tuffs of Tshirege unit 1g; peak moisture contents reach 23%. Moisture contents also are elevated (~20%) in the lowermost part of Tshirege unit 1g and in the underlying Tsankawi Pumice Bed. Although somewhat variable, moisture in LADP-4 generally decreases with depth below the Tsankawi Pumice Bed.

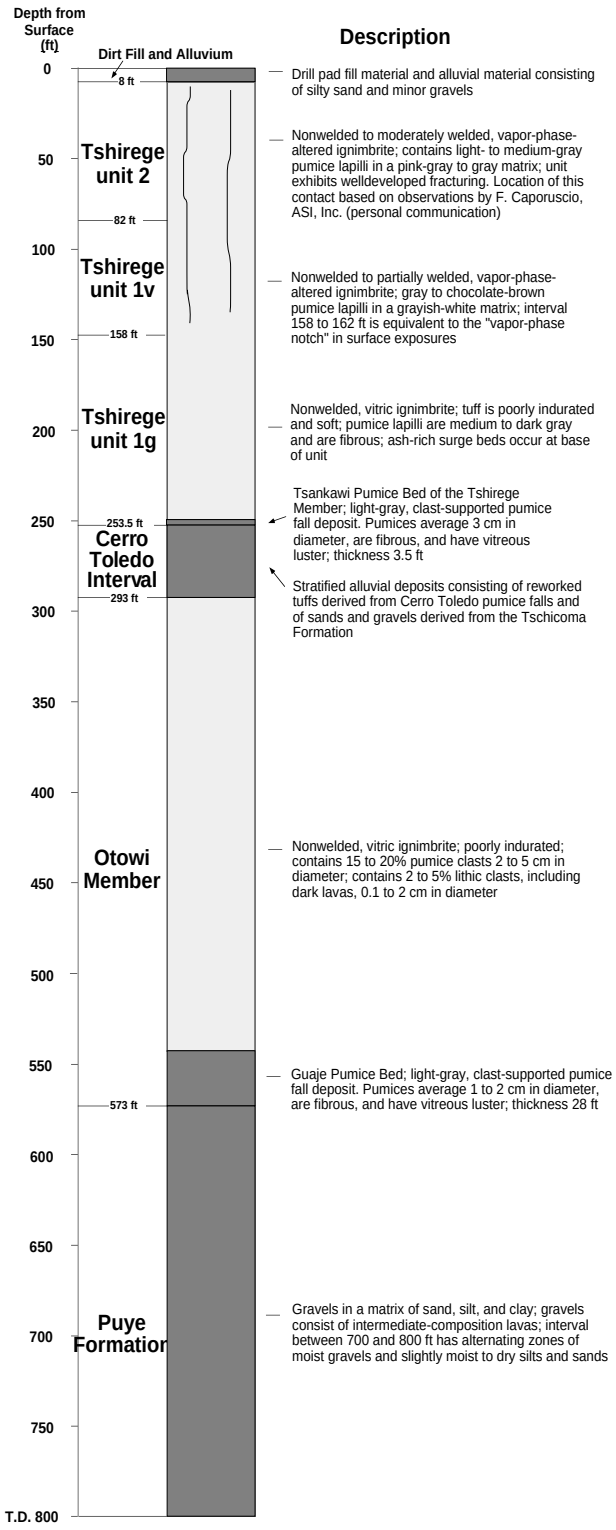

Fig. 6. Preliminary lithologic log for borehole LADP-4, DP Canyon.

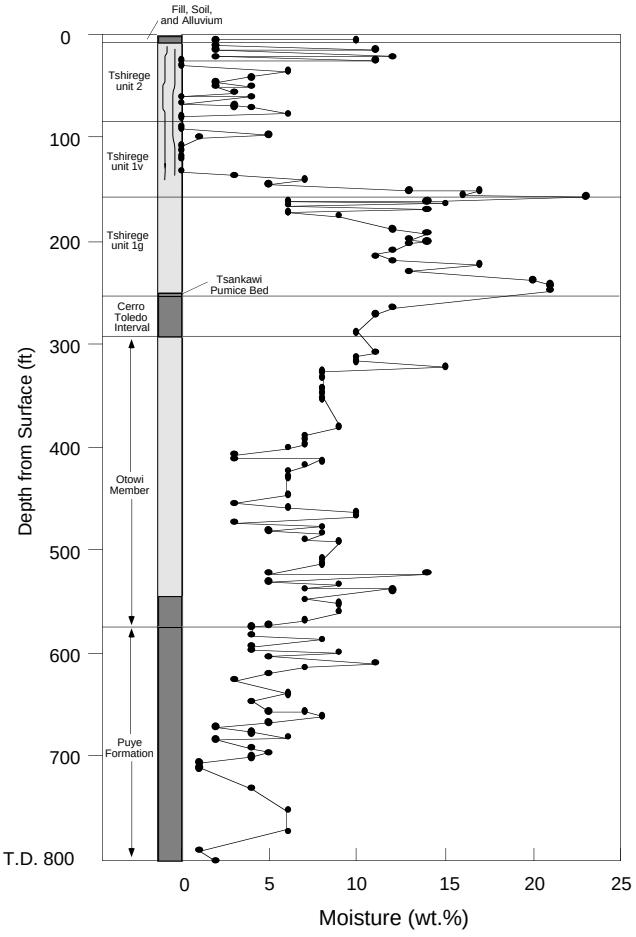

Fig. 7. Variation in moisture content as a function of depth in borehole LADP-4, DP Canyon.

Laboratory tritium results are not yet available for most samples taken from LADP-4. However, initial screening of samples in the field laboratory indicates that low-level tritium is present in some samples. A high-priority laboratory analysis yielded 2.15 ± 0.18 pCi/g tritium in a tuff sample collected from the moist zone associated with the unit 1v/1g boundary at a depth of 158.6 to 160.1 ft. This value is significantly above background but well below the screening-action level of 820 pCi/g for tritium in soils. In general, the tritium concentrations determined by the field laboratory do not correlate well with the moisture content in other parts of the borehole.

DISCUSSION

The alluvial groundwater in LADP-3 was encountered despite attempts to avoid shallow groundwater by siting the hole as far as possible from the stream channel. Evidently, canyon-bottom alluvial groundwaters in the Los Alamos area can extend at least as far laterally as their host alluvial deposits do. Most likely, the alluvial groundwater is confined on its sides and bottom by tuff bedrock, but this not yet confirmed in Los Alamos Canyon.

The chemistry of the Guaje Pumice Bed groundwater is similar in major constituents to that of the alluvial groundwater. This similarity, in addition to the presence of low-level tritium contamination, strongly suggests a hydrologic connection between the two perched groundwaters. Major-ion chemistries and tritium activities of water samples collected from monitor wells LAO-B (background) and LAO-1 as well as a spring in Los Alamos Canyon are compared to analytical results for LADP-3 to evaluate mixing relationships between alluvial and Guaje Pumice Bed groundwaters. Monitor wells LAO-B and LAO-1 are completed in alluvium upstream and upgradient of LADP-3 (Fig. 1). Results of chemical analyses of groundwater samples collected from LAO-B (Fig. 8) show that native alluvial groundwater in Los Alamos Canyon is a Ca^{2+}-Na^{+}-HCO_3^{-}-type solution. This groundwater has a total dissolved solids (TDS) content of 110 ppm. A spring sampled in Los Alamos Canyon north of the skating rink (Fig. 1) contains Na^{+}, Ca^{2+}, and HCO_3^{-} as the dominant species (Fig. 8). This spring has a TDS content of 186 ppm. Groundwater collected from LAO-1 is a Na^{+}-Cl^{-}-HCO_3^{-}-type solution (Fig. 8) and is characterized by a TDS content of 170 ppm. Concentrations of Na^{+} and Cl^{-} increase along the groundwater flow path in the alluvium in Los Alamos Canyon (Fig. 8). These increases result primarily from dissolution of road salt and discharges from Laboratory facilities and secondarily from cation exchange and weathering of the Bandelier Tuff and Tschicoma Formation, which make up the alluvial material (Longmire, unpublished data). Groundwater samples collected from LADP-3 are characterized by a mixed-ion composition in which Na^{+}, Ca^{2+}, HCO_3^{-}, and Cl^{-} are the dominant species. The TDS content of this groundwater is 229 ppm (Table I). LADP-3 groundwater is enriched in Cl^{-} and Na^{+} relative to water from LAO-B and the spring (Fig. 8). Groundwater within the Guaje Pumice Bed is chemically similar to alluvial groundwater collected from monitor well LAO-1 (Fig. 8). This similarity in major-ion chemistries suggests that alluvial groundwater is recharging the Guaje Pumice Bed.

Figure 9 is a volumetric-mixing curve for the Guaje Pumice Bed and alluvial groundwaters that is based on the conservative species Cl^{-}. End members for this mixing curve include an estimated Cl^{-} concentration for noncontaminated groundwater in the Guaje Pumice Bed (3.2 ppm, $10^{-4.06}$ molal) and an average Cl^{-} concentration (64.51 ppm, $10^{-2.74}$ molal) in groundwater samples collected from LAO-1 over 25 years (1966 to 1991). Monitor well LAO-1 is located hydrologically upgradient of LADP-3. Figure 9 suggests that ~70% of the groundwater in the Guaje Pumice Bed is derived from alluvial groundwater.

Figure 10 shows tritium activities observed in alluvial groundwater (LAO-1). Tritium fluctuations observed in LAO-1 probably are the result of the sampling time, variations in source concentration, radioactive decay, and dispersion. Tritium occurs as tritiated water ($^{1}H^{3}HO$), and its retardation factor is equal to unity, which makes this species an excellent radioactive groundwater tracer. A calculated radioactive-decay curve for tritium activities observed in LADP-3 (6.0 ± 0.16 nCi/ℓ) is also shown in Fig. 10. An estimate of groundwater flow velocity in the vertical direction can be calculated from Fig. 10; overlap of the two curves places a plausible time of groundwater recharge from the alluvium to Guaje Pumice Bed (325-ft depth). This

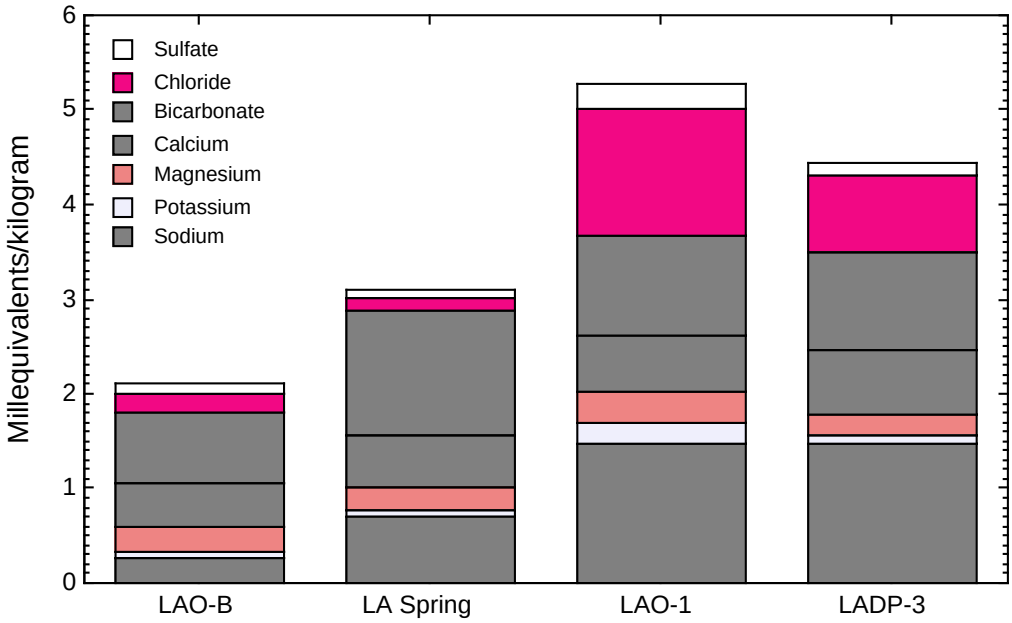

Fig. 8. Major-ion chemistry for selected waters in Los Alamos Canyon.

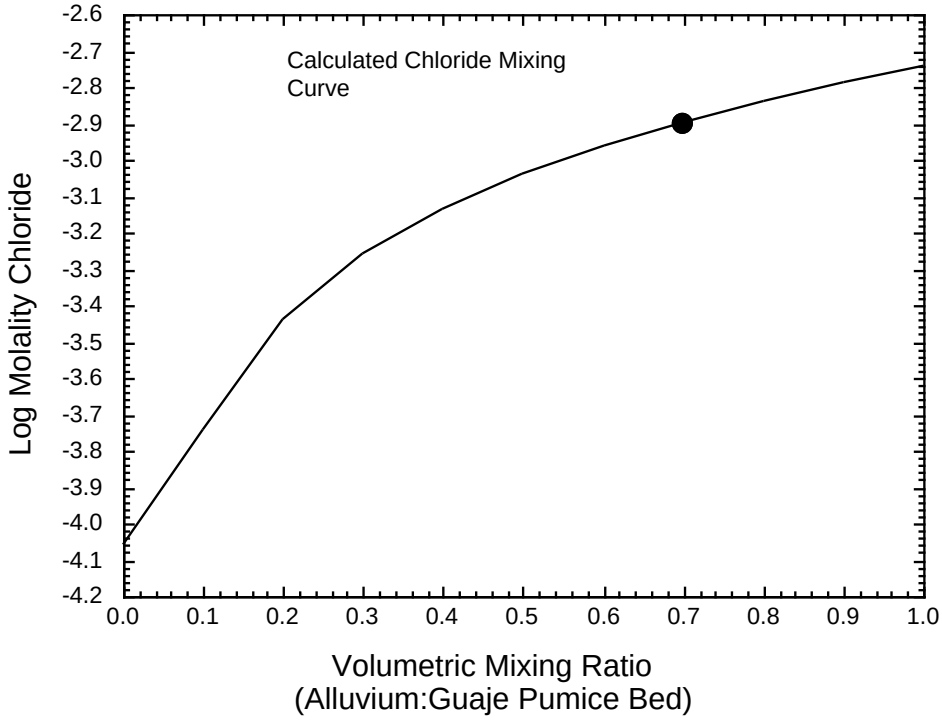

Fig. 9. Calculated volumetric chloride mixing curve for alluvial groundwater (monitor well LAO-1) and Guaje Pumice Bed groundwater (LADP-3), Los Alamos Canyon. The filled circle represents the mixing ratio for groundwater collected from LADP-3.

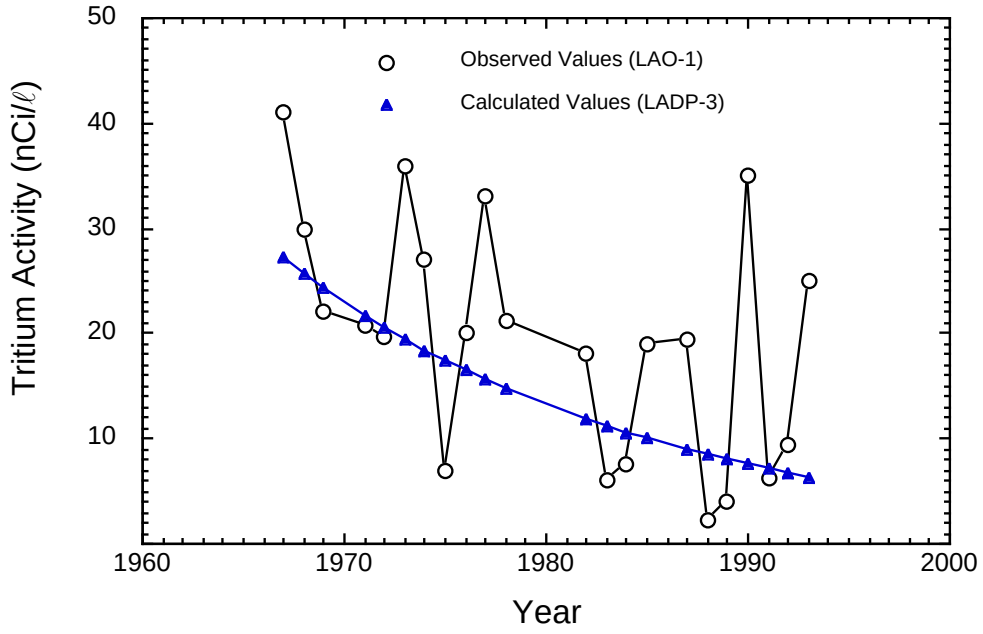

Fig. 10. Observed tritium activities in alluvial groundwater (monitor well LAO-1) and calculated tritium decay in Gauje Pumice Bed groundwater (LADP-3), Los Alamos Canyon.

assumes that (1) tritium concentrations observed at LAO-1 are representative of alluvial groundwater recharging the Guaje Pumice Bed, (2) decreases of tritium activities are mainly due to radioactive decay ($T^{1/2}$ for tritium is 12.33 years), and (3) dispersion and evapotranspiration are insignificant. Based on the data shown in Fig. 10, a realistic recharge event possibly occurred in 1972, which suggests that a minimum vertical groundwater flow velocity, calculated for 1994, is 15 ft/year (325 ft/22 years). This calculation applies to fracture and matrix flow, where the vertical groundwater flow velocity is controlled by the degree of saturation, the unsaturated hydraulic conductivity, and the hydraulic gradient.

One hypothesis for the origin of Guaje Pumice Bed groundwater is that infiltration occurs at several points of recharge or along a line source of recharge on the canyon bottom. Surface water and alluvial groundwater, the likely sources of recharge, may reach the Guaje Pumice Bed as porous media flow through local zones of saturation (Fig. 11). Given the relatively low moisture content (10 to 15%) in the upper part of the Otowi Member (Fig. 5), it is unlikely that LADP-3 penetrated a zone of recharge. These moisture contents represent ~25% saturation in tuffs containing 40 to 50% porosity. Groundwater movement at these low saturation levels could occur only if the smallest pores in the tuff are interconnected. It is possible that recharge occurs upstream of LADP-3 or that the recharge pathways are tortuous and poorly characterized by individual boreholes.

Alternatively, faults, fractures, and joints crossing the canyon floor may act as preferential pathways for recharge that reaches the Guaje Pumice Bed (Fig. 11). Where present, these structural features may act as conduits that allow groundwater to bypass unsaturated rocks before spreading laterally in permeable stratigraphic units. The Guaje Mountain fault, which is projected to cross Los Alamos Canyon in the vicinity of TA-2, is an example of a structural feature that may act as a conduit for recharge of perched systems beneath the canyon floor.

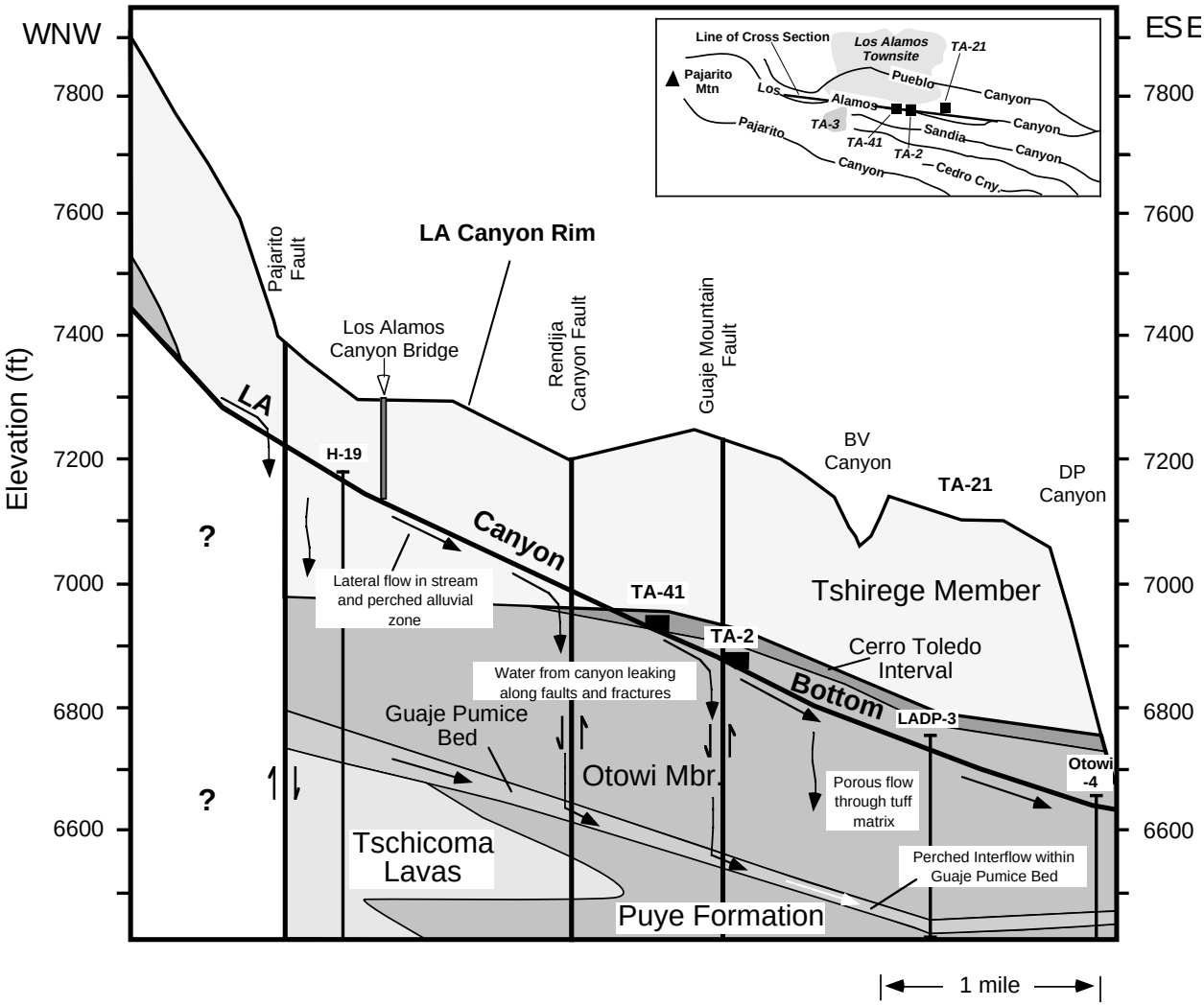

Fig. 11. Schematic cross section showing possible groundwater pathways (black arrows) below the floor of Los Alamos Canyon. Stream-fed shallow groundwater moves downcanyon within alluvial deposits in the canyon bottom. Infiltration of this shallow groundwater feeds at least one intermediate-depth perched zone in the Guaje Pumice Bed. Infiltration may occur either as porous media flow through partially saturated tuffs or as fracture flow along faults, fractures, and joints. Displacements along the Rendija Canyon and Guaje Mountain faults may be significant in pre-Bandelier units but are not shown in this figure because there are insufficient subsurface data. This cross section is based on borehole data from H-19, LADP-3, and Otowi-4 as well as surface geologic studies of Los Alamos Canyon by D.E. Broxton.

Lack of perched conditions in the Guaje Pumice Bed in LADP-4 to the north indicates that the Guaje Pumice Bed groundwater is not a laterally extensive, sheet-like body that extends under DP Mesa. However, present data are insufficient to determine how far northward this groundwater extends under TA-21 (Fig. 12). This perched groundwater may be localized under Los Alamos Canyon because the surface stream and its associated alluvial groundwater provide the likely source of recharge. Perhaps, the perched groundwater is a ribbon-like zone of saturation that follows the canyon course. Because the Guaje Pumice Bed is a pumice fall that mantles paleotopography, the elevation of this deposit may vary significantly from place to place (see Fig. 12). Thus, groundwater in the Guaje

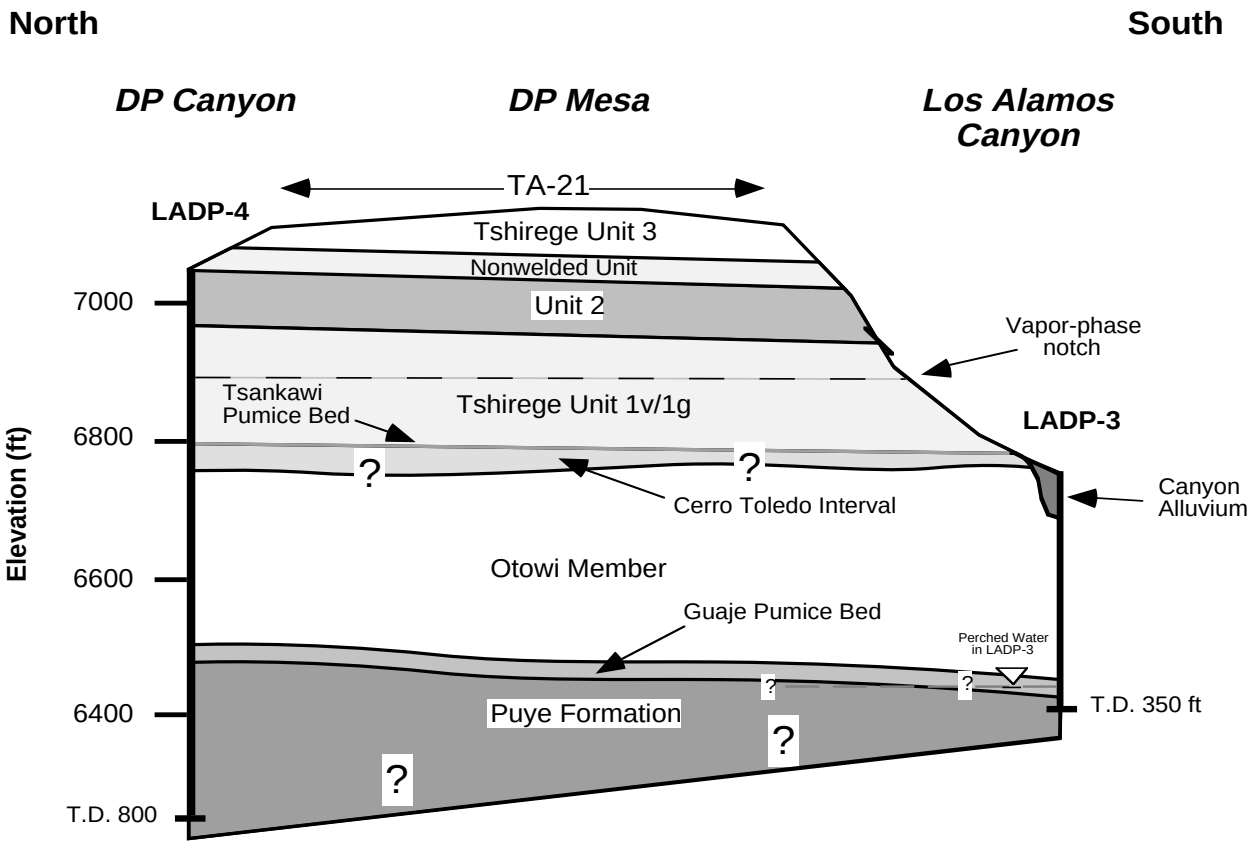

Fig. 12. N-S geologic cross section of TA-21 showing the distribution of principal stratigraphic units. Perched groundwater occurs in the Guaje Pumice Bed under Los Alamos Canyon, but its extent northward under the industrialized areas of DP Mesa is not known.

Pumice Bed at LADP-3 may flow downgradient into the Puye Formation in other parts of Los Alamos Canyon. In the geologic log for well Otowi-4, Stoker *et al.* (1992) observed, *"Some perched water was visible in a video log of the 48-in. hole at about 253 ft where the water cascaded in from large gravel*." The perched groundwater in Otowi-4 occurs in the Puye Formation 0.75 miles downcanyon and 64 ft lower in elevation than the Guaje Pumice Bed groundwater in LADP-3 (Fig. 13). Although these occurrences of perched groundwater may be related, this hypothesis cannot be demonstrated with certainty using the data currently available.

At this point in the investigation, the source of tritium in the Guaje Pumice Bed groundwater in Los Alamos Canyon has not been determined. The Laboratory's TA-2 and TA-41 are located on the floor of Los Alamos Canyon upgradient of the tritium contamination detected at LADP-3. TA-2 is a possible contamination source because it was the source of tritium releases in the past. In January 1992, it was determined that tritium-laden primary coolant water from the Omega West Reactor at TA-2 was leaking into the alluvial groundwater. Surface water and alluvial groundwater from the canyon bottom are possible sources of recharge to the Guaje Pumice Bed groundwater. TA-21 is a less likely source for the tritiated groundwater because thick, unsaturated tuffs, lack of available surface and groundwater, and low recharge rates could serve as effective barriers to contaminant transport from the mesa top.

The discovery of Guaje Pumice Bed groundwater shows that surface water can infiltrate to substantial depths in the unsaturated zone beneath the large canyons of the Pajarito Plateau. Although the presence of the Guaje Pumice Bed perched groundwater raises questions about potential transport through the unsaturated zone, it is important to note that 600 ft of unsaturated Puye Formation separate the Guaje Pumice Bed groundwater from the main aquifer (Fig. 13). In addition, tritium levels in LADP-3 are below EPA drinking-water standards and likely would be diluted further if these groundwaters

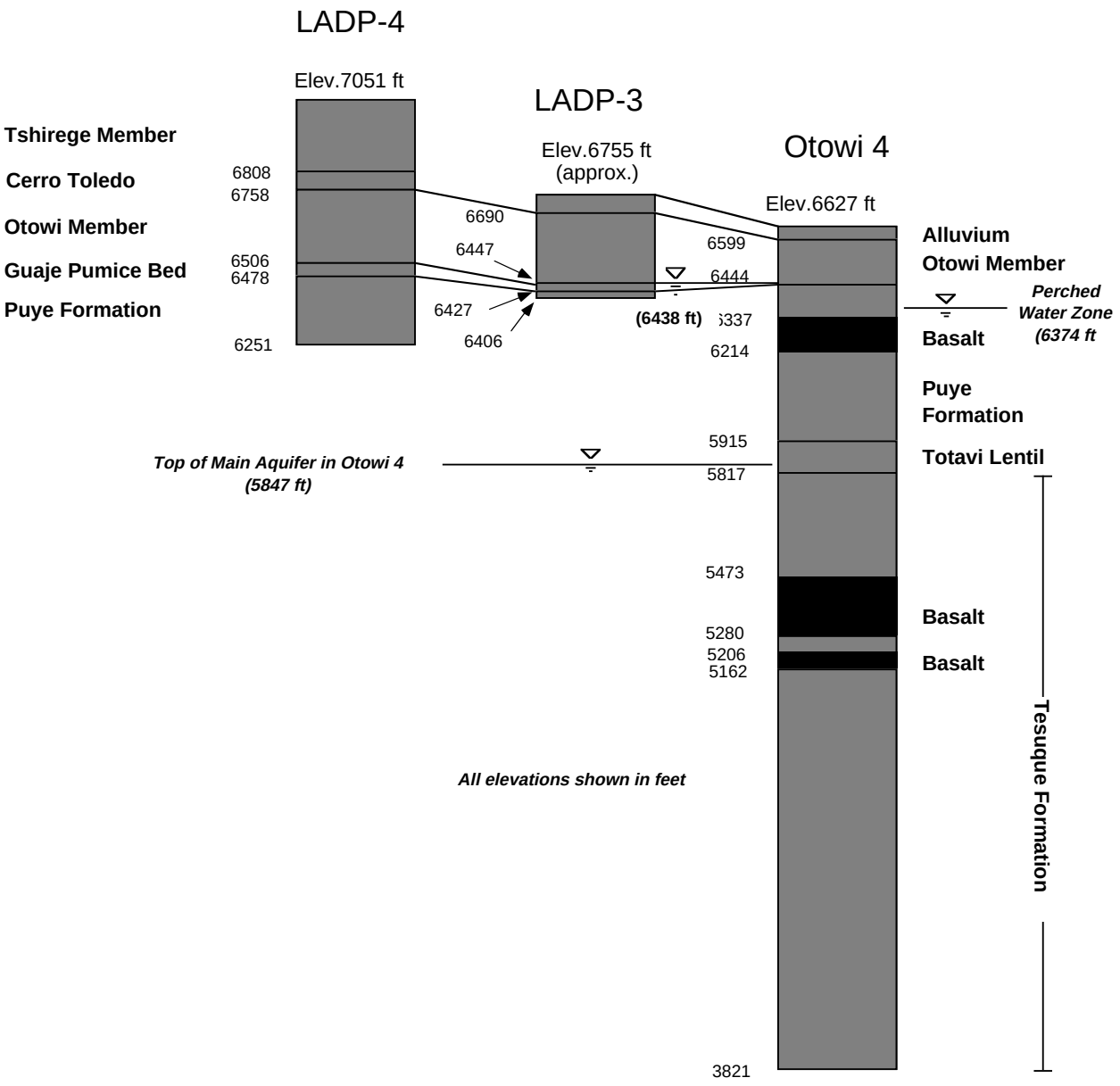

Fig. 13. Summary of subsurface geology in the vicinity of TA-21. Otowi 4 geology is summarized from Stoker* et al. *(1992). Intermediate-depth perched groundwater in LADP-3 and Otowi 4 are ~600 ft above the main aquifer. Guaje Pumice Bed groundwater in Los Alamos Canyon does not extend as far north as LADP-4 in DP Canyon.

entered the main aquifer. Additional boreholes planned for the area around TA-2 and TA-41 should penetrate to the depth of the Guaje Pumice Bed groundwater. These boreholes will provide important information about the lateral extent of the Guaje Pumice Bed perched groundwater and will help identify the source of tritium and groundwaters.

As specified in RFI work plan, LADP-3 was completed as a monitoring well when groundwater was encountered in the Guaje Pumice Bed. The monitoring well was completed with 2-in. PVC inside a temporary ODEX casing, which was subsequently removed. Estimated thickness of the perched zone is 5 to 7 ft, and the well is screened from 326 to 316 ft. Figure 14 shows details of the completed monitoring well. Future plans for the monitoring well include installation of a continuous groundwater-level monitoring transducer and groundwater sampling on a quarterly basis.

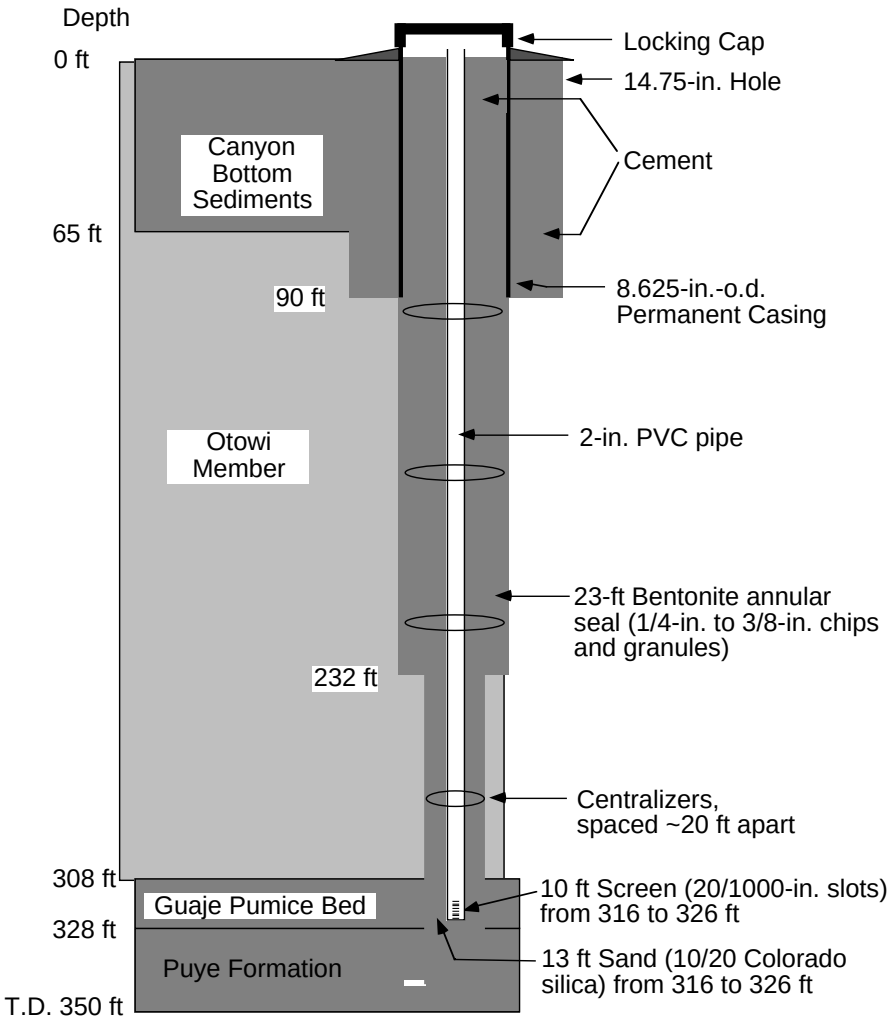

Fig. 14. Completion of LAPD-3 as a monitoring well (prepared from data provided by J.C. Newsom and E.D. Davidson, Jr.).

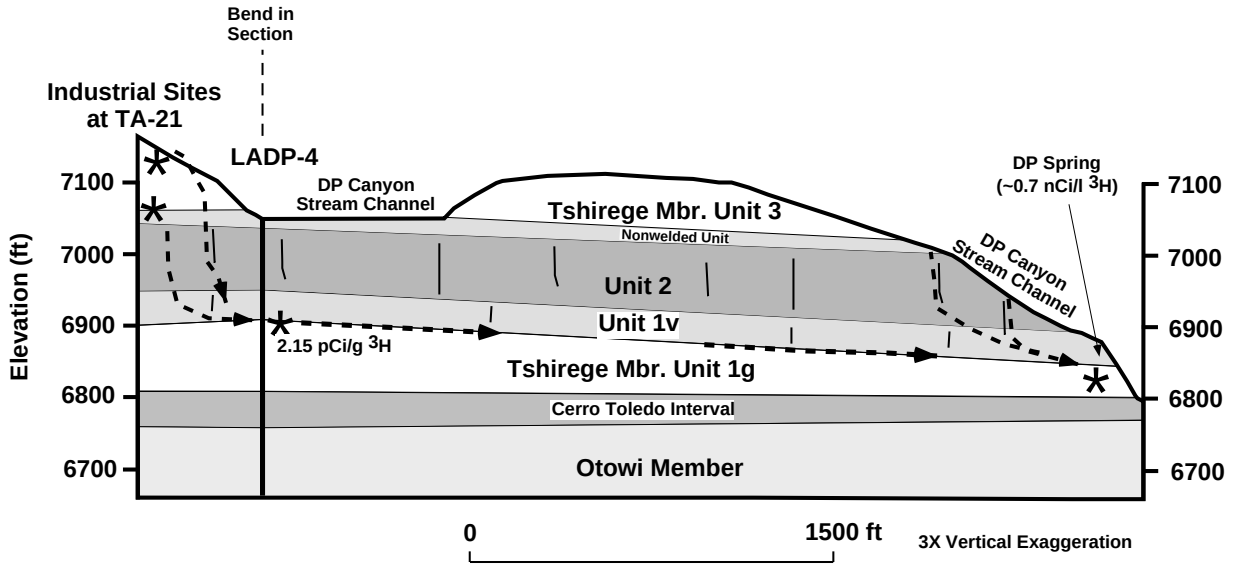

Fig. 15. Schematic geologic cross section showing setting of tritium contamination in the vicinity of DP Canyon (See Fig. 1 for location of cross section). Areas of known tritium contamination are indicated by (*). Tritiated groundwater at DP Spring may be derived from alluvial groundwater in DP Canyon. An alternative hypothesis is that perched groundwater travels laterally along the unit 1v/1g boundary before emerging at DP Spring. In both scenarios, industrialized areas at TA-21 are likely sources of the tritium.

Tritium in LADP-4 in DP Canyon is associated with high moisture content at the Tshirege unit 1g/1v boundary. The origin of the tritium is not yet known, but several industrial sites at TA-21 are potential sources. For example, tritium from TA-21 was released into DP Canyon from outfalls, especially from Building 257. In addition, subsurface tritium contamination has been documented at MDA T, just south of the borehole. Both treated and untreated tritium-bearing effluent from processing of plutonium was disposed of in four absorption beds at MDA T from 1945 to 1966 (Rogers, 1977). In 1974, seven boreholes were drilled to a depth of 40 ft between absorption beds 1 and 3 at MDA T to gather subsurface data for a proposed retrievable-waste storage facility. Samples from these boreholes contained 0.6 to 28 nCi/ℓ in soil moisture.

The localized nature of tritium in LADP-4 suggests that the unit 1v/1g boundary acts as a preferential pathway for the lateral movement of moisture and tritium (Fig. 15). The tritium may have reached its present position in LADP-4 as part of a vapor plume that traveled laterally along a horizon of greater permeability. When ongoing testing of samples is completed, it will be possible to compare the hydrologic properties of the tuffs above, below, and at the unit 1v/1g boundary. Alternatively, the moisture content at the 1v/1g boundary may be high enough for porous-media flow to occur where smaller, interconnected pores in the tuff are water-filled. The highest moisture content at this boundary is 23%—or about two-thirds saturation—assuming 40% porosity.

Tritium is found not only in LADP-4, but also in DP Spring, which is located on the north side of lower DP Canyon (Figs. 1 and 15). The tritium levels in DP Spring vary seasonally with the discharge rate, but they typically average about 0.7 nCi/ℓ (see Adams *et al.*, Sec. VII, this report). The spring occurs at a cascade that marks an abrupt change in streambase level between middle and lower

DP Canyon. Data are not yet available for determining if tuffs in LADP-4 and DP Spring are hydrologically connected, but the occurrence of tritium at both locations suggests that such a connection might exist.

One hypothesis for the origin of tritiated groundwater at DP Spring is that it is derived from alluvial groundwater in DP Canyon, which becomes slightly contaminated as it flows past a source or sources associated with industrialized areas of TA-21 (Fig. 15). Shallow groundwater is unusual in a canyon of this size whose headwaters are on the Pajarito Plateau. Runoff into DP Canyon is probably augmented by diversion of surface water into the canyon from extensive paved areas in the canyon's headwaters. Alluvial groundwater commonly emerges in the stream channel as isolated small pools and short stretches of intermittent surface-water flow in the middle reaches of the canyon. Eastward, DP Canyon becomes steeper, narrower, and deeper as the stream cuts downward through welded-tuff bedrock. Stream alluvium is thinner and more discontinous in this part of the canyon because short, intense summer thunderstorms tend to scour sediments from areas where the stream gradient is high. Surface flow is intermittent in this portion of the canyon. Because DP Spring is perennial and the stream channel is dry for much of the year, water storage probably occurs within stream alluvium—particularly in the middle reaches of the canyon where alluvial deposits are thickest. Downcanyon, where alluvium is thin and discontinuous, some water storage may occur in fractures.

An alternative hypothesis for the origin of the tritiated groundwater at DP Spring is that it derives from a perched groundwater body located beneath DP Canyon (Fig. 15). No perched water was encountered in borehole LADP-4 in the middle reach of the canyon, but relatively high moisture contents and low-level tritium contamination occur along the Tshirege unit 1v/1g boundary. This boundary is ~30 ft above the point where DP Spring emerges in DP Canyon. As noted above, this body may be a preferential pathway for the lateral movement of groundwater or water vapor. Perhaps borehole LADP-4 missed a perched groundwater body in the middle reach of the canyon or perched groundwater occurs beneath one of the mesas adjacent to the canyon.

Two boreholes will be drilled in DP Canyon as part of future ER studies. These boreholes will provide additional information about the source of tritium at DP Spring and possible hydrologic connections between DP Spring and tritium source areas at TA-21.

CONCLUSIONS

Two geologic characterization boreholes were drilled at TA-21 between August 30 and December 17, 1993. These boreholes were drilled to determine if perched groundwater occurs beneath Los Alamos and DP Canyons and to characterize the major hydrogeologic units at TA-21. This report has presented preliminary geologic and hydrologic data collected from these boreholes.

Borehole LADP-3 in Los Alamos Canyon encountered two perched groundwater zones. The upper zone is likely part of the canyon's alluvial groundwater and its occurrence in this borehole shows that these shallow groundwaters can extend at least as far laterally as their host alluvial deposits do. Moisture data for the borehole shows that this upper groundwater is divided into two distinct zones of saturation. Guaje Pumice Bed groundwater occurs at a depth of 325 ft. A water sample of this deeper perched zone contained 6.0 ± 0.16 nCi/ℓ of tritium, which is above regional background for surface water but well below the drinking water standard of 20 nCi/ℓ. Preliminary analyses for low-level ^{137}Cs and Pu isotopes failed to detect these constituents. Mixing calculations suggest that ~70% of the groundwater in the Guaje Pumice Bed is recharge from alluvial groundwater. Additional analyses are being conducted to

determine if other contaminants are present in this perched groundwater and to further investigate the possibility of a hydrologic connection between the alluvial groundwater and the Guaje Pumice Bed groundwater.

The source of tritium in the Guaje Pumice Bed groundwater in Los Alamos Canyon cannot be determined with certainty yet. TA-21 is a less likely source for the tritium contamination because thick, unsaturated tuffs, little or no available water sources, and low recharge rates may serve as effective barriers to contaminant transport from the mesa top. TA-2 is considered a much more likely source of tritium contamination in Los Alamos Canyon because it was the source of tritium releases in the past and because surface water and alluvial groundwater are available to promote recharge through the canyon floor.

Tritium also was found in borehole LADP-4 in DP Canyon. Preliminary laboratory analysis yielded 2.15 ± 0.18 pCi/g tritium for a tuff sample collected from the moist zone associated with the unit 1v/1g boundary at a depth of 158.6 to 160.1 ft. This value is above background but well below the screening action level of 820 pCi/g for tritium in soil moisture. The origin of the tritium is not yet known, but several industrial sites at TA-21 are potential source areas.

Additional characterization of the perched groundwater in Los Alamos Canyon will take place when additional boreholes are drilled as part of both OU-1098 RFI studies at TA-2 and the Canyons RFI investigations. In addition, two boreholes will be drilled in DP Canyon as part of future TA-21 RFI studies to provide additional information about the occurrence of tritium in LADP-4 and at DP Spring.

ACKNOWLEDGEMENTS

We thank J. Gardner, J. Wolff, and E. Springer, who provided critical reviews of this report.

REFERENCES

Adams, A., DeMuth, J., Counce, D., and Goff, F., 1995, Fluorescein dye experiment at DP Spring and sewage outfall, Technical Area 21, Los Alamos, New Mexico, Sec. VII, this report.

Rogers, M.A., 1977, History and environmental setting of LASL near-surface land disposal facilities for radioactive wastes (Areas A, B, C, D, E, F, G, and T), Los Alamos National Laboratory report LA-6848-MS, Vol. 1, 55 pp.

Stoker, A.K., McLin, S.G., Purtymun, W.D., Maes, M.N., and Hammock, B.G., 1992, Water supply at Los Alamos during 1989, Los Alamos National Laboratory Report LA-12276-PR, 51 pp.

FLUORESCEIN DYE EXPERIMENT AT DP SPRING AND SEWAGE OUTFALL

by

A. Adams, J. DeMuth, D. Counce, and F. Goff

Fluorescein dye was released into DP Canyon and one of its tributaries to determine if tritium in the water at DP Spring is supplied all or in part by tritiated effluent released from the sewage outfall on the east end of TA-21. DP Spring and three canyon sampling sites downgradient of the sewage outfall were sampled on a regular basis for 60 days after the dye was released. The fluorescein dye was found in all three canyon sampling sites but was never detected at DP Spring. Chlorate, an industrial processing chemical, is found in DP Spring but not in the effluent from the sewage outfall or in the canyon sample sites. In addition, water collected at the three canyon sampling sites contains much higher concentrations of nitrate, phosphate, and sulphate than is found in DP Spring. These data suggest that the tritium in water at DP Spring did not originate from the sewage treatment outfall at TA-21.

INTRODUCTION

Technical Area 21 is located on a narrow mesa north of Los Alamos Canyon and south of DP Canyon (Fig. 1). DP Canyon is a side canyon that merges with Los Alamos Canyon east of the study area. DP Spring is located in the lower part of DP Canyon. In 1991, water from this spring was found to contain low levels of tritium. This study examines a possible hydrologic connection between DP Spring and the outfall associated with the sewage treatment plant located on the east end of TA-21.

TA-21 has had an interesting and complex history of waste disposal; the site has been used for research determining the chemical and metallurgical properties of nuclear materials from World War II to the present time (Rogers, 1977; Nyhan *et al.*, 1984; Gerety *et al.*, 1989; Merrill, 1990). The recovery and purification of various types of plutonium-bearing residues created during these efforts has involved many industrial processes.

Tritium levels ranging from 3235 to 8915 pCi/kg of water were found at the sewage outfall and levels ranging from 381 to 2704 pCi/kg of water were observed at DP Spring. A fluorescein dye experiment was conducted to determine if the water at DP Spring originated from the sewage outfall at DP site.

FIELD WORK AND ANALYTICAL METHODS

In June 1992, 20 ℓ of fluorescein dye solution was released directly into a small tributary of DP Canyon just below the sewage treatment

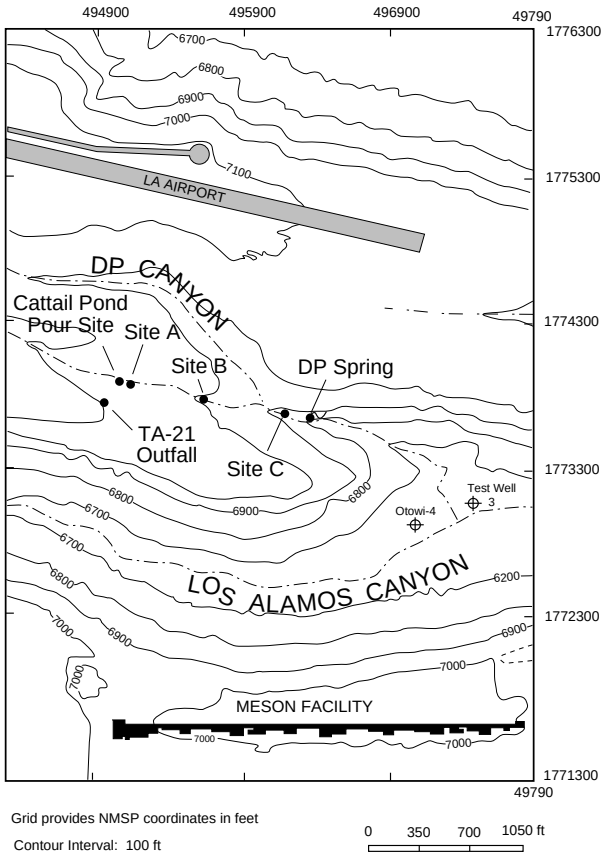

Fig. 1. Location map showing location of DP Spring, the TA-21 sewage treatment outfall, and the sites of the fluorescein dye pour and sampling.

outfall (Figs. 1 and 2). Fluorescein, easily seen by the naked eye because of its bright fluorescent-green color, is a harmless organic dye that breaks down relatively quickly in the environment (Fig. 2). Fluorescein is also easily analyzed in the microgram-per-liter range (Dash *et al.*, 1983).

A solution containing 22.4 g of fluorescein dye/1 ℓ of water was released into a cattail pond just below the outfall (Figs. 1 and 2). Three sampling sites downstream of the cattail pond were located downgradient of the sewage outfall and upslope of DP Spring (Fig. 1). Site A (Fig. 3) is 100 m downstream of the release site. Site B is 400 m downstream of the release point, where the canyon bottom intersects an old logging road. Site C was located in DP Canyon 100 m downstream of the intersection with the tributary canyon and 50 m upstream of DP Spring.

The samples were collected by two different procedures. Those for the fluorescein dye experiment were collected unfiltered in 60-mℓ plastic bottles, rushed to the laboratory, and analyzed for anions only. Another set of samples, collected for a regional surface and groundwater study, were analyzed for tritium, stable isotopes, and a complete suite of major and trace elements using procedures described in Trujillo *et al.* (1987).

RESULTS AND DISCUSSION

Site A was sampled before the fluorescein dye reached the site and was resampled 1 hr after the fluorescein dye arrived (Table 1; samples DP91-1 and DP91-3). From the time of the release until the sampling program was completed, the fluorescein dye was noted in every sample collected from sites A, B, and C; however, fluorescein was never found at DP Spring. The plot of fluorescein dye concentration *vs* time (Fig. 4) shows that the dye reached each of the sampling points downstream of the cattail pond. We were unable to sample site C for nearly 3 weeks—that part of the channel remained dry because of light rainfall and small fluid releases into the sewage outfall. However, DP Spring flows yeararound, and samples were collected from the spring while site C remained dry.

As the fluorescein dye experiment was being conducted, the presence of chlorate (ClO_3) was detected in the water samples collected from DP Spring. This anion is not found in natural groundwater, but is formed by secondary reactions from specific industrial chemicals such as bleach, chloric acid, or perchloric acid. In his report on waste disposal practices at TA-21, Merrill (1990) specifically mentions the perchlorates as a waste-stream chemical disposed of during past activities.

Fig. 2. Pour site in cattail pond below the sewage treatment plant at TA-21. Note the color change as the fluorescein dye becomes diluted with water in pond.

Fig. 3. The dye approaches the first sampling point at Site A.

TABLE I.

CHEMICAL ANALYSES OF SELECTED ANIONS AND FLUORESCEIN DYE IN SAMPLES FROM DP CANYON AND DP SPRING[a]

Sample Number	Description	Date	Temp. °C	B mg/kg	Br mg/kg	BrO_3 mg/kg	Cl mg/kg	ClO_3 mg/kg	Fluorescein µg/kg	F mg/kg	IO_3 mg/kg	NO_2 mg/kg	NO_3 mg/kg	pH (field)	PO_4 mg/kg	SO_4 mg/kg
REGIONAL SAMPLES																
PP-1	DP Spring	05/30/90	8.4	<0.05	<0.05	---	39.5	---	---	1.88	---	---	5.78	---	1.17	14.5
PP-2	DP Spring	08/10/90	10.0	0.53	<0.05	---	24.7	---	---	1.73	---	<0.05	3.41	---	1.1	10.1
PP-4	DP Spring	09/06/90	16.0	0.1	<0.05	---	21.1	---	---	1.69	---	<0.05	2.45	---	1.16	9.23
VA-345	DP Spring	05/14/91	11.4	<0.02	0.03	<0.2	119	0.78	---	1.26	---	<0.05	4.29	5.8	0.47	11.8
VA-346	Outfall at TA-21	05/15/91	12.3	0.1	0.09	---	51.7	<0.05	---	1.6	---	0.83	17.9	6	18.7	34.3
VA-363	DP Spring	06/26/91	8	<0.02	0.02	<0.2	76	0.43	---	1.37	---	<0.05	3.64	5.8	0.6	9.88
VA-364	DP Spring	07/11/91	8.4	0.01	<0.02	---	52.8	0.21	---	1.53	---	<0.02	4.35	5.8	0.62	8.93
TRACER EXPERIMENT																
DP91-1	Site A	06/19/91	20	0.6	0.09	---	75.5	<0.1	<0.05	1.54	---	<0.02	70.6	6.5	16.6	24.9
DP91-2	DP Spring	06/19/91	9.3	0.05	0.02	---	78.3	0.39	<0.05	1.4	---	<0.02	5.22	5.8	0.64	11.2
DP91-3	Site A after dye	06/19/91	20	0.15	0.03	---	30.1	---	16100	1.41	---	0.7	53.4	---	14.6	53.4
DP91-4	DP Spring	06/20/91	9.3	<0.02	0.02	---	76.1	0.42	<0.05	1.38	---	<0.02	4.93	5.5	0.68	11.1
DP91-5	DP Spring	06/21/91	8.9	<0.02	0.02	---	70.7	0.37	<0.05	1.38	---	<0.02	3.96	5.8	0.64	10
DP91-6	DP Spring	06/22/91	9	<0.02	0.02	---	71.8	0.42	<0.05	1.37	---	<0.02	4.25	---	0.65	9.98
DP91-7	Site B	06/22/91	16.8	0.16	0.03	---	36.9	<0.05	0.1	1.81	---	<0.02	0.06	6.5	6.5	29.7
DP91-8	DP Spring	06/23/91	7.9	<0.02	0.02	---	72.6	0.39	<0.05	1.37	---	<0.02	4.25	6.5	0.66	9.92
DP91-9	DP Spring	06/24/91	8	<0.02	0.02	---	73.5	0.44	<0.05	1.34	---	<0.02	4.35	5.8	0.67	9.81
DP91-10	DP Spring	06/25/91	8	<0.02	0.02	---	74.6	0.45	<0.05	1.39	---	<0.02	1.17	6	0.42	9.84
DP91-11	DP Spring	06/26/91	8	<0.02	0.02	---	75.5	0.44	<0.05	1.44	---	<0.02	1.65	5.8	0.47	9.79
DP91-12	DP Spring	06/28/91	8.1	0.02	0.02	---	76.6	0.46	<0.05	1.37	---	<0.02	1.27	5.8	0.46	9.49
DP91-13	DP Spring	06/30/91	8.6	<0.02	0.02	---	77	0.45	<0.05	1.36	---	<0.02	1.92	5.8	0.52	9.44
DP91-14	Site B	06/30/91	---	0.13	0.04	---	28.2	<0.05	0.16	0.99	---	<0.02	<0.05	---	8.6	33.8
DP91-15	DP Spring	07/01/91	7.9	<0.02	0.02	---	77.2	0.45	<0.05	1.4	---	<0.02	2.01	5.8	0.55	9.41
DP91-16	DP Spring	07/03/91	8.2	<0.02	0.02	---	72.9	0.38	<0.05	1.38	---	<0.02	2.45	5.5	0.55	9.5
DP91-17	DP Spring	07/05/91	8.7	<0.02	<0.02	<0.2	60	0.29	<0.05	1	~<0.2	<0.02	1.7	6	0.53	8.69
DP91-18	DP Spring	07/07/91	8	<0.02	<0.02	<0.2	59.9	0.27	<0.05	1.16	---	<0.02	2.19	5.8	0.54	9.37
DP91-19	DP Spring	07/09/91	8	<0.02	<0.02	<0.2	58.7	0.28	<0.05	1.14	---	<0.02	1.67	5.8	0.49	9.49
DP91-20	Site C	07/09/91	---	<0.02	<0.02	<0.2	6.89	<0.05	0.29	0.22	---	<0.02	0.91	---	0.13	3.23
DP91-21	DP Spring	07/11/91	8.4	<0.02	<0.02	<0.2	50.9	0.18	<0.05	1.2	---	<0.02	1.97	5.8	0.61	8.28
DP91-22	DP Spring	07/12/91	8	<0.02	<0.02	<0.2	50.8	0.22	<0.05	1.09	---	<0.02	1.1	5.5	0.51	8.48
DP91-23	DP Spring	07/15/91	8.1	<0.02	<0.02	<0.2	53.4	0.21	<0.05	1.15	---	<0.02	1.15	5.5	0.61	8.69
DP91-24	DP Spring	07/17/91	8.2	<0.02	<0.02	<0.2	53.4	0.22	<0.05	1.05	---	<0.02	1.25	5.8	0.57	8.48
DP91-25	DP Spring	07/19/91	8.6	<0.02	<0.02	<0.2	54	0.21	<0.05	1.07	---	<0.02	2.24	5.5	0.61	8.48
DP91-26	Site C	07/19/91	---	0.06	<0.02	<0.2	15.5	<0.05	0.07	0.56	---	<0.02	1.47	---	0.07	6.06
DP91-27	Site B	07/19/91	---	0.3	<0.02	<0.2	21	<0.05	0.21	2.03	---	<0.02	6	---	4.89	44.6
DP91-28	Site A	07/19/91	---	0.18	<0.02	<0.2	41	<0.05	30.2	1.12	---	<0.02	61.9	---	6.38	79.8
DP91-29	DP Spring	07/22/91	9.1	<0.02	<0.02	<0.2	49.1	0.14	<0.05	1.08	---	<0.02	1.81	5.5	0.69	7.94
DP91-30	Site C	07/22/91	---	<0.02	<0.02	<0.2	12.7	<0.05	<0.05	0.57	---	<0.02	<0.05	---	<0.05	3.7
DP91-31	DP Spring	07/24/91	9	0.02	<0.02	<0.2	37.8	0.11	<0.05	1.49	---	<0.02	2.22	6	0.71	7.47
DP91-32	DP Spring	07/26/91	9.6	<0.02	0.02	<0.2	34	0.08	<0.05	1.69	---	<0.02	1.28	6	0.68	8.85
DP91-33	Site C	07/26/91	---	<0.02	<0.02	<0.2	15.9	<0.02	0.07	0.69	---	<0.02	0.02	5.8	0.17	4.78
DP91-34	Site B	07/26/91	---	0.13	<0.02	<0.2	31.7	<0.05	6.8	1.39	---	<0.02	1.51	6	5.5	48.1
DP91-35	Site A	07/26/91	---	0.09	0.02	<0.2	33.4	<0.1	28.8	1.27	---	<0.02	26.1	6	9.1	46.2
DP91-36	DP Spring	08/01/91	9.4	<0.02	0.02	<0.2	33.1	0.04	<0.05	1.62	---	<0.02	2.95	---	0.83	11.7
DP91-37	DP Spring	08/05/91	10.4	<0.02	<0.02	---	28.1	0.03	<0.05	1.77	---	<0.02	<0.05	6	0.74	7.79
DP91-38	DP Spring	08/07/91	10.6	<0.02	<0.02	---	29.5	<0.02	<0.05	1.75	---	<0.02	<0.05	6	0.69	9.89
DP91-39	DP Spring	08/09/91	10.5	<0.02	<0.02	---	27.9	<0.02	<0.05	1.78	---	<0.02	<0.05	5.8	0.69	10.8
DP91-40	DP Spring	08/12/91	10.9	<0.02	<0.02	---	28.6	<0.02	<0.05	1.66	---	<0.02	<0.05	5.8	0.69	10.5
DP91-41	DP Spring	08/16/91	11.5	<0.02	<0.02	---	30.1	<0.02	<0.05	1.66	---	<0.02	<0.05	6	0.72	9.62
DP91-42	Site B	08/16/91	---	0.14	0.04	---	30.5	<0.02	1.01	1.67	---	<0.02	0.35	6	10.5	9.15
VA-383	DP Spring	05/18/92	9.5	<0.05	<0.02	---	105	<0.1	---	1.23	---	<0.02	1.84	6.5	0.48	10.1

[a]*Analyses by P.E. Trujillo and D. Counce, Geology/Geochemistry Group EES-1, Los Alamos National Laboratory.*

As is seen in Table 1, almost every sample collected at DP Spring contains trace amounts of chlorate; however, samples collected at the sewage outfall and at sites A, B, and C contain no chlorate. Figure 5 shows a plot of chlorate *vs* time (in days). Chlorate concentrations at DP Spring increased until July, when summer rains flushed and diluted the concentration of the chlorate anion. By August, the concentrations of chlorate anion

were no longer detectable because they had been sufficiently diluted by heavier rainfall (Table 1; see EPG, 1993, for meteorological data).

Since chlorate was found at DP Spring, more than 50 wells, springs, and creeks in the Los Alamos region (F. Goff, A. Adams, and D. Counce, unpublished data) have been analyzed. To date, the only other sample containing chlorate is a surface water from Acid Canyon. Because Acid Canyon was once used as a site for disposal of plutonium wastes (US DOE, 1981), it is possible that the chlorate anion is related to plutonium processing and the wastes still linger in Acid Canyon and in DP Canyon.

Nitrate is a good tracer of industrial releases. Site A shows the highest values of nitrate found in the sampled locations—even the sewage outfall (Table 1 and Fig. 6). However, the sewage outfall was sampled in May (a dry month), whereas site A was sampled in June and July (somewhat wetter months). The higher concentration of nitrate at site A may have resulted when increased rainfall flushed this constituent into the tributary canyon. At site B, higher than background concentrations of nitrate found early in the experiment became increasingly diluted in the wetter months. Nitrate concentrations were very low at site C and at DP Spring.

Phosphate and sulfate are also good tracers for industrial waters (Table 1 and Fig. 6). The highest concentration of phosphate is found in the sewage outfall sample. Sites A and B also show high phosphate concentrations. Trends for sulfate are the same as those for phosphate and nitrate: high concentrations (Table 1) are found in samples collected at the sewage outfall and at sites A and B, and low concentrations occurred at DP Spring. When compared to samples of cold waters from springs and wells in the region, all of the samples collected from sites A and B and the sewage outfall contain greater than 1 order of magnitude more phosphate and sulfate than those from regional groundwaters (Shevenell *et al.*, 1987; Meeker *et al.*, 1990).

Boron is detected in varying concentrations at all the sampling sites (Fig. 6). Single samples containing anomalously high boron concentrations were found at sites A and B and at DP Spring. The elevated boron concentrations at these three sampling sites are not temporally related—each was found during a different collection period. Typically, boron is used as a tracer in geothermal waters (Goff *et al.*, 1988). In this study, boron shows no consistent trends but appears to be an indicator of industrial chemical releases.

CONCLUSIONS

The fluorescein dye experiment showed that water from the sewage outfall can be traced into DP Canyon. Fluorescein dye, detected at each of the canyon sampling sites, was not noted at DP Spring. Chlorate was found at DP Spring but not at the other canyon sampling sites. Nitrate, phosphate, and sulfate occur at high concentrations in waters collected from the sewage outfall and in the canyon sampling sites; however, these constituents occur only in low concentrations at DP Spring. These data suggest that DP Spring and the sewage treatment outfall are not hydrologically connected. Therefore, tritium contamination in DP Spring must originate from some source other than those at the sewage outfall, and the source of chemical contamination must be from further upstream in DP Canyon or from sites on the mesa north of DP Canyon.

ACKNOWLEDGMENTS

We thank D. Broxton, G. Eller, and J. Gardner for providing critical reviews of this paper.

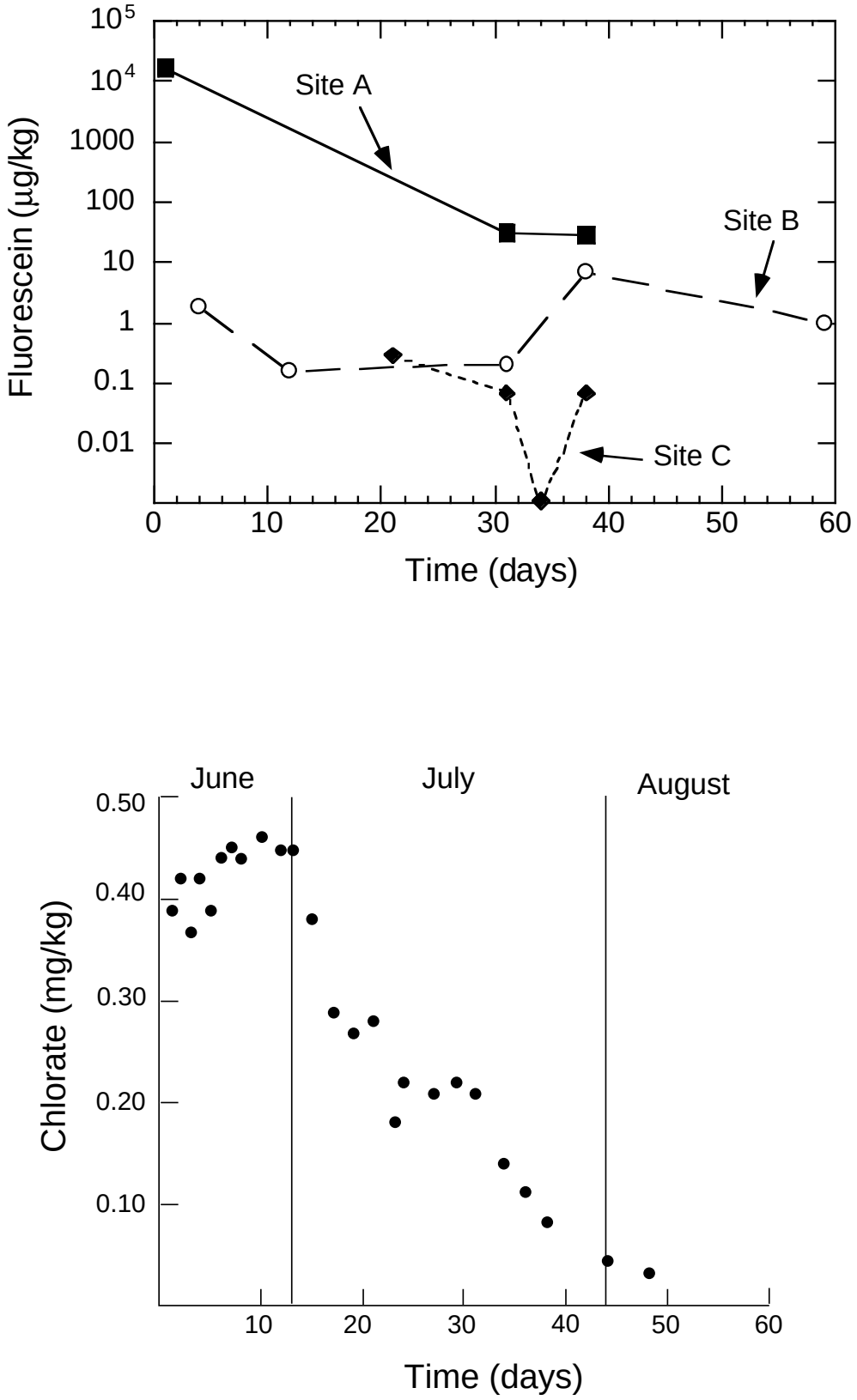

Fig. 5. Plot of chlorate concentration vs time (in days) at DP Spring. Note that chlorate was not detected at sites A, B, and C.

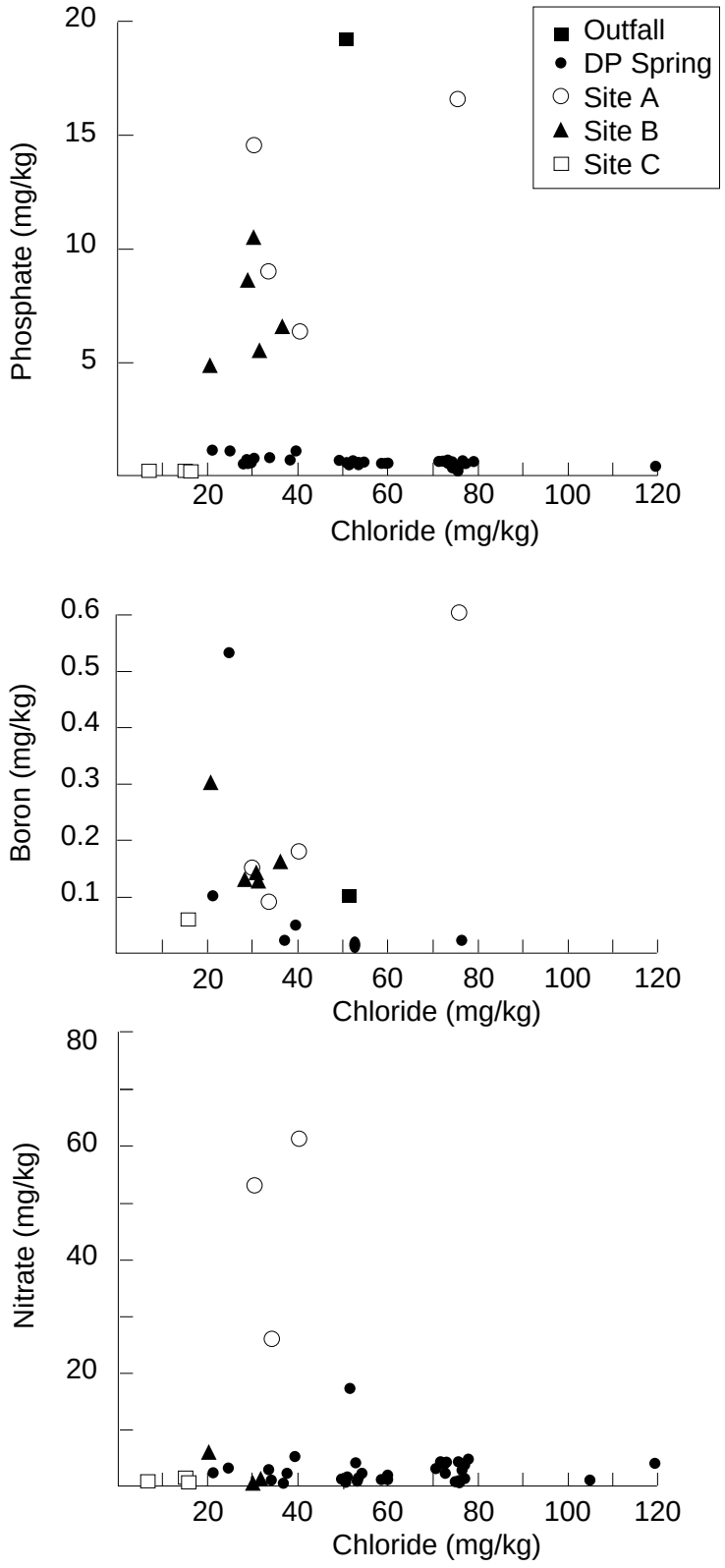

Fig. 6. Plot of nitrate, boron, and phosphate concentrations* vs *chloride at DP Spring and at sites A, B, and C.

REFERENCES

Dash, Z.V., Murphy, H.D., Aamodt, R.L., Aguilar, R.G., Brown, D.W., Counce, D.A., Fisher, H.N., Grigsby, C.O., Keppler, H., Laughlin, A.W., Potter, R.M., Tester, J.W., Trujillo, P.E., and Zyvoloski, G., 1983, Hot dry rock geothermal reservoir testing: 1978 to 1980. In G. Heiken and F. Goff (eds.), Geothermal Energy from Hot Dry Rock, J. Volcanol. Geotherm. Res. 15, 59-99.

EPG, 1993, Environmental Protection Group, Environmental Surveillance at Los Alamos during 1991, Los Alamos National Laboratory report LA-12572-ENV.

Gerety, M., Nyhan, J., and Oliver, R., 1989, History and geophysical description of hazardous waste disposal area A, Technical Area 21, Los Alamos National Laboratory report LA-11591-MS, 90 pp.

Goff, F. Shevenell, L., Gardner, J. N., Vuataz, F-D., and Grigsby, C. O., 1988, The hydrothermal outflow plume of the Valles Caldera, New Mexico and a comparison with other outflow plumes, J. Geophys. Res. 93(B6), 6041-6058.

Meeker, K., Goff, F., Gardner, J.N., Trujillo, P.E., Counce, D., 1990, Environmental sampling and mud sampling program of CSDP core hole VC-2B, Valles Caldera, New Mexico, Los Alamos National Laboratory report LA-11759-OBES, 41 pp.

Merrill, E.S., 1990, History of Waste Disposal at Technical Area 21 1943-1978, Los Alamos National Laboratory document, Group EES-15, 19 pp.

Nyhan, J.W., Drennon, B.J., Abeele, W.V., Trujillo, G., Herrera, W.J., Wheeler, M.L., Booth, J.W., and Purtymun, W.D., 1984, Distribution of radionuclides and water in Bandelier Tuff beneath a former Los Alamos waste disposal site after 33 years, Los Alamos National Laboratory report LA-10159-LLWM, 51 pp.

Rogers, M.A., 1977, History and environmental setting of LASL near surface land disposal facilities for radioactive waste Areas A, B, C, D, E, F, G, and T, Los Alamos Scientific Laboratory report LA-6848-MS, Vol. 1, 55 pp.

Shevenell, L., Goff, F., Vuataz, F., Trujillo, P.E., Counce, D., Janik, C.J., Evans, W., 1987, Hydrogeochemical data for thermal and nonthermal waters and gases of the Valles caldera-southern Jemez region, New Mexico, Los Alamos National Laboratory report LA-10923-OBES, 100 pp.

Trujillo, P.E., Counce, D., Grigsby, C.O., Goff, F., and Shevenell, L., 1987, Chemical analysis and sampling techniques for geothermal fluids and gases at the Fenton Hill laboratory, Los Alamos National Laboratory report LA-11006-MS, 84 pp.

US DOE, 1981, Formerly utilized MED/AEC sites remedial action program: Radiological survey of the site of a former radioactive liquid waste treatment plant (TA-45) and the effluent receiving areas of Acid, Pueblo, and Los Alamos Canyons, Los Alamos, New Mexico, Los Alamos National Laboratory report LA-8890-ENV, 251 pp.

Los Alamos
NATIONAL LABORATORY